

DECAY SCHEME STUDIES OF NEUTRON-DEFICIENT ODD-MASS THALLIUM ISOTOPES

AND THE SYSTEMATICS OF THE ODD-MASS MERCURY LEVELS

A THESIS

Presented to

The Faculty of the Division of Graduate

Studies and Research

By

Gregory Michael Gowdy

In Partial Fulfillment

of the Requirements for the Degree

Doctor of Philosophy in the School of Chemistry

Georgia Institute of Technology

December, 1976

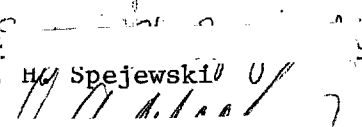
DECAY SCHEME STUDIES OF NEUTRON-DEFICIENT ODD-MASS THALLIUM ISOTOPES

AND THE SYSTEMATICS OF THE ODD-MASS MERCURY LEVELS

Approved:



R. W. Fink, Chairman



E. H. Spejewski

D. A. McClure

Date approved by Chairman:

NOV 29 1976

ACKNOWLEDGMENTS

It gives me great pleasure to recognize those individuals whose support made this research possible.

The largest portion of my thanks must go to my thesis director, Professor R. W. Fink, and my senior postdoctoral research advisor, Dr. J. L. Wood, without whose support, guidance, and encouragement this work could not have been accomplished. In addition, I would like to extend my grateful appreciation to Dr. E. H. Spejewski, Director of UNISOR, and Professor D. A. McClure for valuable suggestions in their review of this manuscript and for serving as members of my final examination committee. My appreciation is also extended to Dr. N. R. Johnson at Oak Ridge National Laboratory and Professor H. M. Newmann for serving on my final examination committee.

The hospitality of the UNISOR, Physics Division, and cyclotron (ORIC) staffs at ORNL is very much appreciated. Drs. Ken Carter and Dave Hensley have been especially kind in helping master the idiosyncrasies of the various UNISOR and ORIC computer systems. The frequent discussions with Drs. Ron Mlekodaj and Art Schmidt have proved both helpful and interesting. Acknowledgments must also be rendered to Professor L. L. Riedinger and E. F. Zganjar and my colleagues Lloyd Collins and Skip Kahler, whose help and discussions, scientific and otherwise, are appreciated. The Physics Division secretaries have been very helpful to me during my stay in Oak Ridge, and the typing assistance of Mrs. Anita Barker, Mrs. Joan Copeland, and Mrs. Christine

Wallace is greatly appreciated. Special thanks go to Miss Carol Proaps and Mrs. Wallace, who have done a great job in the typing of this thesis and Mrs. Barker, who helped cut through red tape, in order to bring the thesis to a speedy conclusion. Thanks are also due Richard Braswell for skillfully preparing many of the thesis drawings.

I sincerely appreciate the advice and assistance given me by Georgia Tech postdoctoral fellows, Drs. M.S. Rapaport, R. A. Braga, K. R. Baker, and A. C. Xenoulis. My colleagues, Drs. Bill Chew, Dale Nix, and Florian Tolea, and Messrs. Stan Lewis, Jerry Pate, and John Uecke will always be remembered for their friendship and help.

I am also thankful for my friendship with the late Dr. Gene Eichler, to whose memory I would like to dedicate this dissertation.

The financial support from Georgia Tech in the form of a teaching assistantship and from ERDA in the form of a research assistantship during my tenure at Georgia Tech is greatly appreciated. I am also grateful for the support given me by Oak Ridge Associated Universities in the form of an Oak Ridge Graduate Fellowship which enabled me to complete this research project at Oak Ridge.

This research project was carried out at the UNISOR facility (located at the Oak Ridge Isochronous Cyclotron of the Oak Ridge National Laboratory which is operated by the Union Carbide Corporation under contract with the U. S. Energy Research and Development Administration) and sponsored by ERDA, Oak Ridge Associated Universities, and the Georgia Institute of Technology.

Finally, I would like to express my sincere appreciation to my parents whose love and guidance will always be cherished; my wife, Donna, whose sacrifices and untiring support and encouragement during the course of this work can never be repaid; and my daughter, Kristyn, whose mere presence was a joy and helped me forget the problems of each day.

TABLE OF CONTENTS

	Page
ACKNOWLEDGMENTS	ii
LIST OF TABLES	vii
LIST OF ILLUSTRATIONS	viii
SUMMARY	xii
Chapter	
I. INTRODUCTION	1
II. MODELS FOR TRANSITIONAL NUCLEI	8
Basic Principles of Vibrational and Rotational Properties in Nuclei	8
Vibrational Models	14
Rotational Models	17
The Rotation-Alignment Model	19
The Triaxial Rotor Model	20
Future Developments for Transitional Nuclei	22
III. THE UNISOR FACILITY - EXPERIMENTAL SYSTEMS	24
Nuclide Production	26
Source Preparation	26
Ion Sources	29
General Features for Data Acquisition	31
Detector Systems	31
Experimental Procedure	35
Calibration and Data Analysis	42
Chemical Separations	44
IV. EXPERIMENTAL MEASUREMENTS, EVALUATION OF DATA, AND EXPERIMENTAL RESULTS	46
Decay of ^{191m}Tl	46
Gamma-Ray Singles Measurements	46
Conversion Electron Measurements	63
Coincidence Measurements	64
The ^{191m}Tl Decay Scheme	81
Levels in ^{191}Hg	90

	Page
Other Decays	91
Decay of ^{195}gTl	91
Decay of ^{189}mTl	101
Decay of ^{193}gTl	107
Decay of ^{193}mTl	115
Decay of ^{197}gTl	117
 V. INTERPRETATION OF EXPERIMENTAL RESULTS AND SYSTEMATICS OF LEVELS IN ODD-A Hg ISOTOPES	123
Population of Levels in Odd-A Hg Isotopes from T1 Isomeric and Ground-State Decays	123
Isomeric and Ground-State Relationships Among Odd-A Mercury Isotopes	126
Systematic Trends and Band Structures in the Odd- Mass Hg Isotopes	130
The Negative Parity States	130
The Postive Parity States and the $i_{13/2}$ Band	144
 VI. CONCLUSIONS AND PROPOSED FUTURE EXPERIMENTAL WORK.	149
 REFERENCES	154
 VITA	163

LIST OF TABLES

Table	Page
4-1. Details of ^{191}Tl Experiments	47
4-2. Energies and Relative Gamma-Ray Intensities for Transitions in the $^{191\text{m}}\text{Tl}$ Decay: Part I - Energies < 650 keV	56
4-3. Energies and Relative Gamma-Ray Intensities for Transitions in the $^{191\text{m}}\text{Tl}$ Decay: Part II - Energies > 650 keV	59
4-4. Experimental and Theoretical Internal Conversion Coefficients, Relative Electron Intensities, and Multipolarities for Transitions in $^{191\text{m}}\text{Tl}$ Decay	66
4-5. Coincidence Relationships Observed in $^{191\text{m}}\text{Tl}$ Decay . . .	73
4-6. Details of ^{195}Tl Experiments	92
4-7. Details of ^{189}Tl Experiments	102
4-8. Details of ^{193}Tl Experiments	108
4-9. Details of ^{197}Tl Experiments	118

LIST OF ILLUSTRATIONS

Figure	Page
2-1. A Schematic Illustration Showing Weak Coupling of an Odd Particle to an Even-Even Harmonic Vibrational Core and Perturbed Coupling (Presented in a Purely Qualitative Manner) Caused by the Presence of Residual Interactions between the Particle and Vibrational Degrees of Freedom	9
2-2. The Low Energy Levels in the Even-Even Hg Core Nuclei	10
2-3. A Strongly Deformed Even-Even Ground State Rotational Band vs the Weakly Deformed ^{194}Hg Ground State Band Shown with Its Coupling to an $i_{13/2}$ Particle . . .	13
3-1. The UNISOR Facility and Its Location Relative to ORIC. .	25
3-2. Original UNISOR On-Line Ion Source	27
3-3. Modified UNISOR Ion Source Using a Graphite Felt Catcher	28
3-4. The UNISOR Tape Transport System	32
3-5. Schematic Diagram of the Electronics for a Typical γ - γ - t Experiment on the Tennecom TP-5000 System	38
3-6. Exploded View of the Tape Vacuum Seal	39
3-7. Photograph of the Tape-Puller System	41
4-1. Low Energy Portion of the A = 191 Singles Gamma-Ray Spectrum	51
4-2. High Energy Portion of the A = 191 Singles Gamma-Ray Spectrum	52
4-3. An Expanded View of the Complex A = 191 Gamma-Ray Structure in the Energy Region 2.0-2.2 MeV	53
4-4. Decay Curves for Selected Transitions (216, 265, 336, 563, and 2360 keV) following the Decay of $^{191\text{m}}\text{Tl}$. .	55

	Page
4-5. The Total Sum of the A = 191 Conversion Electron Data	65
4-6. The γ - γ -t Coincidence Gates for the 216, 265, and 742 keV Transitions Observed in the Decay of ^{191m}Tl . .	71
4-7. The γ - γ -t Coincidence Gates for the 326, 336, and 1611 keV Transitions Observed in the Decay of ^{191m}Tl .	72
4-8. The Gamma-Rays in Coincidence with the 52 keV L Electrons Observed in the Decay of ^{191m}Tl	82
4-9. The Gamma-Rays in Coincidence with the 49 and 103 keV L Electrons Observed in the Decay of ^{191m}Tl . . .	83
4-10 (a) The Decay Scheme for ^{191m}Tl : Part I - Transitions from Levels below 800 keV	84
(b) The Decay Scheme for ^{191m}Tl : Part II - Transitions from Levels between 800 and 1016 keV	85
(c) The Decay Scheme for ^{191m}Tl : Part III - Transitions from Levels between 1016 and 1190 keV	86
(d) The Decay Scheme for ^{191m}Tl : Part IV - Transitions from Levels between 1190 and 1550 keV	87
(e) The Decay Scheme for ^{191m}Tl : Part V - Transitions from Levels between 1550 and 2100 keV	88
(f) The Decay Scheme for ^{191m}Tl : Part VI - Transitions from Levels above 2100 keV	89
4-11. Low Energy Portion of the Chemically-Separated A = 195 Singles Gamma-Ray Spectrum	94
4-12. High Energy Portion of the Chemically-Separated A = 195 Singles Gamma-Ray Spectrum	95
4-13. Singles Gamma-Ray Spectrum of Non-Chemically Separated A = 195 Sources	97
4-14. (a) The Decay Scheme for ^{195g}Tl (with some ^{195m}Tl Admixture): Part I - Transitions from Levels below 1000 keV	98
(b) The Decay Scheme for ^{195g}Tl (with some ^{195m}Tl Admixture): Part II - Transitions from Levels between 1000 and 1700 keV	99

	Page
(c) The Decay Scheme for ^{195g}Tl (with some ^{195m}Tl Admixture): Part III - Transitions from Levels above 1700 keV	100
4-15. (a) The Decay Scheme for ^{189m}Tl : Part I - Transitions from Levels below 760 keV	105
(b) The Decay Scheme for ^{189m}Tl : Part II - Transitions from Levels above 760 keV	106
4-16. (a) The Decay Scheme for ^{193g}Tl (with some ^{193m}Tl Admixture): Part I - Transitions from Levels below 1200 keV	112
(b) The Decay Scheme for ^{193g}Tl (with some ^{193m}Tl Admixture): Part II - Transitions from Levels above 1200 keV	113
4-17. The Decay Scheme for ^{193m}Tl	116
4-18. The Decay Scheme for ^{197g}Tl	121
5-1. Nilsson Diagram for Odd-Proton States, $50 \leq Z \leq 82$. .	124
5-2. The Single-Particle Shell Model States Observed in the Odd-Mass $^{189-201}\text{Tl}$ Isotopes Showing the Isomer and Ground State Relationships	125
5-3. Skeletal Decay Chain for $A = 191$	127
5-4. Nilsson Diagram for Odd-Neutron States, $82 \leq N \leq 126$.	128
5-5. The Single-Particle Shell Model States Observed in the Odd-Mass $^{189-197}\text{Hg}$ Isotopes Showing the Isomer and Ground State Relationships	129
5-6. The $i_{13/2}$ and $f_{5/2}$ Single-Particle States Shown Relative to the $p_{3/2}$ Single-Particle State in the Odd-Mass $^{189-197}\text{Hg}$ Isotopes	131
5-7. Level Systematics for Low-Lying (Energy ≤ 600 keV) States in the Odd-Mass $^{189-197}\text{Hg}$ Isotopes	132
5-8. The Observed Band Structures in ^{189}Hg Showing the Relationships among the $p_{3/2}$, $f_{5/2}$, and Deformed Bands	134
5-9. Band Structure Built on the $p_{3/2}$ Single-Particle State in $^{189-197}\text{Hg}$	135

	Page
5-10. Band Structure Built on the $f_{5/2}$ Single-Particle State in $^{189-197}\text{Hg}$	136
5-11. Band Structure Built on the $p_{1/2}$ Single-Particle State in $^{195-199}\text{Hg}$	137
5-12. The Depopulation of the Strongly Fed High-Energy $1/2^-$ States in $^{193-197}\text{Hg}$ are Shown Feeding the $p_{1/2}$ Single-Particle States by E0 Transitions	140
5-13. A Comparison of Experimental and Theoretical Negative Parity States in ^{193}Hg	141
5-14. A Comparison of Experimental and Theoretical Negative Parity States in ^{195}Hg	142
5-15. A Comparison of Experimental and Theoretical Negative Parity States in ^{197}Hg	143
5-16. The Positive Parity States Observed in $^{191-197}\text{Hg}$ Through In-Beam and Decay Studies	145
5-17. A Systematic Comparison of the Level Structure of Positive Parity States in $^{190-195}\text{Hg}$ Showing the Decoupled Band Structure following the Rotation-Aligned Picture of Stephens	146
5-18. Comparison of Experimental Results for the $i_{13/2}$ Band with the Triaxial Rotor Model Plus VMI (Toki and Faessler), Triaxial Rotor Model (Meyer ter Vehn), and Rotation-Alignment Model Theoretical Predictions.	148

SUMMARY

The study of the decay of the odd-mass nuclides, $^{189-197}\text{Tl}$, by γ -ray, x-ray, and conversion electron singles and coincidence techniques has been undertaken with the university on-line isotope separator (UNISOR) at the Oak Ridge Isochronous Cyclotron (ORIC). This study gives detailed information on energies, intensities, and multipolarities of transitions and energies and spins and parities of the levels in the daughter nuclides, $^{189-197}\text{Hg}$, as well as some branching ratios and $\log ft$ values for the β^+ /EC-decay, from the parents.

A systematic investigation has been made of these Hg levels, together with levels in ^{199}Hg reported in the literature. The present work concentrates on observation of changes in the level energies with changing neutron number, and the band structure trends implied by these level energy systematics. Of particular interest are the systematics of the unique parity high-j $i_{13/2}$ band in these Hg isotopes. The yrast levels (determined by reaction γ -ray spectroscopy studies) together with the non-yrast levels determined in this work are compared to available theory calculations for the $i_{13/2}$ band in the $^{191-197}\text{Hg}$ isotopes. This comparison gives a good indication of the triaxial nature, and thus the rotational nature of this band in the odd-Hg nuclei.

The low-lying negative parity states have also been systematized. These states are compared with the predictions of the complex particle (quasiparticle)-phonon coupling models (developed in order to explain

transitional nuclei, such as the odd-Hg isotopes). These models appear to have very limited success. The level density is reproduced but the energies and level orderings show no particular correlations, indicating that a purely vibrational picture for these nuclei is inadequate. Experimentally three interesting phenomena are observed in the study of the negative parity states. First, and most interesting, is the discovery of evidence for shape coexistence in ^{189}Hg . Three members of a "deformed" band built on the $7/2^-$ [503 \uparrow] Nilsson state and having a bandhead energy of 476.5 keV have been located. This band is predicted to have a rotational constant, $h^2/2I$ of ~ 14.0 keV and a deformation of $\beta \sim +0.27$ (determined from neighboring nuclei), making it a prolate band in a nucleus with an oblate ground state ($\beta \sim -0.17$).

Second, a relatively high energy level (~ 1.0 - 1.6 MeV), giving rise to an intense high energy E0 transition to the $p_{1/2}$ single-particle state and a very intense M1 + E2 transition to the $p_{3/2}$ single particle state, has been uncovered in each of the odd-mass 193 - ^{197}Hg isotopes. These anomalous levels are as yet unexplained.

Finally, a decoupled band structure built on the $p_{3/2}$ single-particle shell model state has been found in 189 - ^{195}Hg , where medium- to high-spin states ($7/2^-$ to $13/2^-$) are populated by decay of the $9/2^-$ isomer in the Tl parents. Band structure has also been found built on the $f_{5/2}$ and $p_{1/2}$ single-particle shell model states, but these structures are difficult to interpret. The decoupled nature of the $p_{3/2}$ band, however, indicates possible rotational character

in these negative parity states. The possible existence of rotational character in both the positive and negative parity systems in the Hg isotopes helps to explain the failure of the pure vibrational model for these nuclei and indicates the need in this region for a model which allows for both vibrational and rotational degrees of freedom.

CHAPTER I

INTRODUCTION

The past thirty years have brought great strides in our understanding of the structure of nuclei. Such techniques as Coulomb excitation, nucleon-transfer reactions, in-beam spectroscopy, elastic and inelastic scattering, and radioactive decay have been used to probe the nature of nuclear structure. Along with these experimental efforts, theoretical nuclear models have been developed in an effort to explain and predict the experimental results and understand the properties of nuclei. The goal of this effort is to account for the complex properties of nuclei in terms of nucleon-nucleon interactions. However, since a fundamental microscopic description of the nucleus is lacking, numerous approximate nuclear models have been proposed in attempts to explain the three broad classes of nuclei - (1) spherical, closed shell nuclei; (2) highly deformed nuclei many nucleons removed from closed shells; and (3) transitional nuclei lying between these two extremes.

The first model which successfully predicted nuclear properties for a broad range of nuclides was the shell model developed in the late 1940's by Mayer, Haxel, Jensen, and Suess (see refs. 1-3). This model assumed that the motion of each nucleon was completely independent of that of the other nucleons and could be described using a harmonic oscillator potential which included

strong spin-orbit coupling. The latter when added to earlier versions of this model permitted realization of a quantitative reproduction of nuclear properties, replacing the limited qualitative picture that had previously existed. The shell model is quite successful in its prediction of various nuclear properties such as spins, parities and magnetic moments for odd-mass nuclei, magic numbers, islands of isomerism, and alpha and beta decay energy systematics.

Despite these accomplishments, its scope is severely limited. Nuclei far from closed shells had properties that were not fully explained; specifically, the existence of large static quadrupole moments and energy levels far below the individual particle excitations, and the enhancement of electric quadrupole transition rates. The first successful explanation of these aspects came in the early 1950's with the realization by Bohr and Mottelson^{4,5)} that these properties are characteristic of collective nucleonic motion in nuclei with permanently deformed ground states (see Hyde et al.⁶⁾ and Sorensen⁷⁾ for historical background). Classically, these collective motions correspond to shape oscillations of the nuclear surface or rotations of the nucleus as a rigid or a fluid body. Shape oscillations (the so-called "vibrational" model) have had much success in describing nuclei near the closed shells, whereas a rotational description (the "rotational" model) has proved applicable to highly deformed nuclei far from closed shells. Neither model does very well, however, for the regions between these two extremes, i.e. the so-called transitional region where nuclei are only slightly deformed,

and asymmetric shapes have been shown to play an important role.^{8,9)}

Microscopic extensions and refinements of the classical vibrational model have been applied to the study of nuclei in transitional regions. The most widely used formalisms involve the use of particle-vibration coupling.¹⁰⁻¹⁷⁾ However, numerical calculations with these models, despite their complexity, have met with only limited success in interpreting transitional nuclei. The rotational model has also been extended in attempts to reproduce the properties found in transitional regions. The rotation-alignment model¹⁸⁾ and triaxial rotor model^{8,9,19)} have produced surprisingly good results for interpreting unmixed unique parity high-spin orbitals in regions where the original rotational model was long thought to be invalid. A complete description of nuclear properties for nuclei in transitional regions has not yet been found in terms of rotational degrees of freedom. The most physically realistic model for transitional nuclei may involve a combination of rotational and vibrational modes, but such a model has not yet been devised.

Detailed and extensive experimental measurements of nuclear properties are vital to the development of models for the description of nuclear phenomena. Many experimental investigations have been carried out on nuclei around the $Z = 50$ closed shell, but very little has been done in the transitional region surrounding the $Z = 82$ closed shell at Pb. The present work, therefore, undertakes a systematic experimental study of the collective excitations present in one isotopic group in this transitional region; specifically, the

neutron deficient odd-mass Hg isotopes. The properties of the excited states in five such nuclei ($A = 189, 191, 193, 195, \text{ and } 197$) have been studied via their population following electron capture and positron decay of their $^{189-197}\text{Tl}$ parents. These systematic studies, including an extension to the more well known ^{199}Hg , have lead to a better understanding of this transitional region.

Previous studies on the levels in $^{189,191,193}\text{Hg}$ have been extremely limited. Vandlik et al.²⁰⁾ found three γ -rays decaying with a 1.4 minute half-life in their study of ^{189}Tl , produced in 660 MeV proton spallation of PbF_2 targets. The reaction products were chemically separated "on-line" by a gas thermochromatographic method and the resulting Tl activities separated by mass separator and counted using Ge(Li) detectors. This group used the same procedure to study ^{191}Tl ,^{21,22)} ^{193}Tl ,^{21,23)} ^{195}Tl ,²⁴⁾ and ^{197}Tl .²⁵⁾ These represent the best decay studies done so far on the odd-Tl nuclei.

Early studies of ^{191}Tl by Chackett and Chackett²⁶⁾ and Andersson et al.²⁷⁾ involved only a half-life determination. Vandlik et al.²²⁾ reported 17 γ -ray lines and five conversion electron transitions, but no decay scheme. An in-beam study by Lieder et al.²⁸⁾ gave information on high-spin ($\geq 21/2$), negative parity states, and the yrast* levels of the $i_{13/2}$ rotational band in

* The yrast state is the lowest-lying energy level of a nucleus having a given spin quantum number.

^{191}Hg and ^{193}Hg . The half-life of the ground state of ^{193}Tl was determined by Chackett and Chackett,²⁶⁾ Andersson et al.,²⁷⁾ and Diamond and Stephens.²⁹⁾ No α -radiation was observed by Karras et al.³⁰⁾ Andersson et al.²⁷⁾ found eight conversion-electron lines in the decay of ^{193}Tl and Vandlik et al.²³⁾ built a tentative decay scheme using γ -ray, conversion electron, and γ - γ coincidence data.

The levels in $^{195,197}\text{Hg}$ have been fairly well studied. In early studies of ^{195}Tl decay by Knight and Baker,³¹⁾ Andersson et al.,³²⁾ Gupta and Jha,³³⁾ Jung and Svedberg,³⁴⁾ Jung and Andersson,³⁵⁾ and Backlin et al.,³⁶⁾ the half-life and decay energy were measured and the conversion-electron spectrum examined with a magnetic spectrometer. Vandlik et al.²⁴⁾ have looked at the decay of ^{195}Tl to low-spin levels in ^{195}Hg in great detail. Proetel et al.³⁷⁾ have done an in-beam study on the yrast states in the $i_{13/2}$ band and the high-spin negative parity states in ^{195}Hg and ^{197}Hg . Early work on the decay of ^{197}Tl by Andersson et al.,^{32,38,39)} Knight and Baker,^{31,40)} Jung and Svedberg,³⁴⁾ and Jung and Andersson³⁵⁾ was done with scintillation spectrometers (γ -rays) and magnetic spectrometers (conversion electrons). Vandlik et al.²⁵⁾ have done a detailed study of the decay of ^{197}Tl with Ge(Li) γ -singles, Si(Li) conversion electron, and γ - γ coincidence measurements. The reaction, $^{198}\text{Hg}(d,t)^{197}\text{Hg}$, has been studied by Moyer.⁴¹⁾ Finally, an in-beam study to determine the low- and high-spin levels in ^{197}Hg has been carried out by Kemnitz et al.⁴²⁾

Building upon the results of these earlier works, the present decay studies have been performed on mass-separated sources of $^{189,191,193}\text{Tl}$ and mass-separated and chemically separated sources of $^{193,195,197}\text{Tl}$. The measurement of the decay properties of these transitional nuclei and interpretation of the results are the subjects of this dissertation. There are three primary goals of this research:

- 1) The measurement of the low-spin states in odd-mass $^{189-197}\text{Hg}$ is to serve as a benchmark for future theoretical interpretations of odd-neutron transitional nuclei.
- 2) The measurement of the non-yrast members of the positive parity $i_{13/2}$ bands is to serve as a test of the ability of the triaxial rotor model to describe pure- j states in these nuclei.
- 3) A systematic comparison among these five odd-Hg nuclei, $A = 189-197$ and the heavier (well known) odd- A Hg isotopes is to yield trends in the level structure which will increase our comprehension of the excitation degrees of freedom which are important in this transitional region.

Chapter II is devoted to theoretical considerations of the vibrational and rotational models, their various modifications, and their applicability to transitional nuclei. Chapter III discusses the UNISOR facility and the experimental systems used in this work. Chapter IV presents the individual experimental studies and their

evaluations and results, Chapter V an interpretation and discussion of the results, and Chapter VI contains a brief concluding summary. Some of the results given in this dissertation have already been published.⁴³⁻⁵²⁾

CHAPTER II

MODELS FOR TRANSITIONAL NUCLEI

Basic Principles of Vibrational and Rotational
Properties in Nuclei

In transitional regions, such as that of the odd-mass Hg isotopes, the vibrational model assumes that the ground-state equilibrium shape of a nucleus is spherical (as for closed-shell nuclei), and superimposed on this shape there are small vibrational oscillations of the surface of the nucleus, most notably quadrupole vibrations, (like waves on the surface of a liquid drop) which can be described by an harmonic oscillator model. Odd-mass nuclei are described by the coupling of the odd particle (or hole) to the vibrations of the surface of the appropriate even-even core. The level structure exhibited by the even-even cores should therefore be a good basis for the description of the structure of the nuclei in the region of interest. An even-even harmonic vibrator has an excitation structure like that shown in Figure 2-1, where the levels are ordered 0^+ (ground state), 2^+ , and a degenerate 0^+ , 2^+ , 4^+ triplet with $E_{4^+}/E_{2^+} = 2$. Figure 2-2 shows the experimental low-lying levels for the even-even nuclei - $^{190-198}\text{Hg}$ - which are core nuclei for the region under study. This figure reveals considerable variation from the harmonic vibrator picture since E_{4^+}/E_{2^+} lies between 2.4 and 2.6 and the 0_2^+ excited state is not observed near the 4_1^+ and

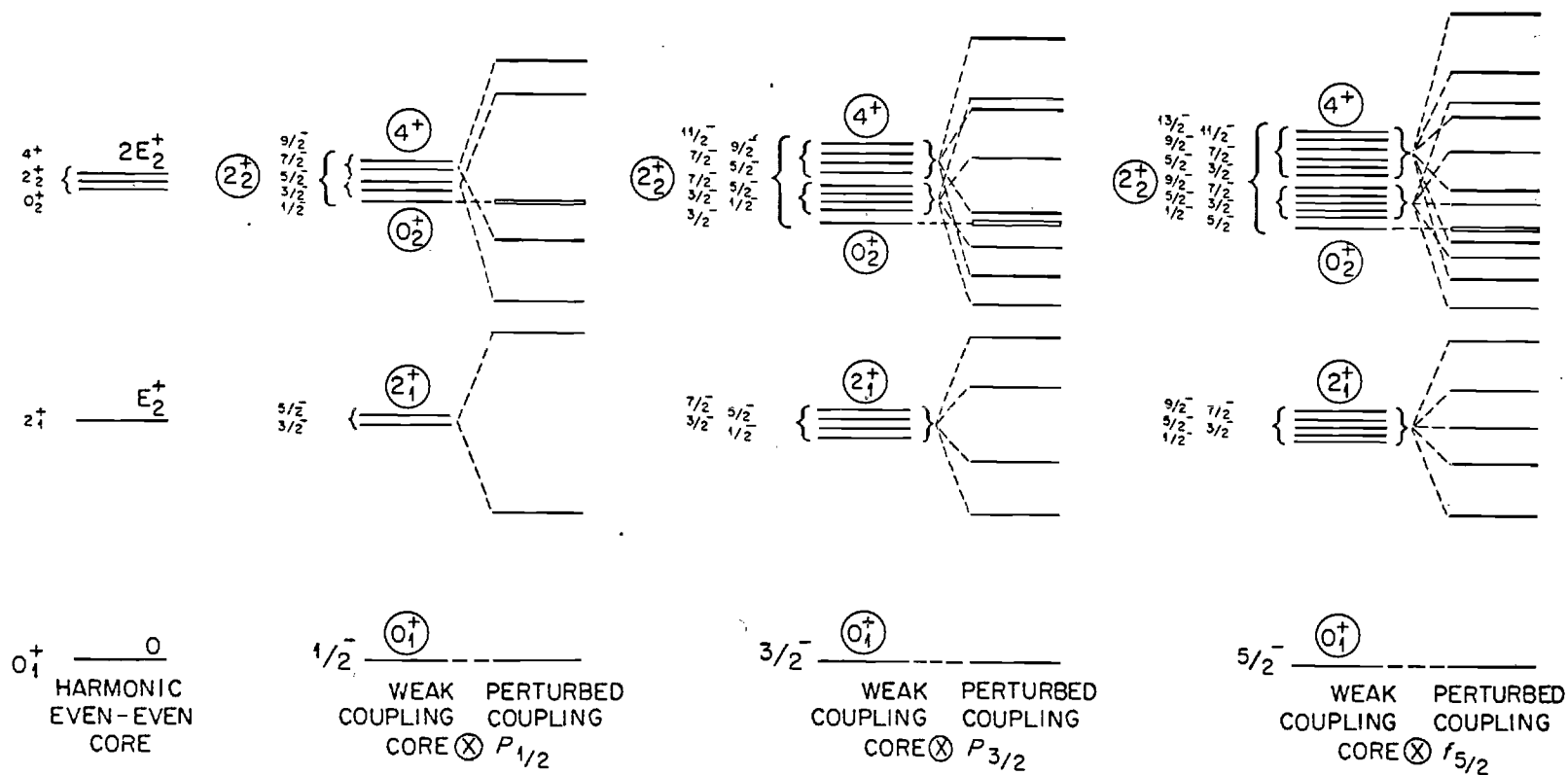


Figure 2-1. A Schematic Illustration Showing Weak Coupling of an Odd Particle to an Even-Even Harmonic Vibrational Core and Perturbed Coupling (Presented in a Purely Qualitative Manner) Caused by the Presence of Residual Interactions between the Particle and Vibrational Degrees of Freedom.

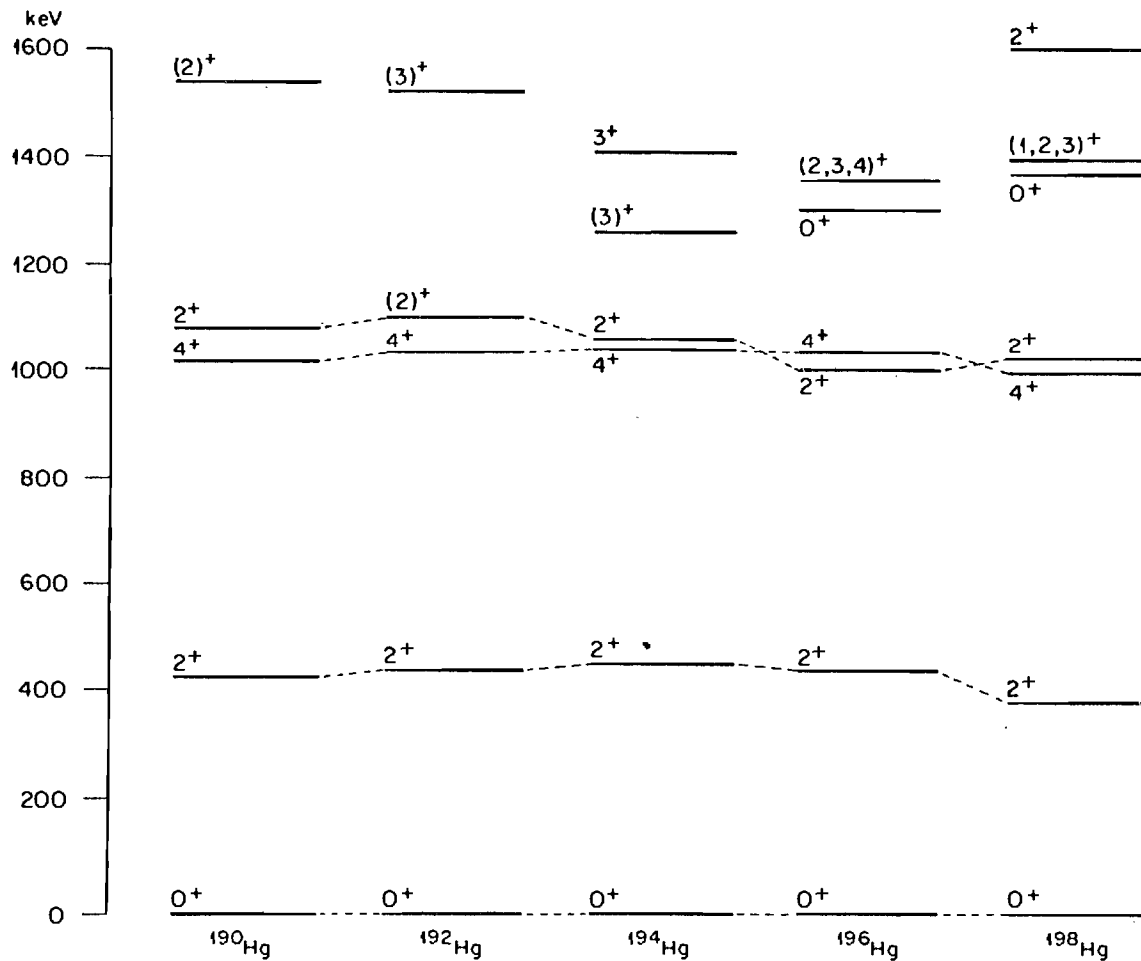


Figure 2-2. The Low Energy Levels in the Even-Even Hg Core Nuclei. Note the E_{4^+}/E_{2^+} ratio (R_4) of 2.4-2.6 suggesting behavior intermediate between pure vibrational ($R_4 = 2$) and pure rotational ($R_4 = 3.33$). Also note the 3^+ states indicative of triaxial rotational behavior. These data are taken from ref. 54 (^{190}Hg), ref. 55 (^{192}Hg), ref. 56 (^{194}Hg), and ref. 57 ($^{196}, ^{198}\text{Hg}$).

2_2^+ states in $^{190-194}\text{Hg}$. Moreover, deformation calculations (see e.g. S. G. Nilsson et al.⁵³⁾) predict that the ground states of the even Hg isotopes are deformed and slightly oblate with β , the quadrupole deformation parameter, between -0.12 and -0.17 . Therefore these core nuclei cannot be pure spherical vibrators. Extension of the quadrupole vibrational model to include anharmonic effects could, in principle, describe the above departures from harmonic behavior. The most recent discussion of the even-Hg isotopes¹⁶⁾ notes that at present a description in terms of quadrupole vibrations including anharmonicities is not yet available.

The high density of low-lying low-spin states present in the odd-mass Hg nuclei causes another effect to become important in a description of nuclei in this region. Figure 2-1 schematically shows the possible weak and perturbed coupling for several low-spin particles (the $p_{1/2}$, $p_{3/2}$, and $f_{5/2}$ "shell model" states expected at low energy in the odd-A Hg isotopes - see Chapter V) to simple harmonic even-even core states. As with the even-even nuclei, the pure harmonic vibrational cases are unrealistic. The perturbed coupling shows, purely qualitatively, the effect of possible mixings of the many low-spin levels at low energies. The effects of perturbed coupling using anharmonic core states have not been illustrated here because of their complexities.

Unlike the vibrational model with its assumption of a spherical equilibrium shape for the nucleus, the rotational model requires permanent deformation of the ground state of the nucleus and in

consequence, an associated rotational degree of freedom. Deformed odd-mass nuclei can be described by coupling the odd particle (or hole) to an even-even rotating core. The energy spectrum of an even-even rotor is shown in Figure 2-3 where the energies follow the relationship

$$E_I = \frac{\hbar^2}{2\mathcal{I}} [I(I+1)] \quad (2-1)$$

(E_I = energy of the level of spin I and \mathcal{I} = moment of inertia). Thus the E_{4+}/E_{2+} ratio has the well-known value of 3.33. The even-Hg isotopes show level spacings with a ratio of E_{4+}/E_{2+} between 2.4 and 2.6. Thus it is concluded that these nuclei lie between rotational and vibrational regions.

The even-Hg core nuclei show relatively low-lying 2_2^+ and 3_1^+ states as illustrated in Figure 2-2. Low-lying 2_2^+ and 3_1^+ states in even-even nuclei have been shown by Davydov^{58,59)} to be characteristic of the axially asymmetric rotor. The axially asymmetric (or triaxial) rotor appears to be well suited to the description^{8,9)} of the excitation spectrum of the doubly even Hg isotopes. The work of Toki and Faessler⁶⁰⁾ has included variable moments of inertia (as described in the classic paper by Mariscotti et al.⁶¹⁾) in addition to triaxial shapes in attempting a rotational description of the even-even transitional nuclei in this region.

The quantitative details of the way in which odd nucleons couple to an even-even core remain to be specified. These details

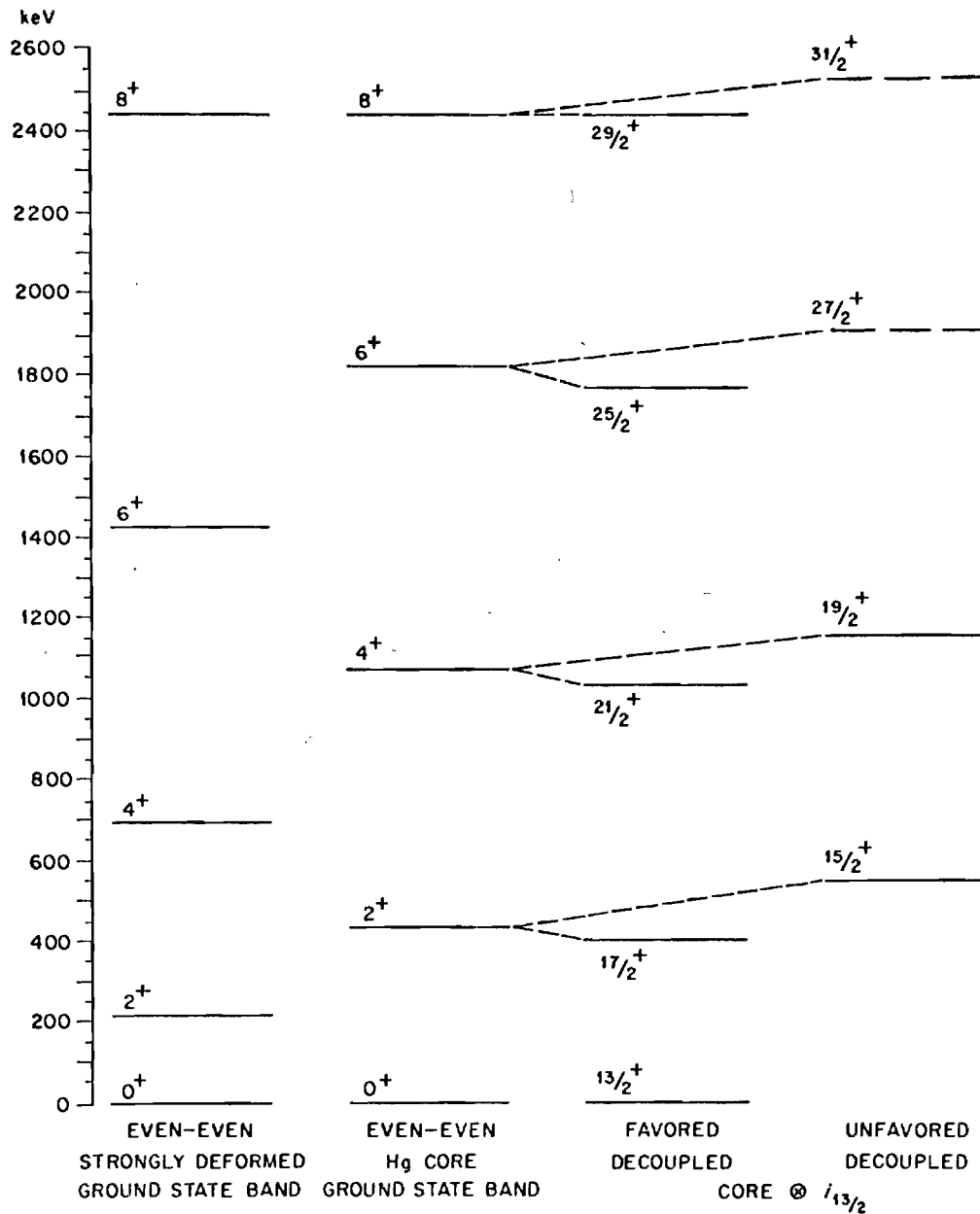


Figure 2-3. A Strongly Deformed Even-Even Ground State Rotational Band vs the Weakly Deformed ^{194}Hg Ground State Band Shown with Its Coupling to an $i_{13/2}$ Particle. The odd-mass $i_{13/2}$ band in ^{194}Hg is shown broken into two bands, the favored decoupled band ($j, j+2, j+4, \dots$) and the unfavored decoupled band ($j+1, j+3, j+5, \dots$) both following the core energy spacings. The dashed levels for $27/2^+$ and $31/2^+$ are expected where they are placed, but have not been experimentally found. The connecting dashed lines indicate the core origins for the levels in the ^{193}Hg . Note that the 8^+ level in the strongly deformed ground state band has been normalized to the 8^+ level in the ^{194}Hg for convenience.

are complex and are fully presented below for both particle-vibrator coupling and particle-rotor coupling. Figure 2-3 schematically shows an example of particle-rotor coupling (for the Stephens model, see below) for comparison with the particle vibrator coupling schemes of Figure 2-1.

Vibrational Models

The main assumption made in vibrational models to describe odd-mass Hg nuclei is that the low-lying states of these transitional nuclei can be treated in terms of the coupling of two basic excitations: particles and quadrupole phonons (quanta of vibrational energy). The doubly-even Hg vibrational cores for the odd Hg-isotopes have been treated as harmonic¹⁰⁻¹⁴⁾ and as anharmonic¹⁵⁻¹⁷⁾ quadrupole vibrators.

The particle-phonon coupling picture was first applied to the odd-mass Hg isotopes by de-Shalit,¹⁰⁾ who used a simple 2^+ core excitation (single quadrupole phonon) configuration coupled to a $p_{1/2}$ particle to explain the first excited $5/2^-$, $3/2^-$ doublet in ^{199}Hg . (See Figure 2-1 for a qualitative picture of the coupling of a $p_{1/2}$ particle to a 2^+ core state.) This model was later extended to include coupling to the second 2^+ vibrational state by Kalish and Gal.¹¹⁾ These models assumed only small single-particle admixtures into the core excited states; however, substantial $p_{3/2}$ and $f_{5/2}$ particle character has been found⁴¹⁾ in all four of the first and second excited $5/2^-$ and $3/2^-$ states in $^{197-203}\text{Hg}$.

Kisslinger and Sorensen¹²⁾ calculated the properties of odd-Hg isotopes by coupling one particle to one or two harmonic quadrupole phonons, using a residual short-range pairing force* and a residual long-range quadrupole force to account for the particle-particle and particle-core interactions. Lo Iudice et al.¹³⁾ extended the formalism of Kisslinger and Sorensen, by insuring the conservation of nucleon number - a well-known problem with pairing force calculations. The results of these calculations are compared with the experimental data in Chapter V. These models using harmonic vibrators crudely reproduce the experimental results, but they are not physically realistic when applied to Hg nuclei owing to anharmonic properties clearly exhibited by the even-even core nuclei.

Mathews et al.¹⁴⁾ have applied the particle-vibration or intermediate coupling model^{5,62-64)} to levels in ¹⁹⁹Hg. In this model, up to three phonons were coupled to the odd nucleon. Variations of the coupling strength and the $f_{5/2}$ single-particle energy were tried in an attempt to fit the experimental level structure, transition rates, and electromagnetic moments of the nucleus. Mathews and Immele¹⁵⁾ have used an expanded version of this quasiparticle-phonon coupling model which is capable of diagonalizing up to third-order anharmonic effects in a basis of up to seven phonons (72 core states) coupled to six single quasiparticle levels to predict the properties of the odd-mass ¹⁹⁵⁻²⁰⁵Hg isotopes. Their model was also modified

* Particles subject to a residual short-range pairing force are referred to as quasiparticles.

to account for the effects of violations of the Pauli exclusion principle in a large phonon basis by ensuring the correct symmetrization of the wave functions. The results of these calculations are compared to the present experimental results in Chapter V.

The calculations of Fenyés et al.¹⁶⁾ and Jolos¹⁷⁾ are the most recent works dealing with the low-spin states in the neutron-deficient Hg isotopes, and have used the pairing-plus-quadrupole force model, by coupling single quasiparticles to an anharmonic vibrator. (See ref. 65 for a detailed description of this model.) Fenyés et al. and Jolos compared these calculations with a harmonic vibrator treatment for the core nuclei: those calculations essentially showed that anharmonic effects in the cores have little influence on the energies and ordering of the lowest lying states ($1/2^-$, $3/2^-$, $5/2^-$) in the odd-mass Hg nuclei, but do cause dramatic variations in the energies of higher levels. Fenyés et al.¹⁶⁾ also interpreted the odd-Hg isotopes in the framework of the cluster-phonon model,⁶³⁾ where the cluster consists of n valence shell proton or neutron particles or holes. The odd-mass Hg nuclei are described by coupling two proton holes (i.e. Hg is two protons below the $Z=82$ closed shell) and an odd neutron to the vibrational field consisting of the mixing of up to three phonon states. The model is unable to do this coupling explicitly, so the effects are approximated by treating the two proton holes as equivalent to two neutron holes thus reducing the problem to coupling a three neutron-hole cluster to the quadrupole vibration. In addition, these authors argued that the Pauli

principle is important in the neutron valence shell in these nuclei, thus it is also included in the model by the correct symmetrization of the wave functions. The results of the model calculations involving the coupling of one quasiparticle to an anharmonic vibrator and involving the coupling of three neutron-hole clusters to a three phonon vibrational field are given in Chapter V, yielding a complete level structure comparison among all the models described above as well as between each model and experiment. The cluster-phonon coupling model has been widely applied to the description of nuclei removed from closed shells by three particles or three holes, e.g. Mn, Ga, Ag, I⁶⁶⁾ and At.⁶⁷⁾ See also the review article by Paar.⁶⁸⁾

Rotational Models

Rotational models of the nucleus necessitate the description of deformed nuclear shapes. The motion of single nucleons in a deformed spheroidal nuclear field was first described by Nilsson.⁶⁹⁾ The further development of single nucleon motion in nuclear fields of various deformation shapes has used the Nilsson model as a starting point. Thus there are descriptions in the literature for single nucleon motion in deformed nuclear fields possessing quadrupole deformation (both axially symmetric⁷⁰⁾ and axially asymmetric^{71,72)}), and hexadecapole shapes.⁷⁰⁾ An essential feature of the rotational degree of freedom is that it results in Coriolis effects acting on the single-particle motion. Bohr⁴⁾ was the first to point out these effects, but Kerman⁷³⁾ was the first to apply the Coriolis force to a specific case (¹⁸³W). In 1972 Stephens and coworkers⁷⁴⁾

developed a model describing single-particle motion under the influence of the Coriolis force, the so-called rotation-alignment model (see the review article by Stephens¹⁸⁾ for a more detailed description), which gives a very simple description of the nuclear system under study and describes surprisingly well those transitional nuclei where the Coriolis effects are large.

There are unique parity high- j orbitals (j is the spin quantum number of the odd particle) within each major shell (such as the $i_{13/2}$ orbital in the $82 \leq N \leq 126$ region) which provide the best cases to observe large Coriolis effects in nuclei. The largest Coriolis effects involve the lowest values of Ω (where Ω is the projection of the nuclear spin on the nuclear symmetry axis and takes the values $1/2, 3/2, \dots, j$, for each j) for a given j in the Nilsson model scheme. These unique parity high- j orbitals are well separated from others of the same parity, and thus their properties are not greatly affected by the small admixtures of other j values; hence, j is treated as being approximately pure and remains a good quantum number for these cases.

Transitional nuclei, in addition to having large Coriolis effects, also tend to be poor rigid rotors (see Figure 2-3 to compare the even-even rigid rotor prediction with that of an even-even Hg transitional nucleus). The single-particle motion in these weakly-deformed nuclei causes centrifugal-stretching effects in the core. The deviations from the rigid rotator picture caused by these effects are a measure of the "softness" of the rotating nucleus and have

most successfully been treated by using the "variable-moment-of-inertia" formalism of Mariscotti et al.⁶¹⁾ This model treats each level as having a different moment of inertia, \mathcal{I} , caused by the increasing centrifugal stretching effects (hence larger \mathcal{I}) as the angular momentum, I , increases.

The Rotation-Alignment Model

The rotation-alignment model¹⁸⁾ for odd-mass nuclei describes the coupling of a particle of spin j to a rotating deformed core with axial symmetry. When a particle is coupled to a rotating core, the particle tends to align its spin axis with that of the core rotation axis, thus tending to decouple it from its alignment in the non-rotating deformed field. This is a manifestation of the Coriolis force in nuclei, the effect of which can be approximated by the expression

$$E_{\text{Cor}}(\text{max}) = 2(\hbar^2/2\mathcal{I})Ij. \quad (2-2)$$

Thus, Coriolis effects increase with increasing I , increasing j , and decreasing \mathcal{I} . The transitional odd-mass Hg isotopes have reasonably small deformation parameters, $\beta \approx 0.15$, leading to small values of \mathcal{I} and hence large values of $\hbar^2/2\mathcal{I}$. The $p_{1/2}$, $p_{3/2}$, and $f_{5/2}$ states mix considerably with each other since they have the same parity (and similar j values) and thus cannot be described by this simple model. The $i_{13/2}$ orbital is the only positive parity orbital in this shell, and is thus well described by the

rotation-alignment model. Figure 2-3 shows one example of how the Coriolis force affects the coupling of the odd particle to an even-Hg core. The $i_{13/2}$ particle is expected to decouple from the core and give rise to the lowest-lying (favored) band having spins $j, j+2, j+4, \dots$, essentially following the energy spacings of the even-even core (as Figure 2-3 illustrates). The unfavored band $j+1, j+3, j+5, \dots$, is also expected to behave like a normal rotational band (following the core spacings) with its energy placement relative to the favored band depending on the magnitude of the Coriolis effect (see Figure 2-3). However, although the rotation alignment model physically explains the spin sequences in transitional nuclei, the calculated energy spacings are found to be more regular than the experimental data indicate. This irregularity in energy spacings can be explained by the presence of shape (γ^*) asymmetry found in transitional nuclei.^{8,9,19)} The asymmetric shapes introduce mixing between states within a pure- j band, moving the favored and unfavored band energy spacings into the irregular patterns found experimentally.

The Triaxial Rotor Model

Meyer ter Vehn^{8,9)} has extended the rotation-alignment model to account for shape asymmetry. His calculations are based on a unique parity, high- j nucleon coupled to an asymmetric rotor as

*The parameter γ denotes the axial asymmetry of a nucleus, and is measured in degrees. Prolate triaxial nuclei have $0^\circ < \gamma < 30^\circ$, while oblate triaxial nuclei have $30^\circ < \gamma < 60^\circ$ with 0° representing an axially-symmetric prolate nucleus and 60° an axially-symmetric oblate nucleus.

developed by Davydov^{58,59)} with the inclusion of Coriolis effects and show that there is a continuous transition from decoupled to strongly coupled bands obtained by changing the shape of the nucleus from prolate to oblate through a (continuous) series of asymmetric shapes specified as the parameter γ varies over $0-60^\circ$. Many states of the model change rapidly in the region of asymmetry $20^\circ < \gamma < 40^\circ$, giving a complex pattern of levels that provide a sensitive test of the model. This, the "triaxial rotor" model, not only gives better energy predictions for the levels in the favored ($j, j+2, j+4, \dots$) and unfavored ($j+1, j+3, j+5, \dots$) yrast bands, but also gives correct predictions for the energies and spin-sequences of the non-yrast states found in the pure- j systems. This is basically because the γ -dependence enters not only through the rotational Hamiltonian as in the even-even nuclei, but also through the Hamiltonian of the single particle, which allows a differentiation between prolate and oblate shapes depending on the value of γ . These non-yrast states, which are populated in β -decay studies such as described here, allow a simple physical interpretation of the system under study, as is pointed out e.g. by Wood et al.⁷⁵⁾ for ^{189}Au .

This model is not entirely satisfactory, however, in the sense that, although the ordering of the levels is reproduced, the energies of the high-spin levels especially are always predicted to be higher than the experimental values. This can be explained by invoking a softness for the core related to centrifugal stretching.

Because of this softness, the rigid rotor approximation, assumed by the triaxial rotor model, does not give a satisfactory reproduction of the level energies. Therefore, Toki and Faessler¹⁹⁾ included core softness by allowing the triaxial core states to have variable moments of inertia (VMI). This VMI formalism, when incorporated into the triaxial rotor model, gives excellent results in comparison with experimental data for pure-j bands. The results of the calculations of this model and the model of Meyer ter Vehn for the pure-j $i_{13/2}$ band in the odd-mass Hg isotopes are given in Chapter V.

Future Model Developments for Transitional Nuclei

None of the above-mentioned models provide a complete description of the nuclei found in the transitional region. However, since the triaxial-rotor-plus-VMI model does so well in explaining the pure high-j systems in this region, a logical extension of this model would be to incorporate j-mixing in order to describe the low-j states. Faessler and Toki⁷⁶⁾ have studied the mixing of two j orbitals in their treatment of ¹⁸⁷Ir, with encouraging results. The complex formalism for mixing three or more j orbitals would allow a description of transitional nuclei in terms of rotational motion alone.

Another approach has been suggested by Yamazaki and Sheline.⁷⁷⁾ They have used the formalism of the Faessler-Greiner microscopic model (e.g. ref. 78) in an explanation of the low-spin level structure in ¹⁹⁵Pt (a transitional nucleus isotonic to ¹⁹⁷Hg). They have

assumed that ^{195}Pt is an extremely γ -soft nucleus, approaching γ -instability, and cannot be well explained in terms of the Nilsson model. Their calculation takes into account the Coriolis, rotation-vibration, and particle-vibration couplings, including the five odd-parity Nilsson orbitals and seven even-parity orbitals near the Fermi surface. The results of using an extension of this type of formalism in future interpretations of the low-spin structure in the odd-Hg isotope could possibly prove useful.

A more physically reasonable interpretation of these transitional nuclei might be given by a mixture of vibrational and rotational degrees of freedom. This kind of formalism is suggested by Arima and Iachello^{79,80)} in their Interacting Boson Model. These bosons are the vibrational quanta of the quadrupole oscillator described earlier. By coupling the odd nucleon to their boson model representation of the even-even core in the manner of Bohr and Mottleson,⁵⁾ Arima and Iachello are in the process of developing a model that can be used possibly to describe the complex odd-mass transitional nuclei in general, and the odd-Hg isotopes in particular, in a relatively simple physical manner. It will be interesting to compare the forthcoming model calculations with the experimental results given here. In this respect, these experiments serve as an extensive future test for theoretical interpretations in this region.

CHAPTER III

THE UNISOR FACILITY - EXPERIMENTAL SYSTEMS

The experimental measurements were carried out at the UNISOR (UNiversity Isotope Separator - Oak Ridge) facility, an isotope separator installed on-line to the Oak Ridge Isochronous Cyclotron (ORIC) located at the Oak Ridge National Laboratory (ORNL). UNISOR is a consortium of 14 institutions [public and private universities, Oak Ridge Associated Universities, (ORAU), and ORNL] formed primarily for the study of nuclei far from stability.⁸¹⁾ ORIC is a 76-inch, variable-energy azimuthally-varying field (AVF) cyclotron⁸²⁾ which provides moderately intense heavy-ion beams necessary for this research. The UNISOR facility and its location relative to ORIC are shown in Figure 3-1.

The UNISOR isotope separator has a 90° homogeneous-field, 150 cm radius-of-curvature sector magnet which gives a dispersion of 0.6 cm for mass 250, a mass resolution $m/\Delta m \geq 2000$ for ion currents up to 50 μA , and a mass range at the focal plane of the collector of $\pm 7.5\%$ of the primary mass selected for study. The operation of the isotope separator on-line to ORIC involves continuous bombardment by the ORIC beam of targets mounted in the UNISOR ion source and continuous extraction of product nuclei into the isotope separator.

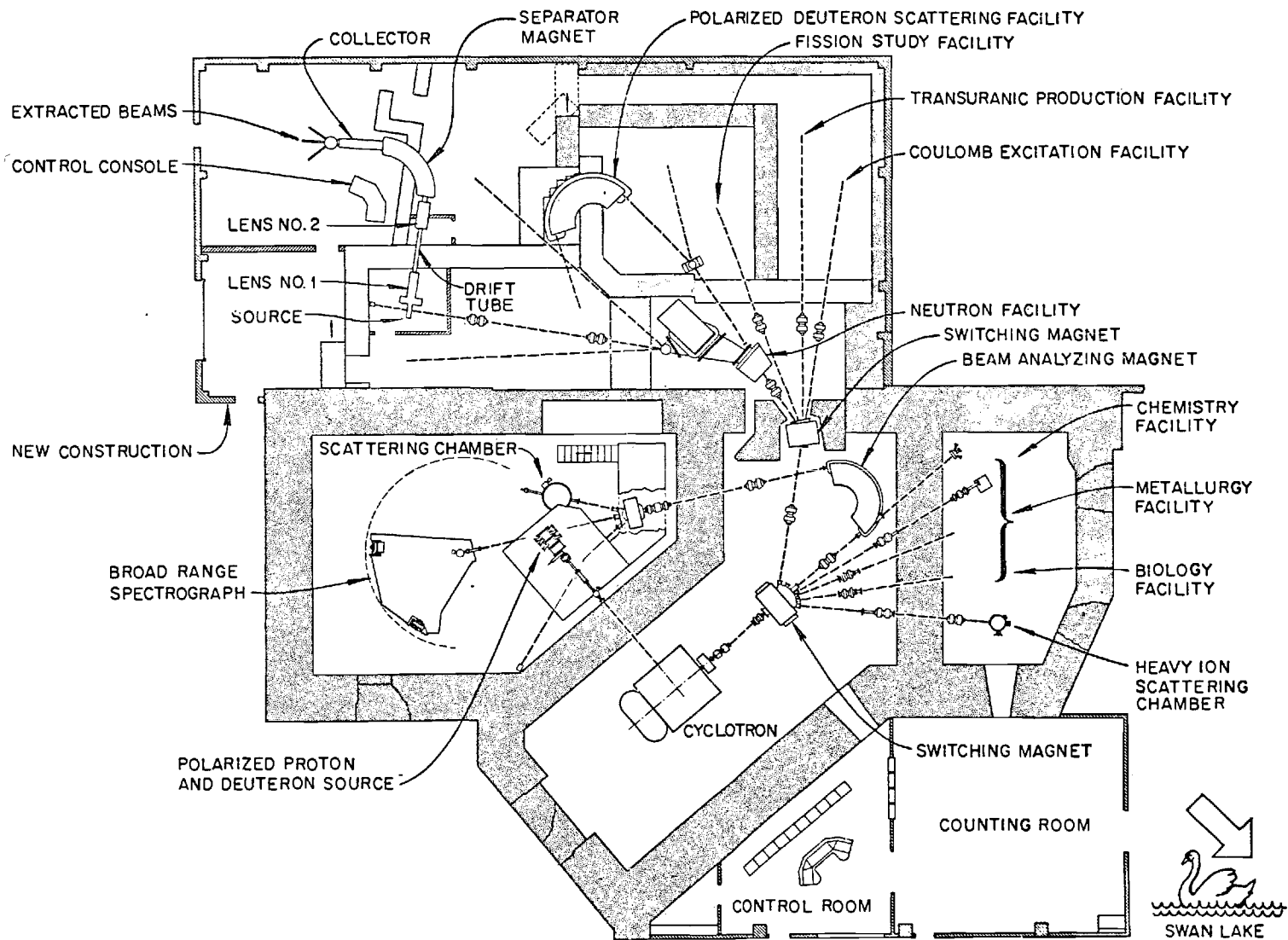


Figure 3-1. The UNISOR Facility and Its Location Relative to ORIC.

Nuclide Production

The heavy-ion beam from ORIC (see Figure 3-1) enters the UNISOR ion source and strikes the selected target. The reaction products recoil out of the target and are collected on a catcher foil which is also thick enough to stop the heavy-ion beam. The heating of the catcher foil by the beam and by the filament of the ion source causes the products to diffuse thermally into the plasma region of the ion source where they are ionized and removed through an extraction electrode (see Figures 3-2 and 3-3). The products are extracted primarily as singly-charged ions and accelerated to approximately 50 kV. They then travel through a drift tube to the magnet where mass dispersion takes place.

Source Preparation

Several target-ion combinations were used to prepare the $^{189-197}\text{Tl}$ activities under study. These odd-mass Tl isotopes were produced by bombarding ^{181}Ta , natural W, or natural Re foils with $^{16}\text{O}^{5+}$ ions using energies ranging from 104 to 146 MeV. A 97% enriched target of ^{186}W bombarded by 131 MeV $^{14}\text{N}^{5+}$ ions from ORIC was also employed in one experiment to produce ^{193}Tl sources. The reactions involved were (a) $^{181}\text{Ta}(^{16}\text{O}, \text{xn})^{189,191}\text{Tl}$; (b) natural W($^{16}\text{O}, \text{xn}$) $^{191,193,195,197}\text{Tl}$ and natural W($^{16}\text{O}, \text{pxn}$) $^{191,193,195,197}\text{Tl}$; (c) natural Re($^{16}\text{O}, \text{pxn}$) $^{193,195,197}\text{Pb}$ followed by β^+ /EC-decay to $^{193,195,197}\text{Tl}$, and natural Re($^{16}\text{O}, \alpha\text{xn}$ or 2pxn) $^{193,195,197}\text{Tl}$; and (d) $^{186}\text{W}(^{14}\text{N}, 7\text{n})^{193}\text{Tl}$. The targets varied in thickness and composition: the ^{181}Ta targets were each 2 mg/cm^2 , the natural W targets ranged from 2.0

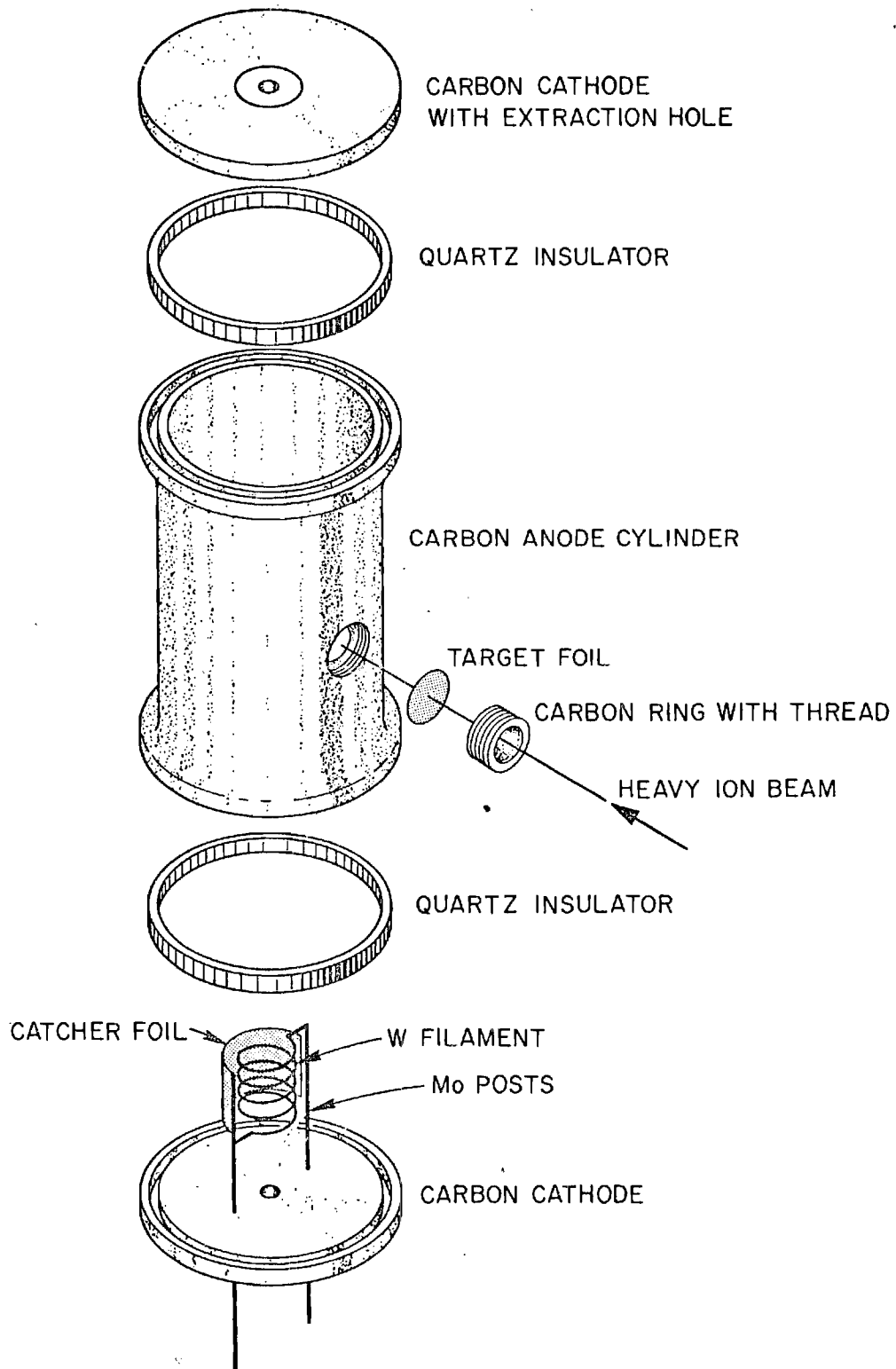


Figure 3-2. Original UNISOR On-Line Ion Source.

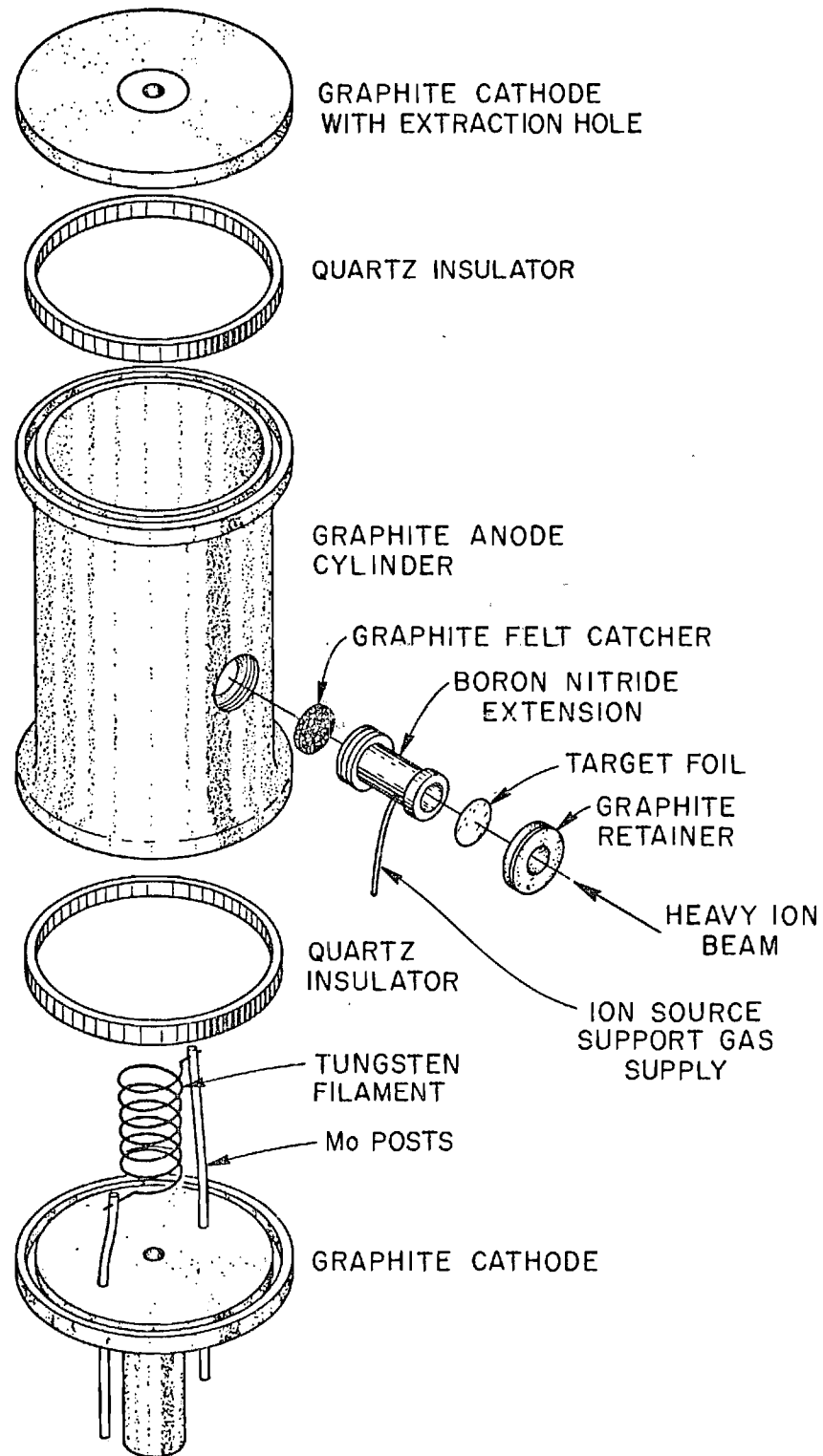


Figure 3-3. Modified UNISOR Ion Source Using a Graphite Felt Catcher.

to 2.3 mg/cm^2 , the ^{186}W target was 4.5 mg/cm^2 , and the natural Re targets ranged from 3.1 to 5.8 mg/cm^2 with 2.2 to 3.0 mg/cm^2 Ta or 2.3 mg/cm^2 Mo/Re alloy backings. All of the Ta and W targets were self-supporting with the exception of the ^{186}W which was mounted directly on the graphite felt described below.

The appropriate energies to maximize the production of the desired nuclides were determined by cross-section calculations using the ALICE^{83,84)} computer code. For a given experiment the production of the primary mass (i.e., the isotope which is separated and counted on-line) was the one for which the projectile energy was optimized for maximum yield. Thus, experiments involving collection of side masses do not always exhibit maximum yields, since the energies are not optimized for these mass numbers. Typically for this region of nuclides, one observes adequate yields for as many as four masses heavier and two masses lighter than the primary on-line mass number for which the bombardment energy is optimized.

Ion Sources

Two UNISOR ion source designs⁸⁵⁾ of the Nielsen oscillating-electron type⁸⁶⁾ have been used in these experiments. This type of ion source is simple, durable, and provides beams over a wide range of elements with reasonable efficiencies. The on-line separation efficiencies for the Tl isotopes are approximately 2-5%.⁸⁵⁾ The initial UNISOR target-ion source configuration is shown in Figure 3-2. Experiments which were performed using this ion source involved the self-supporting targets of ^{181}Ta with a catcher foil about 0.1 mm

in thickness. These targets showed great durability when bombarded with ≤ 10 MeV/amu $^{16}\text{O}^{5+}$ ions at beam currents of up to 0.4 particle- μA .

A problem arose with this initial ion source configuration. During the course of several experiments, a decrease in the output of the desired Tl isotope took place; and in the case of the heavier Tl isotopes ($A \geq 191$), a Pb contaminant appeared. This is attributed to a buildup of tungsten from the ion source filament, due to evaporation or sputtering, onto the back of the Ta target foil. A new design for the UNISOR ion source was developed in order to overcome this problem. The new ion source design⁸⁵⁾ is shown in Figure 3-3. This was employed in the majority of the experiments reported here. The design incorporated a piece of graphite felt 3 mm thick (about 30 mg/cm^2 with individual fiber diameters of 2-5 microns) placed between the tungsten filament (plasma region) and the target. The graphite felt in this position acts as a collector for the tungsten evaporated from the filament, as well as a catcher of the reaction products and a stop for the heavy-ion beam. The felt allows the reaction products to enter the ion source plasma by diffusion from the fibers. Experiments using this ion source involved the self-supporting targets of ^{181}Ta , natural W, and enriched ^{186}W , and targets of natural Re on a Ta or Mo/Re alloy backing. These targets also had great durability when bombarded with ≤ 10 MeV/amu $^{16}\text{O}^{5+}$ of ≤ 14 MeV/amu $^{14}\text{N}^{5+}$ ions at beam currents of about 0.4 particle- μA .

General Features for Data Acquisition

After passing through the 90° sector magnet for mass separation, the reaction products enter the collection chamber. The products of the primary mass number are focussed through a collimator in the collection chamber and pass through a three-meter drift tube to a tape transport system⁸³⁾ (see Figure 3-4) where they are deposited on a movable aluminum-coated Mylar tape for transport to the experimental stations. This arrangement for measuring the radiations of the primary mass is termed an "on-line" experiment. Other product masses near the primary mass were collected in, and periodically removed from the collection chamber for radiation measurements on several experimental arrangements peripheral to the tape transport system. These studies are termed "off-line" experiments.

Standard techniques of conversion electron, γ - and x-ray spectroscopy employing semiconductor detectors were used. Singles spectra for conversion electrons, γ -rays and x-rays were obtained in a multiscaling mode. Three-parameter coincidence information was listed event by event on magnetic tape for e- γ -t, γ - γ -t, and γ -x-t.

Detector Systems

A variety of Ge(Li) γ -ray detectors were used (nine in all) in the various singles and coincidence experiments. These were all large-volume (63 cm³ to 108 cm³) ORTEC Ge(Li) detectors having efficiencies of 10 - 24% at 1332 keV compared to a 3" x 3" NaI(Tl) detector). All detectors had similar specifications which typically

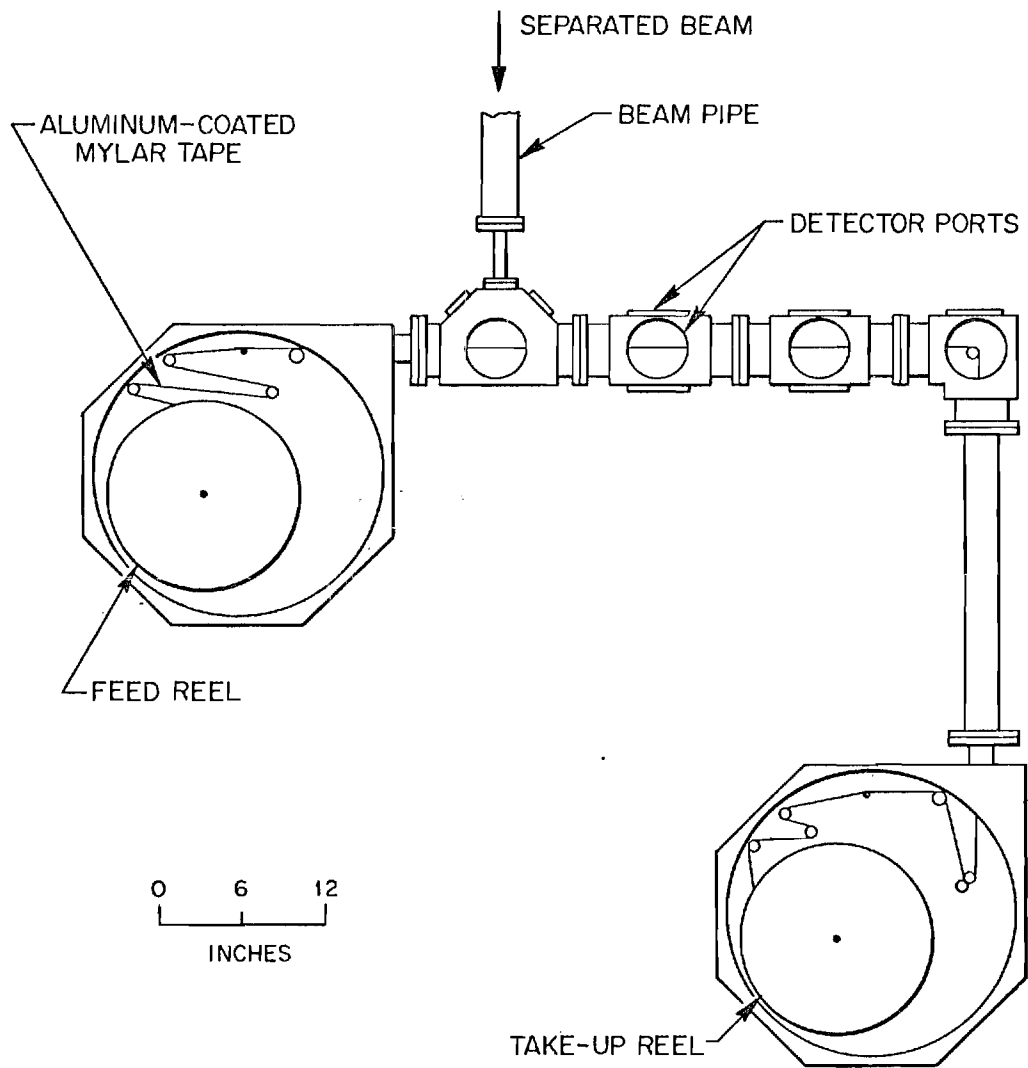


Figure 3-4. The UNISOR Tape Transport System.

were 2.1 keV full-width at half-maximum (FWHM) at 1332 keV, a peak-to-Compton ratio of 45/1, and window-to-detector distance of 5.0 mm. Source-to-detector distances ranged from ~ 1 cm to ~ 2 cm for on-line counting (with a thin Mylar window used for low energy photon measurements) and from ~ 1 cm to ~ 3 cm for off-line counting. Two absorbers, a 10 mil Cd + 5 mil Cu absorber, and a layered absorber consisting of 5 mils each of Cu, Sn, and Ta and 25 mils of Pb, were used in various experiments to cut down or eliminate summing effects, chiefly due to the K x-rays. Varying the source-to-detector distance also helped to identify sum peaks in the spectra. In addition, a specially designed 1.5 cm thick lead shield, lined with 1 mm thick Cd and 0.25 mm Cu on each side and with a 2 cm diameter hole through the middle, was used to minimize Compton back-scattering in off-line γ - γ -t experiments, which were conducted in a 180° detector geometry. This source holder insured reproducible geometry.

Conversion electron spectra were taken using Si(Li) electron detectors. On-line spectra of ^{191}Tl were taken with a Si(Li) electron spectrometer having a ruggedized surface 200 mm^2 in area and a 2 mm depletion depth. This system has a 2.5 keV FWHM and 4.6 keV full-width at one-tenth maximum (FWTM) resolution at the 218 keV electron line from ^{192}Ir . In addition, on-line conversion electron spectra of ^{189}Tl and some spectra of $^{191,193\text{m}}\text{Tl}$ were taken with a different Si(Li) electron spectrometer having specifications similar to those given above. This system gave a FWHM of about 5.5 for K conversion electrons in our spectra and thus was quickly retired in favor of

the above mentioned detector. The source-to-detector distances for both systems ranged from ~ 0.5 cm to ~ 1 cm. The on-line systems were run at the tape transport system's vacuum of 5×10^{-6} to 10^{-5} Torr and were seen to lose some resolution during the course of an experiment. This was most likely caused by trapped gases in the tape feed and take-up reels which caused condensates to form on the detector surface. The on-line detector systems were "recycled" at times during the course of an experiment by warming the systems to room temperature and cooling them down again.

Most of the conversion electron spectra for ^{193}Tl and all for $^{195,197}\text{Tl}$ were taken off-line with a Si(Li) electron spectrometer having an 80 mm^2 active area and 3 mm depletion depth. This detector has 2.2 keV FWHM resolution for 976 keV electron (^{207}Bi). The source-to-detector distance for these experiments was fixed at 1.14 cm. (Note that the source-to- γ -detector distance was fixed at 1.63 cm in the e- γ coincidence system. A special cuplike indentation in the vacuum chamber of the electron spectrometer system allowed the γ -ray Ge(Li) detector to be positioned this close to the source.) The off-line system consisted of a cryostat vacuum chamber, the cooled Si(Li) detector, a cooled preamplifier, and an air lock which allowed the sources to be inserted relatively quickly (~ 2 minutes). This conversion electron system was kept at better than 10^{-6} Torr of vacuum using a small liquid nitrogen cryosorption pump and the pressure was found to increase only slightly during an experiment. The off-line detector was recycled in the same manner as the on-line detector.

Experimental Procedure

The tape transport system used for on-line experiments is shown schematically in Figure 3-4. The system is modular in design so that a wide variety of detector arrangements can be mounted. The system is described in detail in reference 87.

The desired mass-separated product was accumulated at the collection station for a preset length of time (typically 1-4 half-lives of the isotope of interest). The tape was then moved to the desired detector station (typically one of the two intermediate stations in Figure 3-4). A variety of detector systems (detailed above) were available for observation of the resulting radiation. The Ge(Li) detectors used could be positioned as close as 9 mm from the tape through the use of aluminum cups mounted in the detector ports. Photon energies down to approximately 30 keV were observed with these Ge(Li) detectors so that low-energy photon and x-ray data could also be obtained. For low-energy photon measurements, cups with Mylar windows were used. The Si(Li) electron detector was mounted in the chosen station as close to the activity on the tape as desired with a special fitting allowing the detector and its cooled FET preamplifier to be placed in the vacuum of the tape transport. This system allowed a windowless counting arrangement to be used that minimized degradation of the energy resolution for conversion electrons.

A vacuum of 5×10^{-6} to 10^{-5} Torr was maintained in the tape transport through the use of a 450 l/sec diffusion pump mounted

nearby on the beam line and a turbo-molecular pump mounted near to the detector ports. In addition, a cold trap positioned between the diffusion pump and the tape transport was used to reduce contaminants and help maintain vacuum in the system.

The signals from the detectors were shaped and amplified using standard NIM module electronics and were fed into a Tennecomp TP-5000 system which is the primary UNISOR data acquisition system.⁸⁷⁾ This system consists of a PDP-11 computer interfaced to a Tennelec PACE analog-to-digital converter (ADC) with the following peripheral equipment: two magnetic tape drives, a 1.2 million-word disk, a fast line printer, and a light pen - oscilloscope display. A typical experiment, requiring singles data accumulated in a spectrum-multiscaling mode (e.g. 20 time-planes of several seconds per plane, each plane being 8192-channels in length) and a simultaneous set of three parameter coincidence data, could easily be handled by this system. Computer software programs in the TP-5000 control the singles multiscaling and coincidence data operations, allowing for a variety of options. An example of a typical experiment is illustrated by ^{191}Tl ($T_{1/2} = 5.5$ min). In this case the sources from the $W(^{16}\text{O}, xn)$ ^{191}Tl reaction with 142.9 MeV $^{16}\text{O}^{5+}$ ions were collected for only five minutes each (in order to minimize production of the ^{191}Hg daughter) and spectrally-multiscaled in twelve 8192-channel time planes of 23.5 seconds collection per plane with 1.5 seconds between planes, with each plane in turn being collected in the computer core and then transferred to storage on disk. Simultaneously list data were

assembled as data words in temporary buffer storage from which they were transferred directly onto magnetic tape where they were stored as three successive 16 bit words, each having 13 bit resolution (8192 channels). A typical coincidence resolving time for these measurements was about 10 nsec FWHM, resulting in a true-to-chance coincidence ratio of $\geq 20:1$. A schematic diagram of the Tennecomp TP-5000 data-acquisition system is shown in Figure 3-5.

The separated reaction products accumulated in the collection chamber of the isotope separator were studied off-line. Two methods of collection were used for these off-line measurements. The first method involved the use of a removeable plate having collector foils located at the focal points for the various masses. The primary mass for on-line study was allowed to pass through a hole in the collection plate and proceed to the tape transport system. Periodically the collection plate was removed from the collection box through a vacuum lock and the desired foil removed for counting. Several problems made this approach unsuitable. More than 60 sec are required to remove and replace the collection plate through the air lock. Also, all of the off-line samples have to be removed simultaneously which interrupts other experiments. Therefore, this approach is used only for long-lived activities ($T_{1/2} \sim$ several hours) and when more than two off-line experiments are being run simultaneously.

A second, and more successful, technique for collection of off-line products involved the use of a simple tape vacuum seal,⁸⁸⁾ the principle of which is shown schematically in Figure 3-6. This

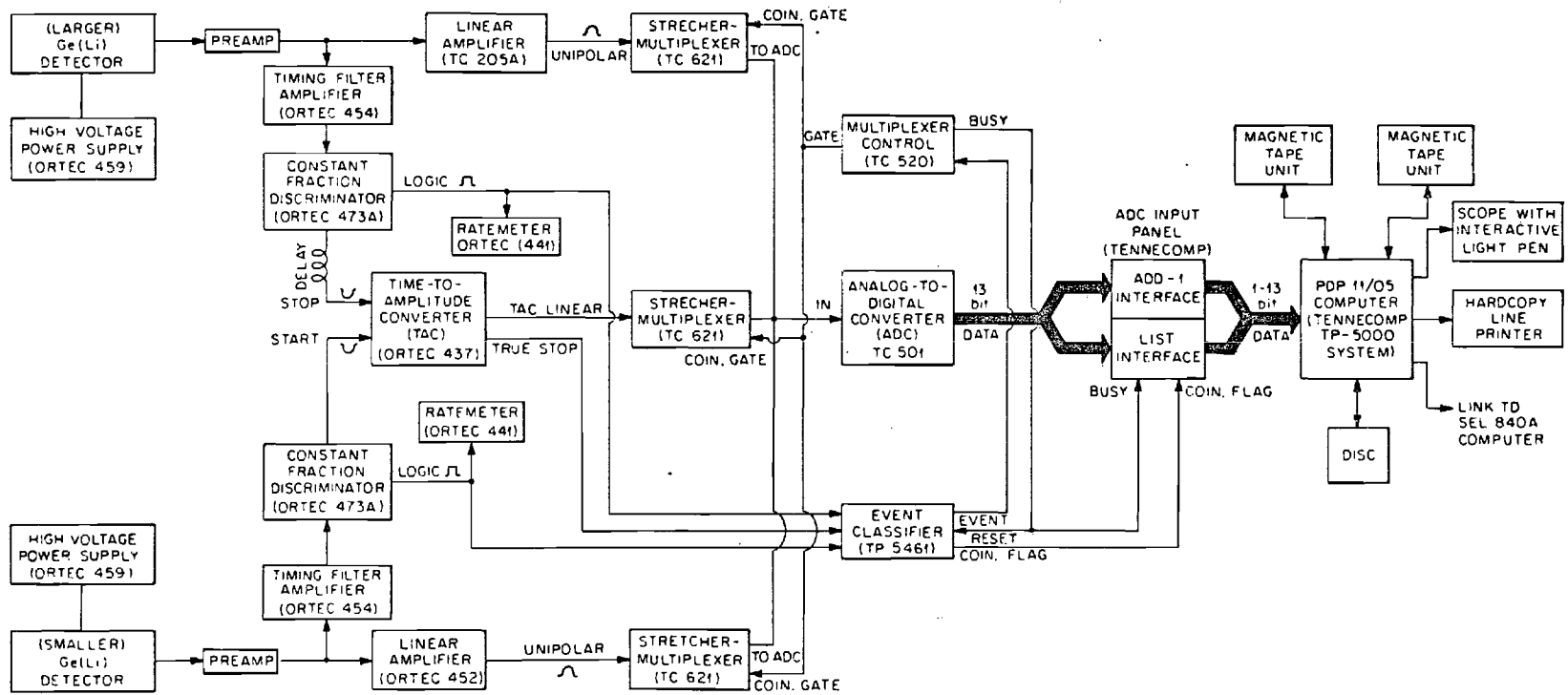


Figure 3-5. Schematic Diagram of the Electronics for a Typical γ - γ -t Experiment on the Tennencomp TP-5000 System.

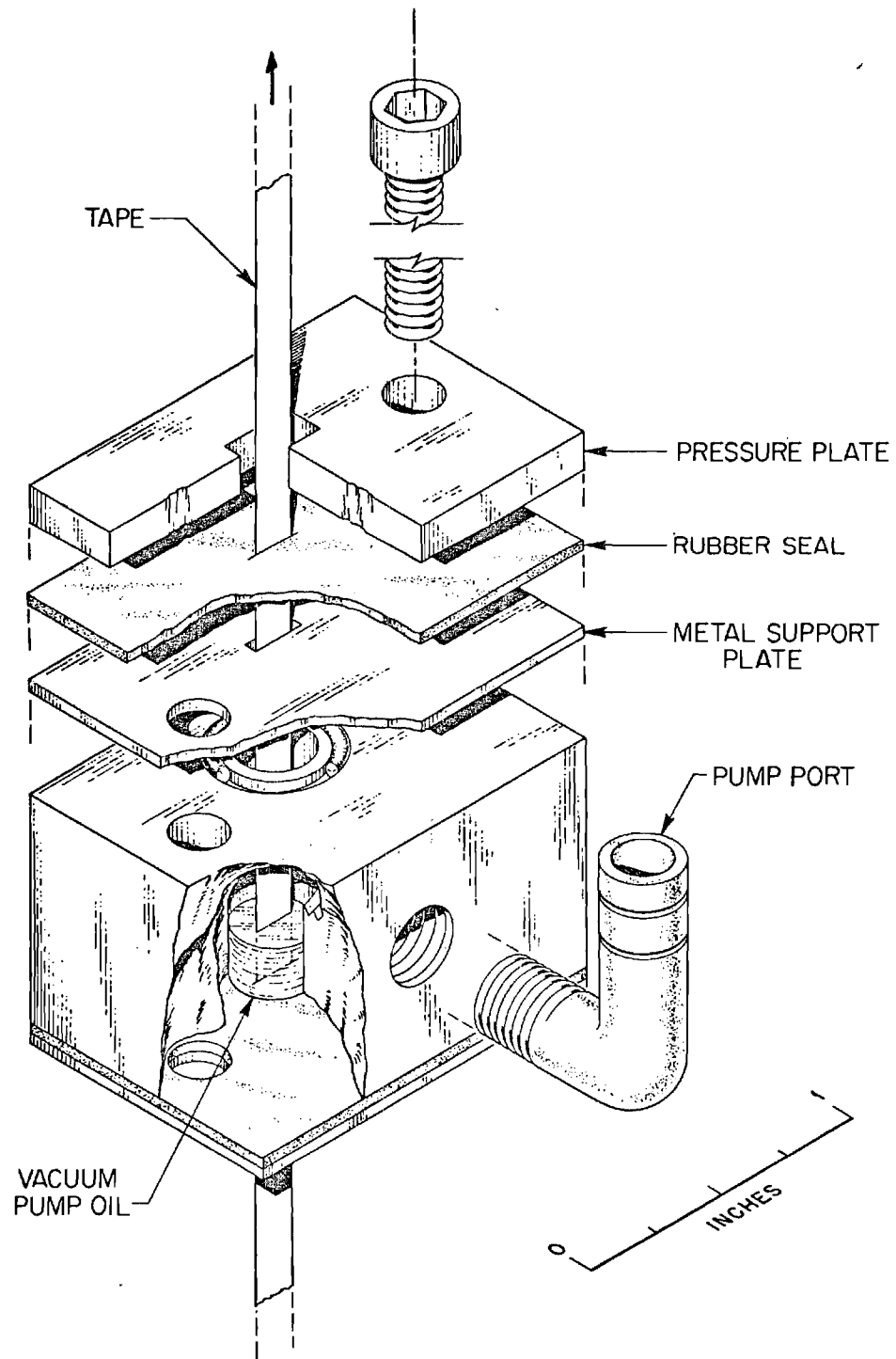


Figure 3-6. Exploded View of the Tape Vacuum Seal.

vacuum seal allows an aluminum-coated Mylar tape, located at a selected mass point in the focal plane, to be pulled directly from vacuum to atmospheric pressure with no appreciable loss of vacuum or activity. The configuration in which this tape seal was used is pictured in Figure 3-7. This vacuum seal-tape puller system is described in reference 88.

Products of the desired mass number were accumulated in the collection chamber and after an appropriate collection time, the separated source was pulled out of the collection chamber, in some cases chemically separated, mounted on an appropriate source holder, and placed in front of the detectors for counting.

These off-line sources were studied in a variety of detector arrangements for γ -ray, x-ray and conversion electron singles spectrum multiscaling and γ - γ -t, γ -x-t, and e- γ -t coincidence measurements. The data were stored and processed by the three additional computer-based systems (apart from the primary UNISOR system). A second Tennecomp TP-5000 system, essentially identical to the UNISOR system, and the SEL-840A interfaced to a Tennelec PACE ADC and a Canberra multichannel analyzer have been used to collect spectral multiscaling and list data for a variety of off-line experiments. The coincidence system using the ORIC SEL-840A computer was very similar to that shown in Figure 3-5 for the Tennecomp TP-5000 and is described in detail in reference 89. Similar to the TP-5000 machine, list data on the SEL was stored in files with essentially 13-bit resolution for the two events and time (each using 9500 channels). The resolving time

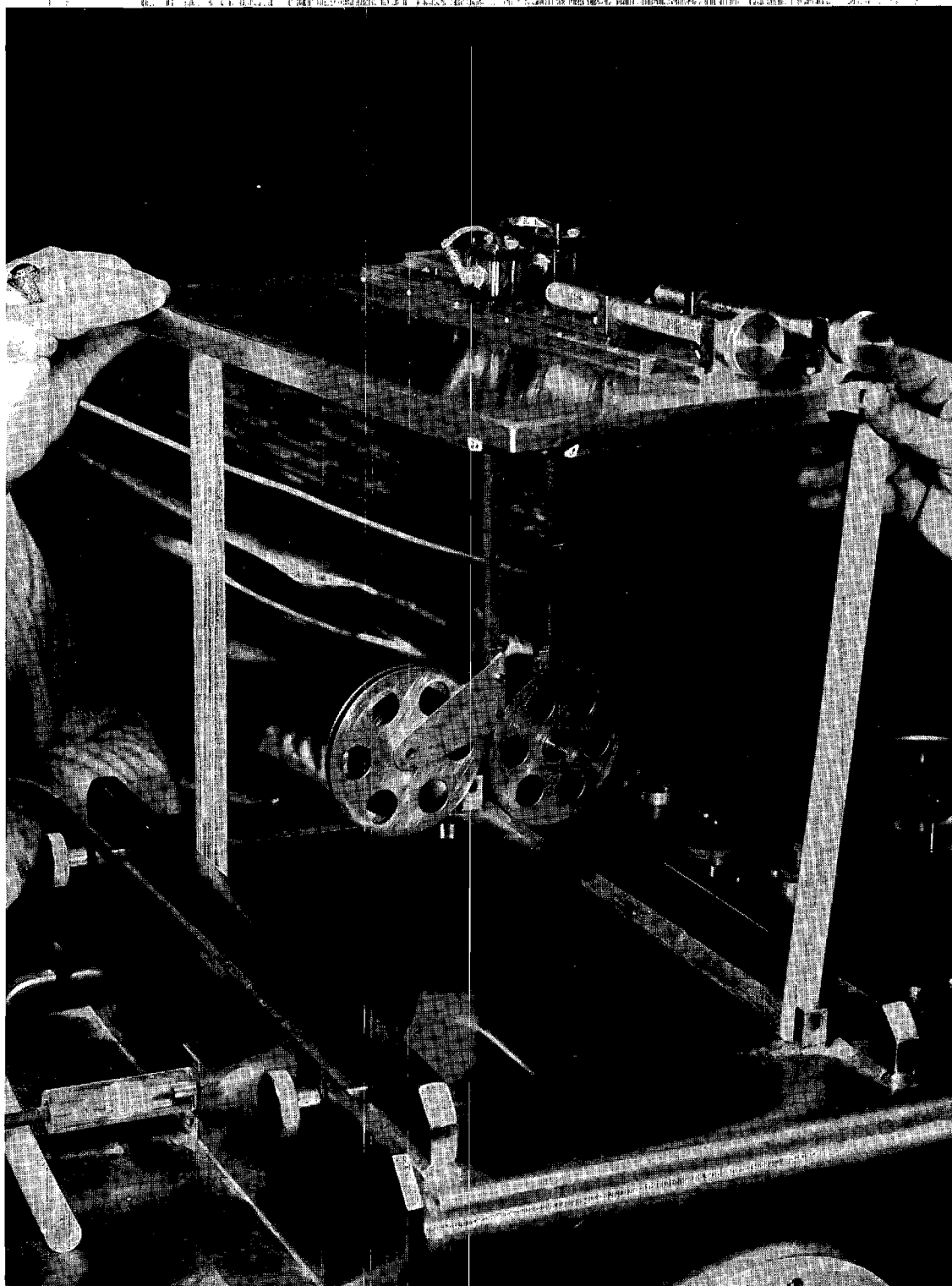


Figure 3-7. Photograph of the Tape-Puller System.

was again about 10 nsec and the true-to-chance coincidence ratio \geq 20:1. In addition, a computer-based Tracor Northern TN-1700 multi-channel analyzer system was used to collect spectrum multiscaling data for other off-line experiments. Thus, in addition to the primary on-line study of a single mass number, up to three off-line experiments have been performed concurrently, by a variety of experimenters, on side masses. Counting procedures were essentially the same as for on-line experiments, with the exceptions noted above. (All electron data were taken on the Tennecomp TP-5000 system.)

Calibration and Data Analysis

Calibration data were recorded both before and after each experiment. A variety of γ -ray energy standards was used including ^{56}Co , ^{60}Co , ^{137}Cs , ^{154}Eu , ^{182}Ta , ^{192}Ir , ^{207}Bi , ^{226}Ra , ^{228}Th , and a National Bureau of Standards (NBS) mixed source containing ^{109}Cd , ^{57}Co , ^{139}Ce , ^{203}Hg , ^{113}Sn , ^{85}Sr , ^{137}Cs , ^{88}Y , and ^{60}Co . In addition, contaminating activities from other nuclides of the same mass (basically Pb and Hg) and to some extent neighboring isotopes (one mass on either side of the separated mass) which could be identified by half-life were used as internal energy calibrations. Naturally occurring ^{40}K , ^{238}U - and ^{232}Th -decay chain γ -rays appeared in all spectra and were also used as internal energy calibrations. Energies for the Tl γ -rays were determined using the precise energy values of Greenwood et al.,^{90,91)} White et al.,⁹²⁾ and others⁹³⁻⁹⁷⁾ and employing the non-linearity mapping method developed by Black and Heath.⁹⁸⁻¹⁰⁰⁾

Gamma-ray intensities were determined relative to lines in the NBS mixed source and ^{56}Co , ^{137}Cs , ^{154}Eu , ^{182}Ta , ^{192}Ir , and ^{226}Ra sources. Spectral peak analysis was performed using the SAMPO^{101,102)} code on the IBM-360/91 computer at ORNL and the CDC-Cyber-70 computer at Georgia Tech. The precise intensity calibration values of Jardine,⁹⁵⁾ Wallace and Coote,¹⁰³⁾ and others^{96,97,104-106)} were used for the above standards.

As in the γ -ray work, electron calibration data were recorded before and after each experiment with thin sources of ^{137}Cs , ^{182}Ta , and ^{192}Ir . The precise intensity values used for these standard sources were taken from references 96, 97 and 107. Accurate conversion coefficient values for these standards^{96,97,107,108)} were used, in order to obtain efficiency curves from which electron intensities could be derived. Electron transitions (especially pure E2 and M1 transitions) from contaminating species (usually the Hg daughter or a neighboring Tl isotope) were then used to check the normalization between gamma and electron efficiencies. The information obtained from the total summed conversion electron and γ -ray singles data with efficiency corrections taken into account then allowed the final conversion coefficients (and subsequently transition multipolarities) for the Tl isotopes to be determined.

Coincidence information was obtained when the list data stored on tape by one of the Tennecomp TP-5000 systems was sorted onto the disk of the PDP-11 computer using available utility software. Interfaces between the TP-5000 systems and the larger SEL-840A computers

allow transmission of data from the core of the PDP-11 to a disk of the SEL (see Figure 4-7). This feature then allowed the sorted spectra to be transferred to a disk on one of the SEL-840A computers from which they could be printed or plotted on the fast line printer for final hand analysis. Coincidence data files produced on the SEL system were sorted using a special utility program TS01¹⁰⁹) developed specifically for extremely fast analysis of this particular type of list data.

Chemical Separations

Isotopically-separated sources of masses 193, 195, and 197 were radiochemically separated, in order to provide pure samples of ^{193}Tl , ^{195}Tl , and ^{197}Tl for decay studies. The heavy-ion reactions in which these isotopes were made, and the resulting decay during collection, lead to the formation of mixtures of Pb, Tl, and Hg isotopes. Thus, a chemical procedure was devised to remove the Pb and Hg contaminations from the Tl activities in the mass-separated sources.

The mass-separated products were collected for an appropriate time to maximize the activity of the Tl isotopes relative to other members of the mass chain. The source on the aluminum-coated Mylar tape was then removed from the collection chamber, and the aluminum coating containing the embedded recoil products was dissolved in a 3 ml solution of hot 1N NaOH contained in a 50 ml beaker. Then 0.5 ml portions of Pb, Tl, and Hg carriers were added in the form of $0.2\text{N Pb}(\text{NO}_3)_2$, $0.2\text{N Tl}(\text{NO}_3)_3$, and $0.2\text{N Hg}(\text{NO}_3)_2$, respectively.

The hot solution was then cooled in an ice or cold water bath to room temperature, acidified with concentrated HNO_3 (about 0.3 ml) and transferred to a 15 ml centrifuge tube. Next 3-5 ml of a 50% ethanol solution was added [to help prevent Tl-Pb from complexing as $\text{Tl}_2\text{Pb}(\text{SO}_4)_2$] and was followed by addition of 1-2 ml 1N H_2SO_4 . The solution was centrifuged and decanted, and the PbSO_4 precipitate was discarded after washing it with 1 ml of Tl carrier solution. About 3-5 ml of 1M KI was added to the decantate. This precipitates both the Tl and Hg. Additional KI (approximately 2 ml) was added until the solution turned from an orange-yellow color to bright yellow. The Hg complexes went back into solution as K_2HgI_4 , while the Tl remained precipitated as TlI. The solution was then centrifuged, filtered, and washed with excess KI, Hg carrier, and distilled water. Finally, the filter paper containing the separated source was enclosed in a small polyethylene bag and mounted in front of the detector for radiation measurements.

CHAPTER IV

EXPERIMENTAL MEASUREMENTS, EVALUATION OF DATA, AND EXPERIMENTAL RESULTS

Experimental measurements on the decay properties of the odd-mass Tl isotopes ($A = 189-197$) to levels in Hg have been carried out at the UNISOR facility as outlined in Chapter III. Gamma-ray, x-ray and conversion electron singles and singles multiscaling measurements, and γ - γ -t, γ -x-t, and e- γ -t coincidence measurements have been made on these nuclei. From these data, accurate energies, relative γ -ray and conversion electron intensities, conversion coefficients, multipolarities, level spins and parities, β^+ /EC branching ratios, and log ft values have been assembled. A detailed analysis for one system, the decay of ^{191m}Tl to levels in ^{191}Hg , is presented in its entirety below. The results of the decay studies on the other Tl isotopes are presented in abbreviated discussions, the detailed analysis being left for future publication, and are summarized in tables of experimental measurements and decay scheme diagrams below.

Decay of ^{191m}Tl Gamma-Ray Singles Measurements

The γ -ray emissions from mass-separated $A = 191$ sources were studied in several experiments. Singles data were accumulated in spectral multiscaling runs made in four separate experiments emphasizing the production and decay of ^{191}Tl (the complete experimental details are given in Table 4-1). In Run 191-1, mass-191 sources collected for ten

Table 4-1. Details of ^{191}Tl Experiments

Run Number	Reaction(s) and Projectile Energy	Detectors Used and Their Energy Ranges ^a	Measurement(s) Made and Data Acquisition System Used	Collection Times and Counting Times	Number of Coincidence Events Collected
191-1	$^{181}\text{Ta}(^{16}\text{O}, 6n)^{191}\text{Tl}$ 141.1 MeV	16% Ge(Li) 30-2450 keV (8192 channels)	γ -ray singles multiscaling using the on-line Tenne- comp TP-5000	10-min collection; counted as 10 sequential 1-min spectra	
191-2	$^{181}\text{Ta}(^{16}\text{O}, 6n)^{191}\text{Tl}$ 104.2 MeV	18% Ge(Li) on-line Si(Li) electron detector (5.5 keV FWHM) both 30-1200 keV (2048 channels)	ce^- and γ -ray singles multi- scaling and e γ t using the on-line Tennecomp TP-5000	(1) 16.7-min collection; counted as 10 sequential 100-sec spectra ($\text{Ce}^- + \gamma$). (2) e- γ -t collected for 2.4 hours	9×10^5
191-3	$^{181}\text{Ta}(^{16}\text{O}, 6n)^{191}\text{Tl}$ 104.2 MeV	16% Ge(Li) and 10% Ge(Li) both 30-2700 keV ^b	γ -ray singles multiscaling (off-line Tenne- comp TP-5000) and γ - γ -t coincidences (SEL 840A)	(1) 15-min collection; counted as 10 sequential 90-sec spectra (2) γ - γ -t collected for 3.5 hours	5.9×10^6

Table 4-1 (Continued)

Run Number	Reaction(s) and Projectile Energy	Detectors Used and Their Energy Ranges ^a	Measurement(s) Made and Data Acquisition System Used	Collection Times and Counting Times	Number of Coincidence Events Collected
191-4	Nat. W(¹⁶ O, pxn) ¹⁹¹ Tl 142.9 MeV	16% Ge(Li) 30-2700 keV ^b and 18% Ge(Li) ^c 30-2000 keV	γ-ray singles multiscaling and γ-γ-t coincidences using the on-line Tennecomp TP-5000	(1) 5-min collection, counted as 12 sequential 25-sec spectra (2) γ-γ-t collected for 5 hours	8.3 x 10 ⁶
191-5	Nat. W(¹⁶ O, pxn) ¹⁹¹ Tl 142.9 MeV	16% Ge(Li) 30-2700 keV (4096 channels) on-line Si(Li) electron detector (2.5 keV FWHM) 30-1600 keV (4096 channels)	Ce ⁻ and γ-ray singles multi- scaling and eγt coincidences using the on- line Tennecomp TP-5000	(1) 5-min collection; counted as 12 sequential 25- sec spectra (2) e-γ-t collected for 18 hours	1.8 x 10 ⁶
191-6	¹⁸¹ Ta(¹⁶ O, 6n) ¹⁹¹ Tl 143 MeV	16% Ge(Li) and 10% Ge(Li) both 30-2300 keV	γ-γ-t coincidences using the off- line SEL 840A	γ-γ-t collected for 3 hours	3.5 x 10 ⁶

Table 4-1 (Continued)

^aAll coincidence measurements made on one of the Tennecomp TP-5000 systems had data collected 8192 channels each for the two events and the TAC; the data was similarly collected on the SEL 840A system 9500 channels each for the three parameters.

^bSingles measurements were done as 8192 channels on the 16% Ge(Li) detector.

^cThe Cu + Cd absorber was used on this detector.

minutes were moved in front of a 16% Ge(Li) detector (2.0 keV FWHM resolution at 1333 keV) which recorded ten sequential one-minute 8192-channel spectra. Freshly deposited sources were then moved to the detector and the counts were added to the ten spectra. Run 191-2 involved recording ten sequential 100-second 2048-channel spectra (16.7 minutes total), Run 191-3 ten 90-second spectra (15 minutes total), and Run 191-4 twelve 25-second spectra (five minutes total), both 8192-channels. Runs 191-3 and 191-4 used the same 16% Ge(Li) detector employed in Run 191-1, while Run 191-2 used an 18% Ge(Li) detector having similar characteristics. The study of the ^{191}Tl activities was hampered by the presence in all sources of 35.0 minute ^{191}gHg and 50.8 minute ^{191}mHg activities having several origins: the release of Hg products from the UNISOR ion source is favored over that of Tl products, direct production of Hg via (Heavy Ion, pxn) or (Heavy Ion, oxn) depending on the production mode for the Tl) is possible at the beam energies employed, and build-up of the Hg daughter through decay of the Tl parent also contributed. With this in mind, Run 191-4 was found to give the best Tl/Hg ratio due to the short (five minute) source collection and counting times. Figures 4-1 and 4-2 show the sum of the 12 sequential spectra for about half of the sources collected in Run 191-4. Figure 4-3 shows an expanded view of a section of this summed spectrum covering 2.0-2.2 MeV and illustrates the grouping of a collection of relative intense lines present at a high energy in the decay spectrum. Gamma-ray transitions following the decay of ^{191}Hg and other minor contaminants have been labeled as such, while those following the decay of ^{191}Tl have been labeled only with the decay energy.

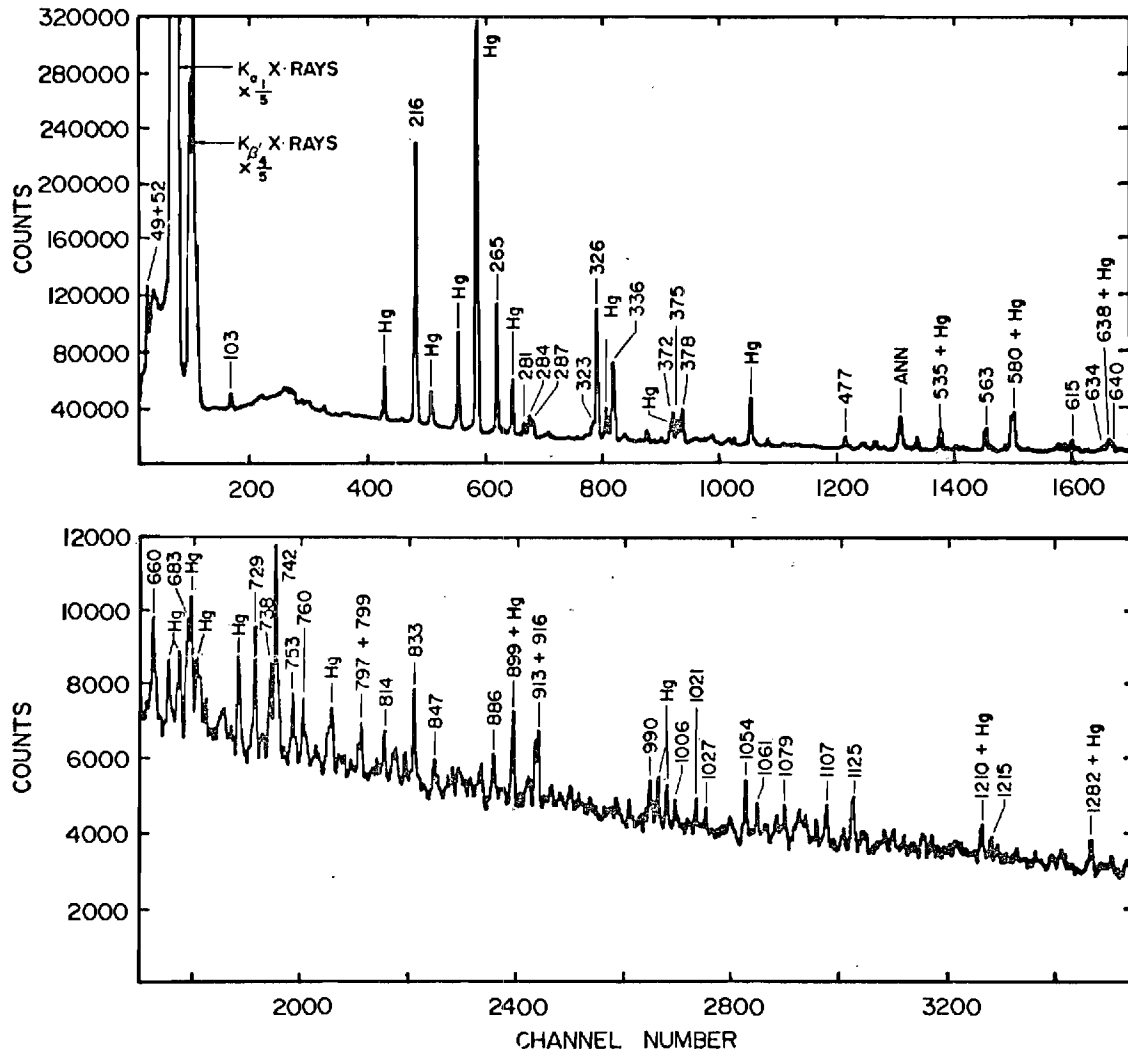


Figure 4-1. Low Energy Portion of the $A = 191$ Singles Gamma-Ray Spectrum: Total Sum of Run 191-4 Data. Those transitions following the decay of ^{191}Hg or other contaminating species have been given special labels, while those associated with the decay of ^{191}mTl have been labeled only with the decay energy.

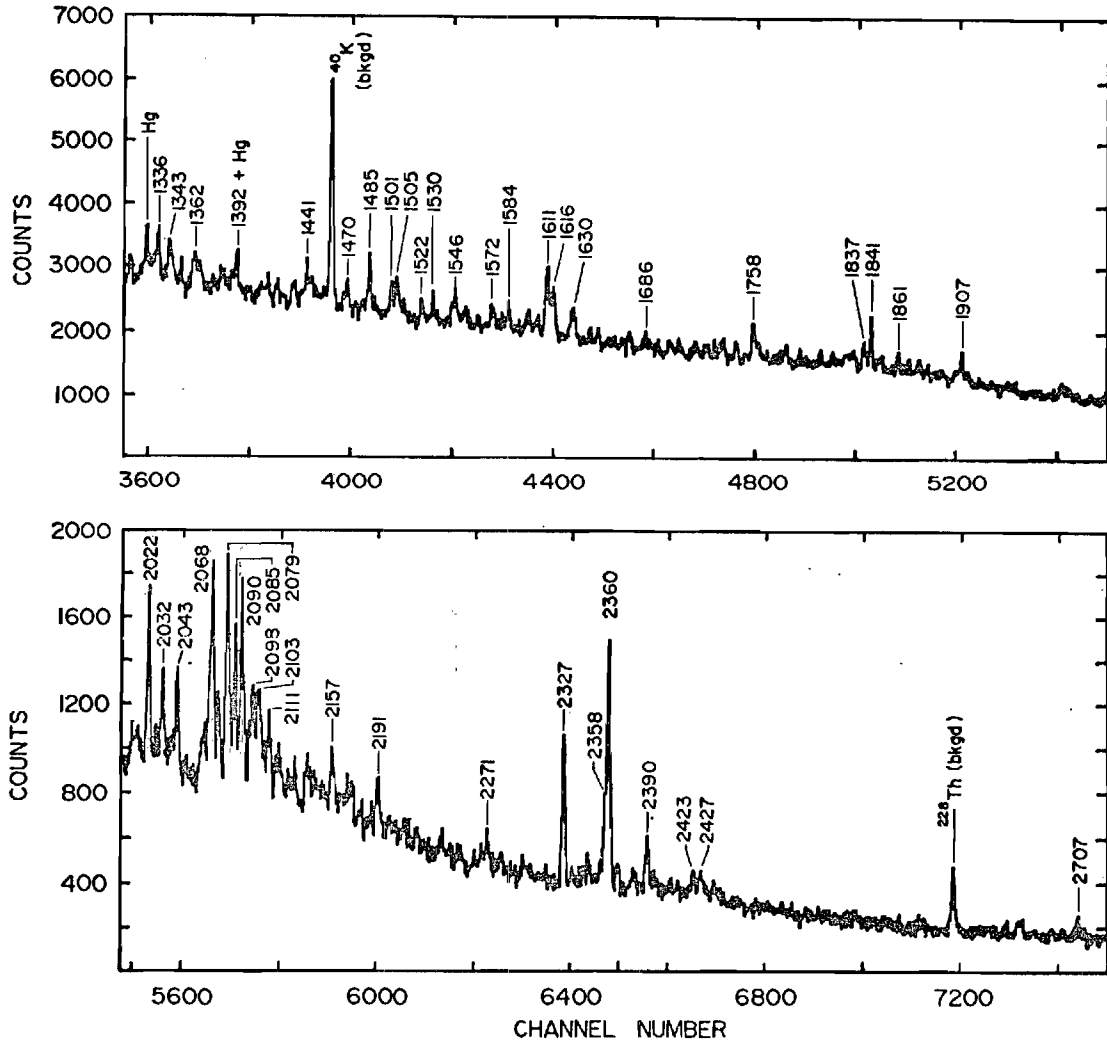


Figure 4-2. High Energy Portion of the $A = 191$ Singles Gamma-Ray Spectrum: Total Sum of Run 191-4 Data. Those transitions following the decay of ^{191}Hg or other contaminating species have been given special labels, while those associated with the decay of $^{191\text{m}}\text{Tl}$ have been labeled only with the decay energy.

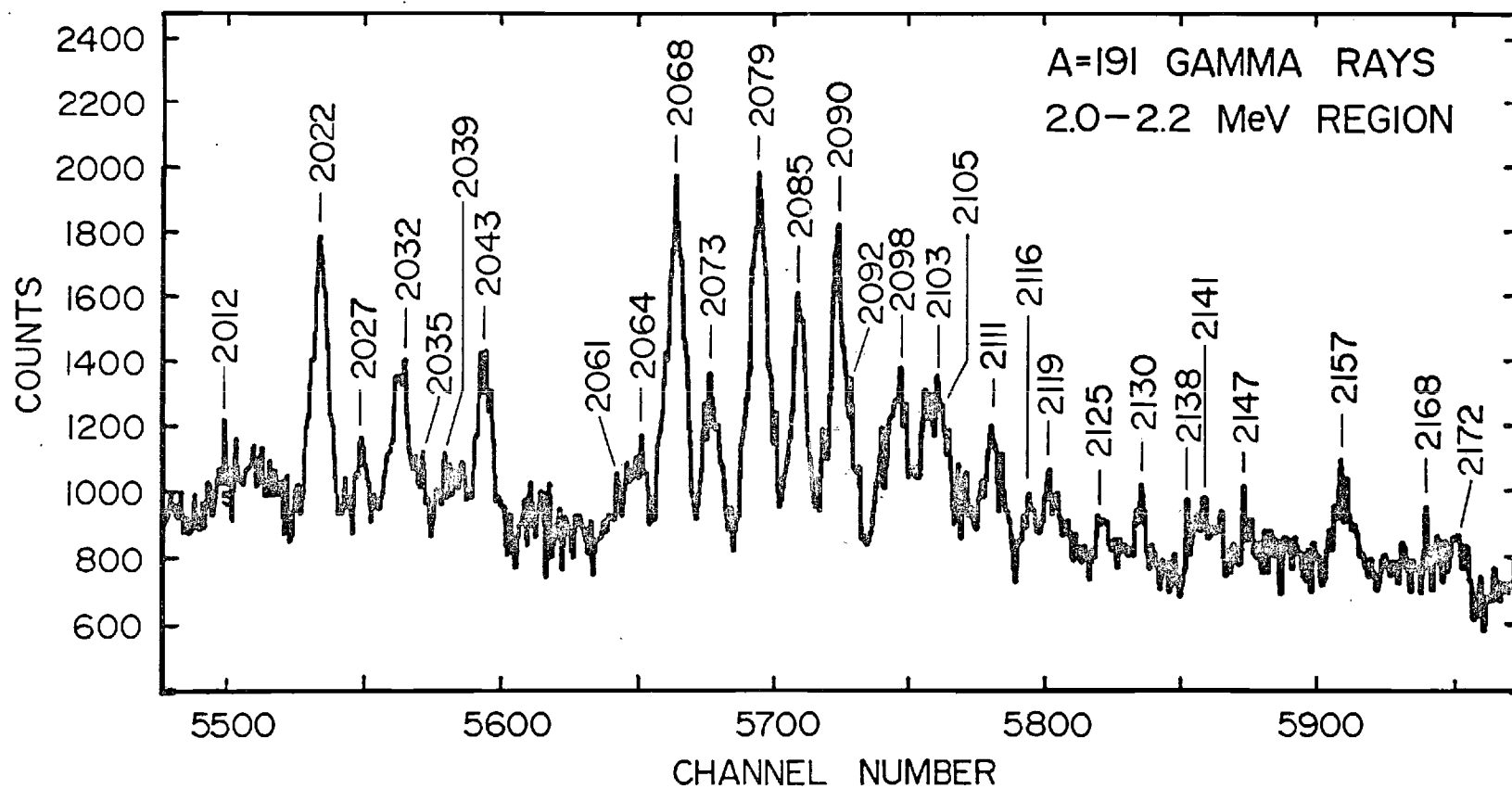


Figure 4-3. An Expanded View of the Complex A = 191 Gamma-Ray Structure in the Energy Region 2.0-2.2 MeV for the Data from Run 191-4. Note that only lines having areas > 1000 counts are labeled.

The best information concerning the ^{191m}Tl half-life came from Run 191-3, due to the good statistical quality of the data and the total length of the run (almost three half-lives, 15 minutes total collection for each source). The decay characteristics of some of the transitions are shown in Figure 4-4. Combining the results in Figure 4-4 with similar results for other transitions, the half-life for ^{191m}Tl is deduced to be 5.42 ± 0.30 min. This value agrees well with a previous half-life reported in Nuclear Data Sheets¹¹⁰⁾ and Vandlik et al.,²²⁾ but they attribute this half-life to the ground state, while we have shown it to be the decay of the $9/2^-$ isomer (see Chapter V).

The relative intensities of γ -rays observed to follow the decay of ^{191m}Tl were measured in the four experiments mentioned earlier. The intensities of the γ -rays were determined by correcting the peak areas for detector efficiency and for the degrading effects of the absorber used. The error in the relative intensities of the most intense peaks arises from the error in the efficiency calibration and is conservatively estimated to be $\pm 5\%$. The error in weak peaks comes from a combination of the $\pm 5\%$ maximum error in these intensity determinations and the statistical uncertainties present. The energy values of the ^{191m}Tl transitions were obtained using the non-linearity mapping method of Greenwood (as detailed in Chapter III). The energy and intensity results from the combined experimental data are given in Table 4-2 along with the energy and intensity values of Vandlik et al.²²⁾ and in Table 4-3 for energies above those reported by Vandlik. The results from the other three experiments were similar to those of

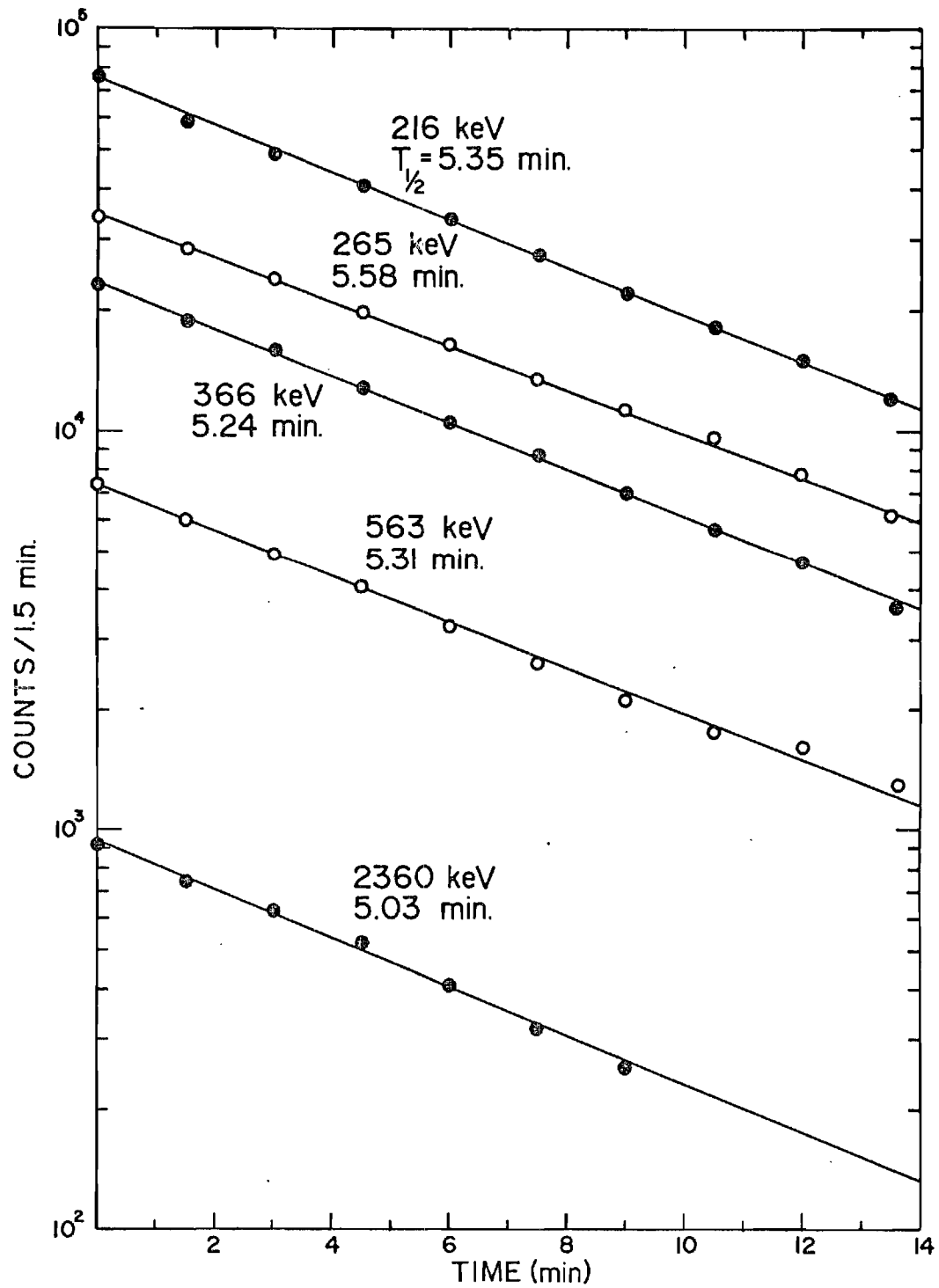


Figure 4-4. Decay Curves for Selected Transitions (216, 265, 336, 563, and 2360 keV) following the Decay of ^{191m}Tl during Run 191-3.

Table 4-2. Energies and Relative Gamma-Ray Intensities for Transitions in the ^{191}mTl Decay: Part I - Energies < 650 keV

Present Work		Vandlik et al. ^a	
E_{γ}^b (keV)	$I_{\gamma}^{b,c}$	E_{γ}^b (keV)	$I_{\gamma}^{b,c}$
49.0 (4)	1.9 (4)		
52.1 (3)	11.1 (11)		
93.5 (5)	0.29 (15)		
103.5 (4)	2.6 (5)		
118.5 (10)	0.27 (14)		
120.3 (10)	0.65 (33)		
122.1 (10)	0.68 (34)		
123.1 (10)	0.38 (19)		
165.9 (5)	0.20 (10)		
167.3 (5)	0.08 (6)		
172.1 (5)	0.81 (41)		
174.3 (5)	0.75 (38)		
184.8 (5)	0.20 (10)		
203.9 (5)	0.28 (14)		
207.1 (4)	1.3 (5)		
212.9 (4)	0.87 (44)		
215.6 (2)	100	215.71 (12)	100
226.7 (5)	1.0 (5)		
239.9 (4)	3.1 (6)		
248.6 (7)	1.7 (5)		
250.7 (7)	2.9 (6)		
254.3 (7)	1.8 (5)		
261.4 (4)	1.8 (5)		
264.7 (2)	58.9 (30)	264.66 (12)	51 (3)
268.6 (8) ^d	1.0 (5)		
271.4 (5)	1.1 (5)		
274.0 (8) ^d	2.1 (6)		
277.5 (5)	1.0 (5)		
280.9 (4)	6.7 (7)	281.0 (6)	7 (3)
284.4 (3)	10.5 (10)	284.4 (5)	9 (4)
286.6 (4)	8.4 (8)		
295.8 (4)	3.0 (6)		
298.5 (8)	0.50 (25)		
308.8 (8)	0.65 (33)		
310.3 (8)	0.48 (24)		
313.6 (5)	1.4 (5)		
318.9 (4)	3.6 (7)		
321.2 (4)	4.0 (8)		
323.4 (5)	10.0 (10)	323.1 (5)	7 (4)
326.0 (3)	76.5 (38)	325.6 (3)	67 (7)
333.7 (5)	3.7 (7)		

Table 4-2 (Continued)

Present Work		Vandlik et al. ^a	
E_{γ}^b (keV)	$I_{\gamma}^{b,c}$	E_{γ}^b (keV)	$I_{\gamma}^{b,c}$
336.1 (2)	53.0 (27)	335.91 (25)	45 (5)
344.9 (5)	1.4 (5)		
347.5 (5)	1.2 (5)		
355.4 (5)	1.2 (5)		
365.1 (4)	4.3 (8)		
372.3 (4)	20.5 (20)	374.3 (5)	16 (6)
375.4 (4)	16.8 (30)		
378.2 (4)	23.8 (20)	378.1 (3)	27 (5)
383.6 (5)	1.5 (5)		
387.6 (5)	1.7 (5)		
390.1 (7)	0.75 (50)		
394.9 (5)	4.1 (8)		
396.8 (5)	5.6 (7)		
400.0 (6)	1.2 (4)		
404.0 (6)	1.2 (4)		
405.5 (5)	3.2 (6)		
406.9 (5)	4.6 (9)		
409.9 (10) ^d	1.1 (10)		
413.6 (8)	0.45 (23)		
427.5 (7)	0.54 (27)		
430.3 (4)	6.1 (8)		
433.8 (7)	0.97 (49)		
443.3 (6)	1.8 (6)		
446.5 (6)	1.5 (5)		
449.0 (6)	2.3 (5)		
452.4 (10)	0.47 (24)		
474.6 (6)	1.5 (7)		
477.4 (4)	11.4 (12)	477.55 (27)	11 (2)
480.5 (6)	1.3 (5)		
487.1 (6)	3.5 (7)		
489.1 (7)	1.6 (5)		
495.8 (5)	7.7 (8)		
501.1 (6)	2.2 (4)		
514.0 (6)	2.2 (4)		
516.9 (6)	1.9 (4)		
526.3 (8)	1.6 (4)		
532.8 (6)	2.7 (6)		
535.1 (5)	12.0 (12)	535.1 (4)	10 (5)
539.6 (6)	3.1 (6)		
541.8 (7)	1.4 (5)		
545.2 (9) ^d	2.9 (10)		

Table 4-2 (Continued)

Present Work		Vandlik et al. ^a	
E_{γ}^b (keV)	$I_{\gamma}^{b,c}$	E_{γ}^b (keV)	$I_{\gamma}^{b,c}$
546.8 (8)	1.4 (5)		
563.2 (5)	26.7 (14)	563.1 (3)	20 (4)
566.5 (6)	4.7 (9)		
574.6 (10) ^d	3.7 (12)	574.7 (6)	8 (3)
580.4 (4)	44.6 (22)	579.7 (4)	35 (8)
583.0 (6)	3.2 (6)		
586.3 (8)	0.98 (50)		
588.4 (6)	3.5 (7)		
590.7 (7)	1.0 (4)		
606.9 (5)	10.1 (10)	606.1 (6)	6 (3)
610.4 (5)	9.8 (10)		
615.3 (4)	16.2 (20)	615.3 (4)	12 (2)
618.8 (5)	6.5 (8)		
624.3 (10) ^d	2.6 (10)		
630.1 (6)	2.1 (4)		
632.1 (6)	2.7 (5)		
634.5 (5)	8.9 (9)		
637.6 (8) ^d	15.7 (31)	639.0 (4)	16 (3)
639.8 (5)	13.3 (13)		
643.5 (7)	2.0 (5)		
645.1 (10) ^d	3.0 (12)		
647.0 (7)	2.8 (6)		
649.0 (7)	2.3 (5)		

^aRef. 20. Note that the highest energy gamma-ray reported is 639.0 keV.

^bErrors are given in parentheses and indicate the uncertainties in the last significant figures reported.

^cIntensities are relative to $I_{\gamma}(215.6) \equiv 100$.

^dContamination from ^{191}Hg .

Table 4-3. Energies and Relative Gamma-Ray Intensities for Transitions in the ^{191}mTl Decay: Part II - Energies > 650 keV

Present Work		Present Work	
E_{γ}^a (keV)	$I_{\gamma}^{a,b}$	E_{γ}^a (keV)	$I_{\gamma}^{a,b}$
650.9 (6)	3.8 (8)	840.8 (12)	0.45 (23)
656.3 (8)	1.1 (5)	846.7 (8)	3.1 (6)
658.2 (8)	1.4 (5)	858.5 (8)	2.0 (5)
660.3 (5)	7.3 (8)	862.4 (8)	1.7 (5)
676.3 (7)	2.5 (5)	866.6 (9)	1.3 (6)
683.5 (7)	7.7 (8)	870.3 (9)	1.3 (6)
685.8 (10)	5.5 (11)	874.5 (9)	1.1 (6)
689.8 (8)	1.5 (5)	877.4 (8)	2.8 (6)
691.7 (7)	3.0 (7)	885.7 (7)	4.0 (8)
695.9 (7)	2.5 (6)	890.9 (9)	1.1 (5)
699.2 (12)	0.70 (35)	898.7 (11) ^c	6.0 (9)
701.7 (12)	0.57 (29)	903.2 (14)	0.38 (20)
705.3 (9)	1.3 (5)	913.3 (7)	4.5 (9)
708.5 (10)	0.99 (50)	915.7 (7)	5.5 (9)
712.5 (12)	0.87 (44)	923.9 (8)	2.1 (5)
726.0 (10)	1.3 (7)	929.1 (13)	0.41 (20)
728.5 (6)	9.3 (10)	937.2 (15)	1.0 (5)
738.4 (7)	6.7 (7)	942.8 (10)	1.1 (5)
741.8 (6)	14.5 (15)	944.8 (10)	0.65 (33)
743.9 (7)	4.4 (8)	950.5 (9)	1.4 (5)
747.4 (10)	1.2 (6)	959.7 (12)	0.53 (27)
751.6 (20)	0.15 (15)	963.7 (10)	1.2 (5)
753.1 (8)	4.4 (8)	967.4 (8)	2.2 (5)
755.4 (8)	1.5 (5)	978.4 (12)	0.68 (34)
760.0 (7)	3.9 (8)	983.4 (9)	1.1 (5)
768.3 (8)	1.5 (5)	989.8 (8)	3.6 (7)
770.5 (11)	0.87 (44)	1006.2 (8)	2.2 (5)
775.7 (8)	1.4 (5)	1008.6 (9)	1.3 (5)
779.2 (14) ^c	1.4 (10)	1015.1 (10)	0.93 (47)
796.8 (7)	2.0 (6)	1020.6 (8)	2.6 (5)
798.8 (7)	3.3 (8)	1024.0 (15) ^c	<0.57
809.6 (8)	1.4 (5)	1044.0 (15) ^c	<1.5
814.0 (6)	3.5 (7)	1046.4 (15)	0.35 (20)
821.6 (7)	2.5 (5)	1053.5 (8)	5.6 (6)
827.3 (12) ^c	2.1 (8)	1061.0 (8)	2.6 (5)
830.5 (9)	1.0 (7)	1073.8 (9)	2.2 (5)
833.0 (7)	7.7 (9)	1078.9 (8)	3.0 (6)

Table 4-3 (Continued)

Present Work		Present Work	
E_{γ}^a (keV)	$I_{\gamma}^{a,b}$	E_{γ}^a (keV)	$I_{\gamma}^{a,b}$
1088.1 (10)	1.9 (4)	1340.6 (12)	0.51 (26)
1089.4 (9)	2.4 (5)	1343.2 (10)	2.9 (6)
1091.6 (10)	1.1 (5)	1345.1 (10)	2.2 (5)
1093.3 (9)	1.8 (6)	1360.2 (11)	1.8 (8)
1100.4 (9)	2.3 (5)	1362.2 (10)	2.4 (7)
1105.0 (10)	1.4 (7)	1380.9 (10)	1.5 (5)
1107.2 (8)	4.0 (8)	1385.0 (13)	0.56 (28)
1122.6 (15)	\sim 1.0 (10)	1388.5 (18) ^c	1.0 (6)
1124.5 (8)	6.0 (8)	1391.9 (15) ^c	2.5 (9)
1131.0 (10)	2.0 (5)	1412.1 (13)	0.80 (50)
1133.5 (10)	1.1 (5)	1413.7 (12)	1.4 (7)
1145.9 (10)	1.8 (6)	1424.5 (12)	1.0 (4)
1151.3 (9)	2.3 (5)	1430.8 (12)	1.3 (4)
1158.3 (10)	1.9 (5)	1437.3 (12)	1.3 (4)
1170.5 (10)	2.0 (5)	1440.7 (9)	3.2 (6)
1176.8 (10)	1.5 (5)	1444.0 (10)	2.1 (5)
1188.0 (15) ^c	1.2 (6)	1458.1 (14)	1.0 (6)
1192.1 (10)	1.4 (6)	1469.8 (10)	2.6 (5)
1193.6 (12)	0.82 (41)	1485.2 (8)	5.1 (9)
1198.8 (20)	0.18 (18)	1504.7 (10)	2.6 (5)
1204.1 (15)	0.53 (27)	1517.7 (11)	1.7 (5)
1208.7 (15)	1.7 (5)	1522.4 (8)	4.5 (9)
1210.1 (9)	2.5 (5)	1530.4 (8)	5.2 (9)
1215.7 (9)	2.4 (5)	1540.1 (20)	>0.1
1245.0 (11)	1.2 (4)	1543.7 (10)	2.4 (5)
1248.7 (11)	1.0 (4)	1552.7 (11)	2.3 (5)
1257.0 (10)	1.4 (5)	1553.8 (12)	1.7 (5)
1261.7 (10)	2.1 (5)	1557.0 (11)	2.7 (6)
1264.1 (12)	0.87 (45)	1562.9 (12)	1.2 (4)
1270.7 (15)	0.33 (18)	1572.0 (10)	3.8 (8)
1279.1 (11)	1.3 (4)	1574.9 (12)	1.9 (5)
1282.2 (15) ^c	2.4 (5)	1580.3 (11)	2.9 (6)
1288.4 (11)	1.2 (4)	1583.7 (9)	5.7 (9)
1296.0 (10)	1.8 (5)	1587.0 (11)	2.7 (6)
1305.0 (10)	2.2 (5)	1591.6 (11)	3.1 (6)
1315.8 (11)	1.6 (5)	1595.1 (10)	3.9 (8)
1327.1 (18) ^c	1.7 (8)	1598.4 (10)	5.3 (9)
1333.7 (11)	1.1 (4)	1604.2 (10)	3.7 (7)
1335.7 (9)	3.4 (6)	1611.0 (6)	11.9 (12)

Table 4-3 (Continued)

Present Work		Present Work	
E_{γ}^a (keV)	$I_{\gamma}^{a,b}$	E_{γ}^a (keV)	$I_{\gamma}^{a,b}$
1614.3 (11)	3.5 (7)	1906.6 (12)	4.0 (8)
1616.0 (8)	7.9 (8)	1977.2 (14)	1.8 (5)
1624.7 (12)	2.5 (5)	1983.5 (12)	2.6 (5)
1628.6 (10)	4.5 (9)	2011.8 (13)	2.2 (5)
1629.6 (9)	7.2 (10)	2021.5 (10)	7.7 (8)
1630.4 (10)	5.2 (9)	2031.9 (12)	5.3 (9)
1633.9 (15) ^c	0.80 (65)	2035.0 (15)	1.3 (6)
1641.0 (12)	3.0 (6)	2043.2 (12)	6.8 (8)
1650.9 (20) ^c	<1.0	2060.5 (15)	1.8 (5)
1669.9 (12)	2.5 (5)	2063.6 (14)	3.2 (6)
1685.9 (12)	2.1 (5)	2068.4 (10)	12.2 (12)
1697.3 (12)	2.0 (5)	2073.0 (14)	4.8 (9)
1712.1 (13)	1.7 (5)	2079.4 (10)	12.2 (12)
1716.8 (11)	3.1 (6)	2085.0 (12)	7.3 (8)
1722.9 (12)	2.0 (5)	2089.5 (11)	8.0 (9)
1725.5 (11)	3.0 (6)	2097.9 (12)	6.4 (8)
1731.4 (12)	2.8 (6)	2102.9 (13)	5.1 (9)
1735.0 (13)	2.1 (5)	2105.2 (15)	2.1 (5)
1737.1 (10)	5.6 (9)	2111.0 (15)	2.9 (6)
1746.6 (10)	4.0 (8)	2137.8 (15)	2.2 (5)
1752.9 (12)	2.4 (5)	2147.5 (20)	0.94 (50)
1757.7 (9)	7.5 (8)	2157.0 (14)	3.6 (7)
1761.5 (16) ^c	1.8 (7)	2168.1 (15)	2.1 (5)
1780.9 (12)	2.7 (6)	2190.6 (15)	2.8 (6)
1806.1 (12)	2.5 (5)	2270.7 (15)	2.4 (5)
1814.5 (12)	2.0 (5)	2327.4 (12)	8.2 (9)
1823.6 (13)	2.2 (5)	2334.5 (20)	0.94 (50)
1827.0 (13)	1.5 (4)	2342.2 (20)	0.80 (40)
1828.8 (13)	2.1 (5)	2357.6 (14)	4.1 (7)
1836.9 (10)	4.3 (8)	2360.4 (10)	13.1 (13)
1841.4 (9)	9.7 (10)	2366.7 (16)	1.8 (5)
1846.0 (12)	2.5 (5)	2389.8 (14)	3.3 (6)
1849.5 (12)	3.4 (7)	2406.4 (16)	1.4 (4)
1854.0 (13)	1.8 (5)	2411.4 (20)	0.88 (44)
1860.8 (12)	2.5 (5)	2420.8 (20)	0.64 (32)
1872.9 (13)	2.1 (5)	2427.1 (17)	1.1 (4)
1875.9 (12)	3.0 (6)	2439.2 (20)	0.87 (44)
1881.1 (18)	0.40 (20)	2457.6 (25)	0.58 (35)
1887.6 (13)	2.0 (5)	2476.9 (25)	0.57 (35)
1892.4 (13)	2.2 (5)	2606.5 (25)	0.78 (40)
1902.6 (12)	2.3 (5)	2782.3 (30)	0.26 (20)

Table 4-3 (Continued)

^aErrors are given in parentheses and indicate the uncertainties in the last significant figures reported.

^bIntensities are relative to I_{γ} (215.6) \equiv 100.

^cContamination from ^{191}Hg is present in this line.

Run 191-4. Note that some of the lines were contaminated by ^{191}Hg lines which were subtracted from the spectrum by using the energy and relative intensity values determined by Wood et al.¹¹¹⁾ in ^{191}Hg experiments done concurrently with ^{191}Tl ; and ^{191}Hg measurements by Beuscher et al.¹¹²⁾ at Jülich.

From our measurements, a total 361 γ -rays are assigned to the $^{191\text{m}}\text{Tl}$ decay. Half-life measurements for 225 of the transitions are consistent with their assignment to 5.42 min $^{191\text{m}}\text{Tl}$, a majority of them exhibiting a single half-life, while some are found to overlap with ^{191}Hg lines and thus exhibit a two-component decay curve. The remaining 136 weak γ -rays are assigned to the decay of $^{191\text{m}}\text{Tl}$ through coincidence relationships.

Conversion Electron Measurements

Conversion electrons were detected in a Si(Li) detector cooled to liquid nitrogen temperature during Run 191-2. This detector was positioned on the opposite side of the source from an 18% Ge(Li) γ -ray detector, and multiscaled singles spectra of the conversion electrons and γ -rays were obtained simultaneously. Because of the high density of electron lines found to exist in the mass-191 data, the resolution of approximately 5.5 keV FWHM typically for K electron lines using this detector was insufficient for studying this decay. In order to improve the resolution, a new Si(Li) detector was used, which has resolution for K electron lines ranging between 2.5 and 3.0 keV FWHM. This detector was run simultaneously in singles mode with a γ -ray detector, as before, with the sources in this experiment (Run 191-5) being collected for five minutes and recorded as 12 sequential 25-second

4096-channel spectra for γ -rays and electrons. The sum of the 12 sequential electron spectra is shown in Figure 4-5. Using the pure E2 and M1 transitions present in the $^{191g,m}\text{Hg}$ decay (111,112) for normalization, K-conversion coefficients of the previously unknown transitions were deduced. For some very strong lines, L- and M-conversion coefficients were also determined. These experimental conversion coefficients are compared to the theoretical values calculated by Hager and Seltzer,¹¹³⁾ and a resulting multipolarity is assigned for each transition. The conversion electron intensities, conversion coefficients, theoretical values, and deduced multipolarities are given in Table 4-4.

Coincidence Measurements

Coincidence data on γ -rays from ^{191m}Tl decay were obtained in three separate experiments. Runs 191-6 and 191-3 (see Table 4-1) were carried out using the off-line γ - γ -t counting setup described in Chapter III with 10% and 16% Ge(Li) γ -ray detectors recording the γ -coincidence events on the SEL 840A computer. Run 191-6 involved energy ranges on both γ -ray detectors of ~ 30 -2300 keV and coincidence data are collected for about three hours, resulting in the accumulation of over 3.5×10^6 coincidence events. Run 191-3 showed an increase in the total data collected and a somewhat improved Tl/Hg ratio, and it involved increased energy ranges of ~ 30 -2700 keV on both Ge(Li) detectors. The coincidence rates approached 11.00 counts/sec, accumulated over 3.5 hours, giving 5.9×10^6 coincidence events. The most favorable experiment was Run 191-4. In this experiment, 16% and 18% Ge(Li) detectors were used in the on-line γ - γ -t experimental configuration employing the UNISOR tape

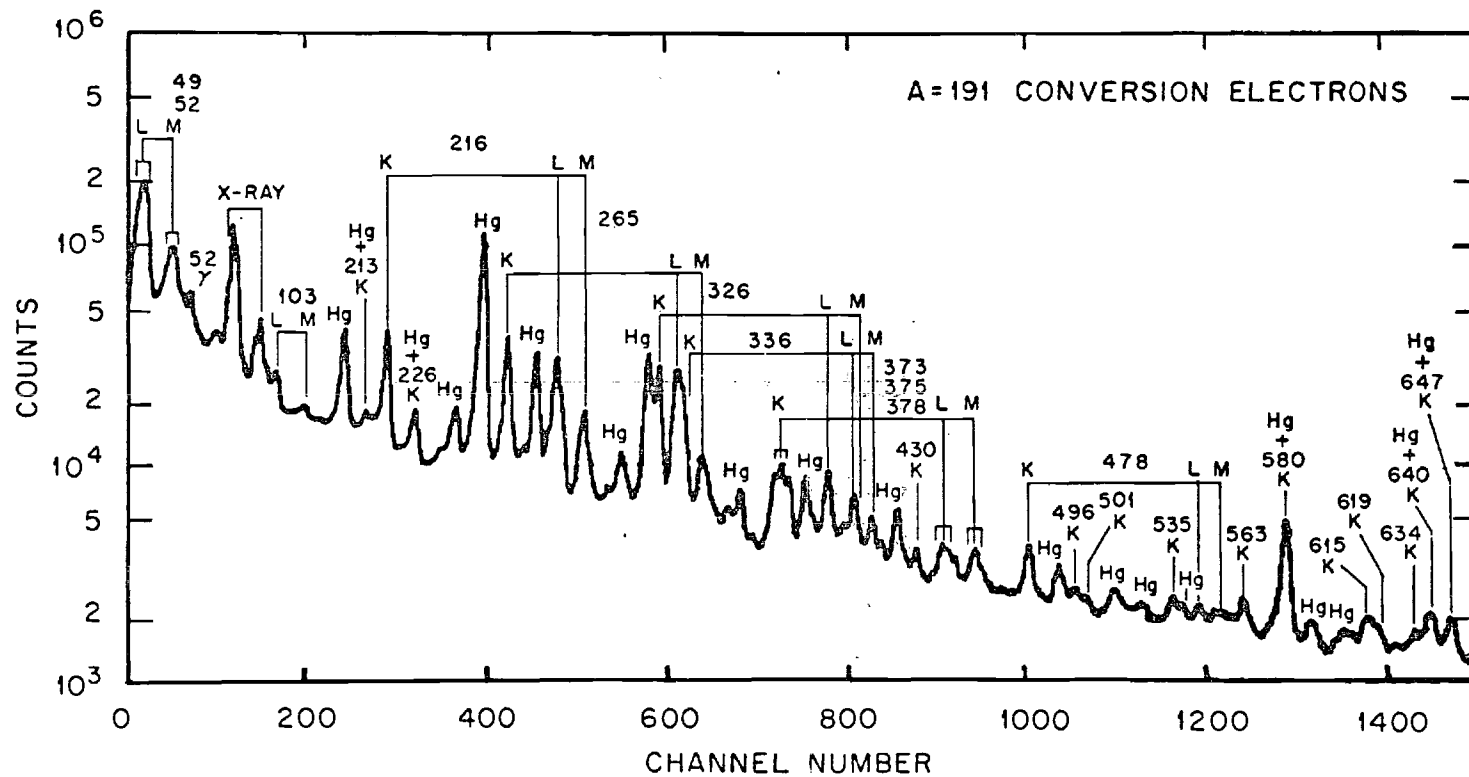


Figure 4-5. The Total Sum of the A = 191 Conversion Electron Data Taken during Run 191-5. Those transitions following the decay of ^{191}Hg have been given special labels, while those associated with the decay of $^{191\text{m}}\text{Tl}$ have been labeled with the decay energy and the shell of conversion (K, L, or M).

Table 4-4. Experimental and Theoretical Conversion Coefficients, Relative Electron Intensities, and Multipolarities for Transitions in ^{191}mTl Decay

E_{γ} (keV)	$I_{\text{Ce}^-}^{a,b}$	$\alpha_K^{b,c}$ ($\times 10^3$)	Theoretical $\alpha_K^{c,d}$ ($\times 10^3$)			Multipolarity Assigned
			E1	M1	E2	
49.0	276 (54)	L_{109000}^e	460	9160	113000	E2
		M_{33300}^e	108	2130	29500	
52.1	455 (90)	L_{30900}^e	390	7660	83400	M1 + (39+6%)E2
		M_{9680}^e	91.6	1780	21900	
103.5	97.0 (97)	L_{1350}	60.2	1040	3170	M1 + (15+2)%E2
		M_{389}	14.0	241	829	
212.9	1.0 (3)	880	52.2	790	147	M1
215.6	18.8 (19)	141	50.6	762	142	E2
226.7	2.1 (20)	1530^e	44.8*	664	127	>M1 (some E0?)
238.4	0.36 (7)	171	39.7	578	110	E2 + (13+6)%M1
264.7	15.6 (20)	199^e	30.9	434	86.1	E2 + (33+10)%M1
280.9	2.0 (4)	230	26.9	369	74.5	M1 + (47+15)%E2
284.4	3.0 (15)	213^e	26.1	356	72.3	E2 + (49+22)%M1
323.4	2.3 (6)	174^e	19.3	251	53.1	M1 + (39+20)%E2
326.0	15.1 (15)	146	19.0	246	52.1	E2 + (48+5)%M1

Table 4-4 (Continued)

E_{γ} (keV)	$I_{\text{Ce}^-}^{a,b}$	$\alpha_{\text{K}}^{b,c}$ ($\times 10^3$)	Theoretical $\alpha_{\text{K}}^{c,d}$ ($\times 10^3$)			Multipolarity Assigned
			E1	M1	E2	
336.1	6.6 (13)	97.8 ^e	17.7	226	48.5	E2 + (28+10)%M1
360.7	0.72 (36)	218 ^e	15.1	187	41.0	>M1
372.3	2.0 (5)	72.6 ^e	14.0	172	38.1	E2 + (26+12)%M1
375.4	3.6 (5)	160	13.8	168	37.3	M1
378.2	3.0 (4)	86.3 ^e	13.5	165	36.7	E2 + (39+10)%M1
405.5	0.45 (22)	107 ^e	11.6	137	31.2	M1 + (28+25)%E2
430.3	0.63 (25)	77.6 ^e	10.2	117	27.3	M1 + (44+25)%E2
449.0	0.085 (55)	27.9 ^e	9.30	104	24.8	E2 + (\leq 10)%M1
474.4	1.0 (3)	67.3 ^e	8.17	88.7	21.7	M1 + (32+18)%E2
488.5	0.07 (7)	14.1 ^f	7.78	83.5	20.6	E1 ^f
495.8	0.50 (25)	48.3 ^e	7.54	80.3	19.9	E2 + (47+40)%M1
501.1	0.20 (5)	71.7	7.37	78.1	19.5	M1 + (11+80)%E2
535.1	0.37 (37)	23.2 ^e	6.43	65.7	16.9	E2 + (\leq 40)%M1
539.6	0.30 (25)	<73.3 ^e	6.32	64.3	16.6	\leq M1
545.2	0.069 (40)	30.2 ³	6.19	62.6	16.3	E2 + (30+40)%M1
563.2	0.55 (25)	15.4 ^e	5.79	57.5	15.2	E2

Table 4-4 (Continued)

E_{γ} (keV)	$I_{\text{Ce}}^{a,b}$	$\alpha_{\text{K}}^{b,c}$ ($\times 10^3$)	Theoretical $\alpha_{\text{K}}^{c,d}$ ($\times 10^3$)			Multipolarity Assigned
			E1	M1	E2	
580.4	0.83 (35)	14.0 ^e	5.44	53.2	14.3	E2
606.9	0.17 (9)	$\sim 13.1^e$	4.97	47.4	13.0	E2(?)
615.3	0.35 (17)	16.3 ^e	4.84	45.7	12.7	E2 + (11+20)%M1
618.8	0.25 (9)	28.8 ^e	4.78	45.1	12.5	E2 + (50+25%)M1
634.5	0.29 (10)	24.2 ^e	4.55	42.2	11.9	E2 + (\leq 70)%M1
683.5	0.088 (55)	8.59 ^e	3.93	34.9	10.2	E2(?)
738.4	0.043 (21)	4.76	3.38	28.6	8.76	E1
741.8	0.16 (6)	8.28 ^e	3.35	28.2	8.68	E2
753.1	0.060 (20)	10.2	3.26	27.1	8.42	E2 + (10+10)%M1
833.0	0.051 (30)	4.96 ^e	2.70	20.9	6.91	<E2
846.7	0.025 (15)	6.07 ^e	2.62	20.1	6.70	E2 + (\leq 4)%M1
898.7	0.048 (30)	6.07 ^e	2.34	17.2	5.97	E2 + (\leq 19)%M1
913.3	0.015 (15)	7.54 ^e	2.28	16.5	5.79	E1(?)
915.7	0.063 (40)	8.60 ^e	2.27	16.4	5.76	E2 + (27 + 25)%M1
1053.6	0.015 (15)	2.06	1.76	11.5	4.42	<E2
1124.6	0.017 (17)	2.19	1.57	9.75	3.92	<E2

Table 4-4 (Continued)

E_{γ} (keV)	$I_{\text{Ce}}^{\text{a,b}}$	$\alpha_{\text{K}}^{\text{b,c}}$ ($\times 10^3$)	Theoretical $\alpha_{\text{K}}^{\text{c,d}}$ ($\times 10^3$)			Multipolarity Assigned
			E1	M1	E2	
1215.7	0.017 (17)	5.48	1.37	8.03	3.39	E2 + M1
1335.7	0.017 (17)	3.72	1.16	6.36	2.86	E2 + M1
1380.9	0.007 (7)	3.33	1.10	5.85	2.69	E2 + M1
1444.0	0.010 (10)	3.45	1.02	5.23	2.48	E2 + M1
1453.2	0.012 (12)	9.40	1.01	5.15	2.45	>M1
1485.2	0.010 (10)	1.48	0.970	4.88	2.35	<E2
1595.1	0.014 (14)	2.45	0.860	4.07	2.06	E2 + M1
1611.0	0.024 (24)	1.51	0.848	3.98	2.02	<E2

^a Intensities are relative to I_{γ} (215.6) \equiv 100.

^b Errors in I_{Ce} - (in parentheses) also reflect the errors in the conversion coefficients. The errors quoted are the uncertainties in the last digit.

^c All conversion coefficients are α_{K} unless otherwise marked - superscripts L and M mean the values given are for α_{L} and α_{M} , respectively.

^d Taken from Hager and Selzer (ref. 113).

^e Electron lines were overlapped by at least one contaminating line.

^f A contamination of this electron line is possible, but the amount could not be calculated. This would lower the α_{K} , thus the multiplicity of this line is thought to be E1.

transport system, as described in Chapter III. The 16% Ge(Li) detector had an energy range of ~ 30 -2700 keV for γ -rays and was also used to take singles data in the spectrum-multiscaling mode (see Figures 4-1 and 4-2) simultaneously with the γ - γ -t data accumulation. The 18% Ge(Li) detector was set to cover the ~ 30 -2000 keV range and used the Cd + Cu absorber to remove most of the x-ray summing effects for that detector. The data were accumulated at coincidence rates up to 1500 counts/sec for about five hours and resulted in the collection of over 8.3×10^6 coincidence events on the UNISOR Tennecomp TP-5000 computer system. Six of the gated spectra (the 216, 265, 742, 326, 336, and 1611 keV gates) from this third coincidence experiment are shown in Figures 4-6 and 4-7. Similar gated spectra were obtained for 129 γ -rays originating from ^{191m}Tl decay. The results of the coincidence measurements are given in Table 4-5. The entries (S, M, and W, which represent strong, moderate, and weak, respectively) indicate the relative magnitudes of peak areas observed in a spectrum coincident with a particular gate. The various peak areas described by the three entries usually differ by approximately an order of magnitude within a spectrum.

In addition to the γ - γ -t data, e- γ -t data were collected in two experiments, both using the on-line counting setup, including the tape transport and Tennecomp TP-5000 data acquisition system (as described in Chapter III). The first experiment, Run 191-2, involved an 18% Ge(Li) detector (~ 30 -1200 keV energy range over 8192 channels) and the on-line Si(Li) electron detector (~ 5.5 keV FWHM resolution for K electrons, ~ 30 -1200 keV energy range over 8192 channels), but only a

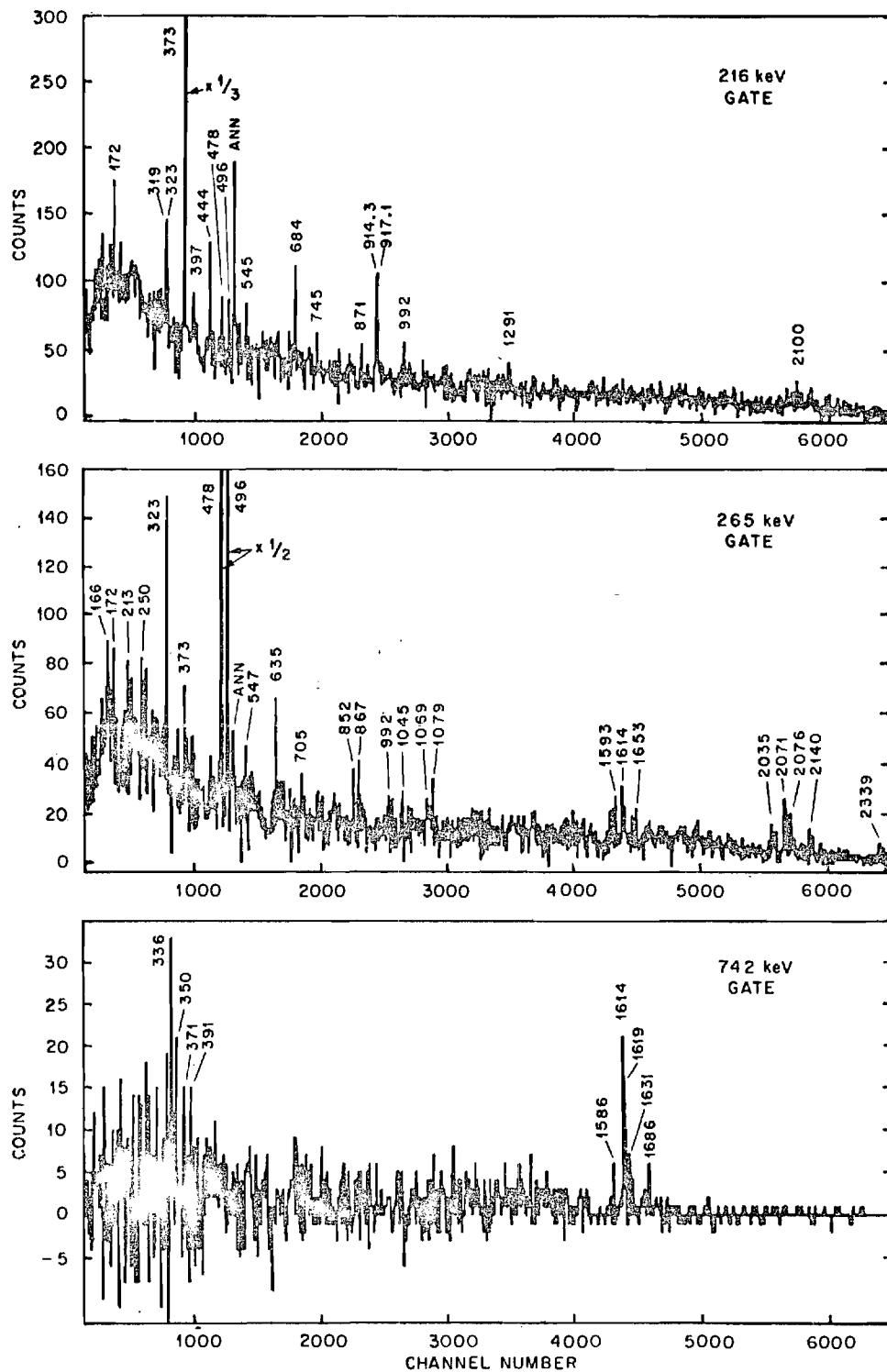


Figure 4-6. The γ - γ -t Coincidence Gates Taken in Run 191-4 for the 216, 265, and 742 keV Transitions Observed in the Decay of ^{191}mTl .

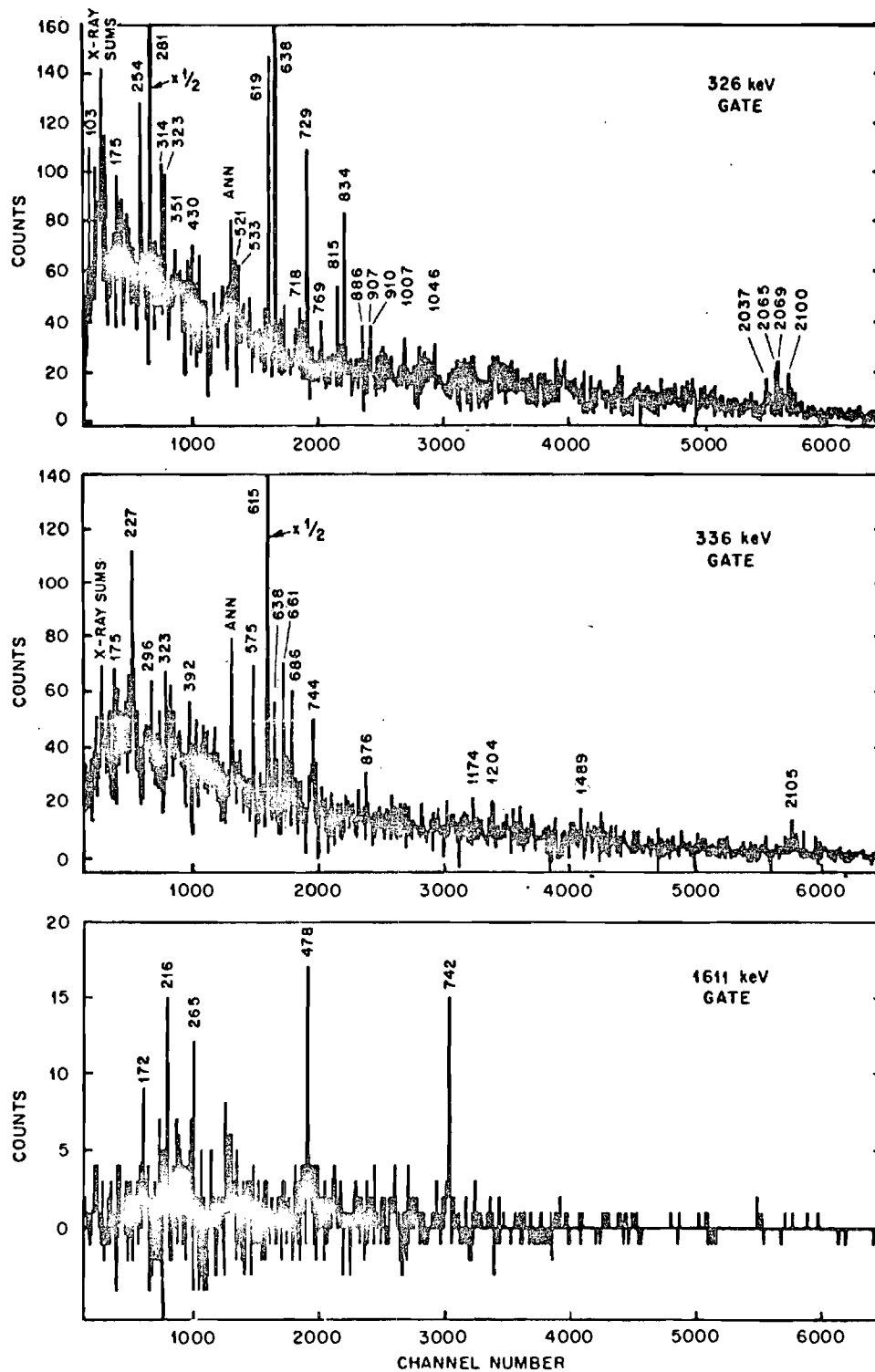


Figure 4-7. The γ - γ -t Coincidence Gates Taken in Run 191-4 for the 326, 336, and 1611 keV Transitions Observed in the Decay of ^{191m}Tl .

Table 4-5. Coincidence Relationships Observed in ^{191m}Tl Decay

Gate Energy* (keV)	Energy of Coincident Gamma-Rays and Their Relative Strengths ^a
49.0 ^{b,c}	172.1(M), 174.3(M), 184.8(W), 212.9(W), 215.6(S), 254.3(M), 261.4(W), 280.9(M), 284.4(M), 323.4(W), 326.0(S), 378.2(S), 383.5(W), 396.8(W), 580.4(S), 606.9(W), 637.6(M), 639.8(M), 731.8(W)
52.1 ^{b,c}	254.3(M), 261.4(W), 280.9(M), 284.4(M), 298.5(W), 313.6(W), 323.4(M), 326.0(S), 336.1(W), 344.9(W), 378.2(S), 383.5(W), 394.9(W), 396.8(M), 501.1(W), ann(M), 521.4(W), 535.1(W), 566.5(W), 580.4(S), 606.9(M), 618.8(W), 637.6(M), 639.8(M), 685.8(W), 728.5(M), 768.3(W), 814.0(M), 827.3(M), 833.0(M), 923.9(M), 1053.5(M), 1124.5(M), 1145.9(W), 1257.0(W), 1335.7(W), 1469.8(W), 1690.2(W), 1697.1(W), 1780.9(W), 1828.8(W), 1841.4(M), 2068.4(W), 2079.4(M), 2085.0(W), 2138.0(W), 2190.6(W), 2210.6(W)
103.5 ^b	150.6(W), 215.6(S), 239.9(W), 264.7(W), 271.4(M), 274.0(W), 284.4(W), 286.6(W), 323.4(W), 325.6(S), 355.4(W), 372.3(S), 378.2(W), 387.6(W), ann(W), 586.3(W), 588.4(W), 676.3(W), 695.9(W)
172.1	215.6(S), 246.5(M), 303.6(W), 323.4(W), 326.0(M), 372.3(S), 762.4(W), 830.5(W)
207.1	326.0(S), 355.4(W), 456.8(W), 532.8(S), 545.1(W), 726.0(W), 1026.9(M)
212.9 ^c	162.8(M), 217.9(M), 225.4(W), 232.3(W), 372.3(S), 378.2(M), 443.3(W), ann(M), 915.7(M), 1065.0(W)
215.6 ^c	139.4(M), 162.8(M), 172.1(S), 318.9(S), 323.4(M), 372.3(S), 396.8(M), 443.3(S), 477.4(M), 495.8(M), ann(S), 526.3(M), 545.2(M), 683.5(S), 743.9(M), 753.1(W), 870.3(M), 913.3(S), 915.7(S), 989.8(M), 1100.4(W), 1124.5(W), 1291.0(M),

Table 4-5 (Continued)

Gate Energy* (keV)	Energy of Coincident Gamma-Rays and Their Relative Strengths ^a
	1413.7(M), 1611.0(W), 1633.9(W), 1761.5(W), 1787.8(M), 1887.6(M), 1924.2(M), 1944.1(M), 2068.4(M), 2097.9(M), 2111.0(M), 2138.0(M)
226.7	336.1(S), 705.3(W), 934.3(W), 1053.5(W), 1802.2(W)
254.3	264.7(M), 326.0(S), 489.1(M), 798.8(M)
264.7	165.9(M), 172.1(M), 212.9(M), 250.7(M), 323.4(S), 372.3(M), 441.5(W), 477.4(S), 495.8(S), ann(M), 516.9(W), 546.8(M), 557.4(W), 566.5(M), 634.5(S), 705.3(W), 749.9(W), 821.6(W), 851.6(W), 870.3(W), 866.7(M), 989.8(M), 1078.8(M), 1237.9(W), 1583.7(M), 1591.6(M), 1611.0(M), 1737.1(W), 2031.9(M), 2068.4(M), 2073.0(M), 2089.5(M), 2138.0(W), 2147.5(W), 2339.2(W)
274.0 ^d	49.0(W), 52.1(S), 135.4(W), 236.7(S), 295.8(W) 308.8(M), 329.6(W), 356.7(S), 370.8(S), 385.6(M), 439.8(M), 449.0(W), 557.4(W), 656.3(W), 699.1(W), 717.7(M), 1031.2(W), 1089.9(W), 1107.2(M), 1162.9(W), 1391.9(W)
280.9	224.5(M), 326.0(S), 378.2(M), 1006.2(W), 1920.9(W)
284.4	274.0(M), ann(W), 615.3(S), 637.6(W), 1089.5(W)
313.6	326.0(S)
323.4 ^c	186.8(W), 212.9(W), 215.6(S), 264.7(S), 280.9(S), 336.1(W), 351.8(M), 396.8(W), 419.1(W), ann(M), 535.1(M), 618.8(W), 637.6(M), 743.9(M), 770.5(M), 967.4(M), 1140.4(W), 2021.5(M)
326.0 ^c	52.1(S), 56.8(S), 103.5(M), 174.3(W), 184.8(W), 254.3(S), 280.9(S), 313.6(M), ann(W), 532.8(M), 618.8(S), 637.6(S), 645.1(W), 708.5(W), 717.7(M), 728.5(S), 867.3(W), 814.0(M), 833.0(M), 885.8(W), 907.6(W), 1006.2(W), 1046.4(W), 1158.3(W), 1725.6(W), 2035.0(W), 2063.6(M), 2068.4(M), 2097.9(M)

Table 4-5. (Continued)

Gate Energy* (keV)	Energy of Coincident Gamma-Rays and Their Relative Strengths ^a
336.1	174.3(W), 226.7(S), 295.8(W), 323.4(M), 355.4(W), ann(M), 574.6(M), 615.3(S), 637.6(M), 660.3(S), 685.8(M), 743.9(M), 770.5(W), 855.8(W), 874.5(W), 1122.6(W), 1172.3(W), 1204.1(W), 2102.9(M), 2138.0(W)
372.3 ^c	137.4(M), 172.1(M), 187.1(M), 215.6(S), 286.6(S), 441.5(M), 516.9(M), 535.1(M), 618.8(M), 948.6(W), 1089.9(W), 1382.9(W), 1412.1(W), 1854.0(W)
375.4 ^c	186.4(M), 211.1(W), 356.7(M), 535.1(S), 1369.8(W)
378.2 ^c	52.1(W), 261.4(S), 356.7(M), 521.4(M), 566.5(S), 650.9(W), 1064.3(W), 2351.0(W)
383.6	196.3(M), 580.4(S), 676.4(M)
387.6 ^c	188.9(S), 192.5(S), 615.3(W), 1175.6(W)
390.1 ^c	188.9(S), 934.0(W)
409.9 ^d	215.6(S), 241.1(S), 252.4(S), 331.6(W), 678.1(M), 1365.7(M)
430.3	261.4(W), 521.4(M), 566.5(W), 1530.4(W)
474.6	212.9(W), 264.7(S), 580.4(W), 1268.3(W)
477.4	139.4(M), 161.4(W), 190.0(W), 215.6(S), 264.7(S), 336.1(M), 347.5(W), 452.4(W), 1100.4(M), 1611.0(M)
480.5	430.3(W), 1107.2(M)
487.1	172.1(W)
495.8	135.4(M), 215.6(S), 241.1(W), 264.7(S), 336.1(M), 421.6(M), 441.5(M), 809.6(W), 907.6(W), 1485.2(W)

Table 4-5 (Continued)

Gate Energy* (keV)	Energy of Coincident Gamma-Rays and Their Relative Strengths ^a
501.1	639.8(S), 1151.3(W)
514.0	264.7(M), ann(S), 580.4(M), 650.9(M)
516.9	182.5(W), 331.6(W), 372.3(S), 664.7(M), 1018.1(M)
532.8 ^c	207.1(M), 326.0(M), 356.7(W), 375.4(M), 913.3(W)
535.1 ^{c,d}	207.1(M), 241.1(M), 252.4(S), 266.3(W), 320.0(M), 343.0(M), 375.4(S), 466.8(W), 662.4(W), 670.8(M), 830.5(W), 1151.3(M), 1165.3(W), 1188.0(M)
545.2 ^d	172.1(W), 215.6(S), 331.6(S), 402.3(W), 1215.7(W)
563.2	224.5(W), 252.4(W), 329.1(M), 514.0(M), 583.0(S), 610.4(W), 753.1(M), 1122.6(M), 1977.2(W)
566.5	336.1(W), 378.2(S)
574.6 ^d	103.5(S), 224.5(S), 252.4(M), 268.6(M), 326.0(M), 336.1(S), 467.8(M), 521.4(M), 934.7(M)
580.4	52.1(W), 198.6(M), 286.6(W), 383.6(S), 474.6(M), 504.7(W), ann(S), 514.0(M), 685.8(M), 1841.4(S), 1860.8(W)
583.0	563.2(S)
606.9	488.5(W), 539.6(W), 1078.9(M), 1299.8(W)
615.3	103.5(W), 252.4(M), 284.4(S), 336.1(S), 370.8(W), 1002.1(W), 1257.0(W)
618.8	215.6(S), 326.0(S)
624.3 ^d	252.4(M), 375.4(W), 420.0(W), 535.1(S)
634.5 ^e	264.7(S), 326.0(S), 333.7(W), 422.6(M)

Table 4-5 (Continued)

Gate Energy* (keV)	Energy of Coincident Gamma-Rays and Their Relative Strengths ^a
637.6 ^c	286.6(W), 326.0(S), 336.1(M), 378.2(S), 396.8(M), 406.9(M), 885.9(M), 1044.0(W), 1440.7(W)
639.8 ^c	326.0(S), 336.1(M), 501.1(M)
645.1	318.8(W), 387.6(W)
660.3	336.1(S)
683.5	120.3(W), 215.6(S), 286.6(M), 409.9(M), 495.8(W)
691.7	ann(M)
728.5	215.6(W), 326.0(S), 1345.1(M)
738.4	199.3(W), 336.1(M)
741.8 ^c	336.1(S), 350.0(M), 370.8(M), 1583.7(M), 1611.0(S), 1616.0(W), 1629.6(W), 1685.9(W)
743.9 ^c	252.4(W), 274.0(W), 336.1(S), 370.8(M)
753.1	ann(M), 563.2(S)
760.0	320.0(W)
798.8	184.8(W), 390.1(W), 563.2(M)
814.0	201.1(W), 326.0(S), 378.2(W), 417.7(W), 522.6(W)
833.0	241.1(M), 252.4(S), 326.0(S), 378.2(M)
898.7	103.2(W), 762.4(W)
913.3	127.4(W), 215.6(S), 284.4(M)
915.7	215.6(S), 634.5(W)
923.9	203.9(M), 717.7(W)
937.2	184.8(W), 1305.0(W)

Table 4-5 (Continued)

Gate Energy* (keV)	Energy of Coincident Gamma-Rays and Their Relative Strengths ^a
950.5	103.2(M)
989.8	215.6(S), 264.7(S), 630.1(M)
1006.2	215.6(M), 264.7(M)
1053.5	161.2(M), 239.9(W)
1061.0	378.2(W)
1078.9	188.9(M), 209.2(W), 212.9(W), 297.1(W)
1088.1	215.6(W), 241.1(M), 264.7(W), 326.0(M)
1091.6	215.6(W), 233.6(W), 326.0(M)
1093.3	ann(W), 1100.4(W)
1100.4	215.6(S), 241.1(M), 498.4(W)
1107.2	215.6(S), 271.4(M)
1124.5	165.9(W), 372.3(W)
1158.3	190.0(W), 203.9(W), 326.0(M)
1188.0 ^d	203.9(M), 272.5(W), 578.5(M)
1192.1	632.1(M)
1210.1	215.6(M), 326.0(W)
1215.7	215.6(S)
1257.0	202.0(M), 336.1(W), 615.3(M)
1261.7	202.0(W), 295.8(W)
1264.1	261.4(W), 420.0(M)
1282.2	159.7(M), 326.0(W), 329.4(W), 580.4(M)
1296.0	199.3(W), 473.0(W)
1305.0	224.5(W), 264.7(M)

Table 4-5 (Continued)

Gate Energy* (keV)	Energy of Coincident Gamma-Rays and Their Relative Strengths ^a
1327.1 ^d	254.3(W), 326.0(W), 578.5(M)
1333.7	326.0(M)
1345.1	250.7(W), 685.8(M)
1380.9	370.8(M)
1440.7	326.0(M)
1457.5 ^f	326.0(M), 637.6(W)
1459.0 ^f	193.5(W), 215.6(M), 263.1(W), 336.1(W)
1469.8	215.6(S)
1485.2	131.4(W), 615.3(M)
1504.7	336.1(M), 375.4(M)
1522.4	248.6(M)
1546.1	172.1(W), 291.4(W)
1553.8	326.0(W), 580.4(W)
1583.7	264.7(M), 741.8(M)
1611.0 ^c	215.6(M), 264.7(M), 477.4(S), 526.3(W), 741.8(S)
1614.3 ^c	326.0(M), 477.4(M), 741.8(M)
1616.0 ^c	215.6(W), 264.7(M), 477.4(M), 741.8(M)
1841.4	580.4(S)
1911.0	264.7(W)
1977.2	563.2(W)
2021.5	375.4(W)
2031.9	264.7(M), 326.0(M)

Table 4-5 (Continued)

Gate Energy* (keV)	Energy of Coincident Gamma-Rays and Their Relative Strengths ^a
2043.2	264.7(M), 326.0(M)
2063.6	326.0(S)
2068.4	215.6(S), 264.7(S)
2073.0	215.6(W), 264.7(M)
2079.4	246.5(M)
2085.0	215.6(S), 264.7(S)
2089.5	215.6(M)
2097.9	215.6(S), 326.0(W)
2102.9	336.1(M), 341.2(W)
2111.0	215.6(M), 246.5(W)
2138.0	215.6(M), 231.7(W), 264.7(W)
2190.6	215.6(S)
2327.4	215.6(W)
2334.5	215.6(W)

* Note: γ - γ -t data were taken mainly from Run 191-4. Gates were also set on γ -rays of 1551.9, 1562.9, 1604.2, and 2360.4 keV. Each of these gates showed no coincidences.

^a Relative coincidence strengths are given by:
 S = strong coincidence relationship, >90% confidence level;
 M = moderate coincidence relationship, >70% confidence level;
 W = weak coincidence relationship, >40% confidence level.

^b Data taken from e- γ -t experiment, Run 191-5.

^c Gate set in a region having multiple peaks, overlapping coincident γ -rays from neighboring gate are probable.

^d Hg and Tl are present in this gate.

^e Contamination from ¹⁹²Tl is present in this gate.

^f Gate energy not found in singles.

sparse amount of poor quality data were accumulated ($\sim 9 \times 10^5$ events) in a 2.4-hour period. The second experiment, Run 191-5, employed a 16% Ge(Li) γ -ray detector (~ 30 -2700 keV energy range over 4096 channels) and the better on-line Si(Li) detector (2.5-3.0 keV FWHM resolution for K electrons, ~ 30 -1600 keV energy range over 4096 channels), and the statistical quality of the data was much improved. The e- γ coincidences were collected for 18 hours resulting in 1.8×10^6 coincident events. The analysis of the coincidence relationships from these experiments yielded no new information (compared to the γ - γ -t measurements) for γ -ray energies above 200 keV and so is not included among the reported results. The coincidence data between low-energy conversion electron lines and γ -rays proved to be extremely useful. Coincidence gates set on the L-conversion lines of the 49, 52, and 103 keV transitions are shown in Figures 4-8 and 4-9. These low-energy coincidences are included in Table 4-5 and replace the gates set on weak 49, 52, and 103 keV γ -rays in the γ - γ -t coincidence work.

The ^{191m}Tl Decay Scheme

The decay scheme of ^{191m}Tl , shown in Figure 4-10, was constructed through use of the coincidence results and energy sums and differences. As is indicated in Figure 4-10, most of the transitions are placed by coincidence relationships (denoted by dots at the decaying levels). Note that in transitions having multipolarities that appear to be admixtures, the dominant component is given first.

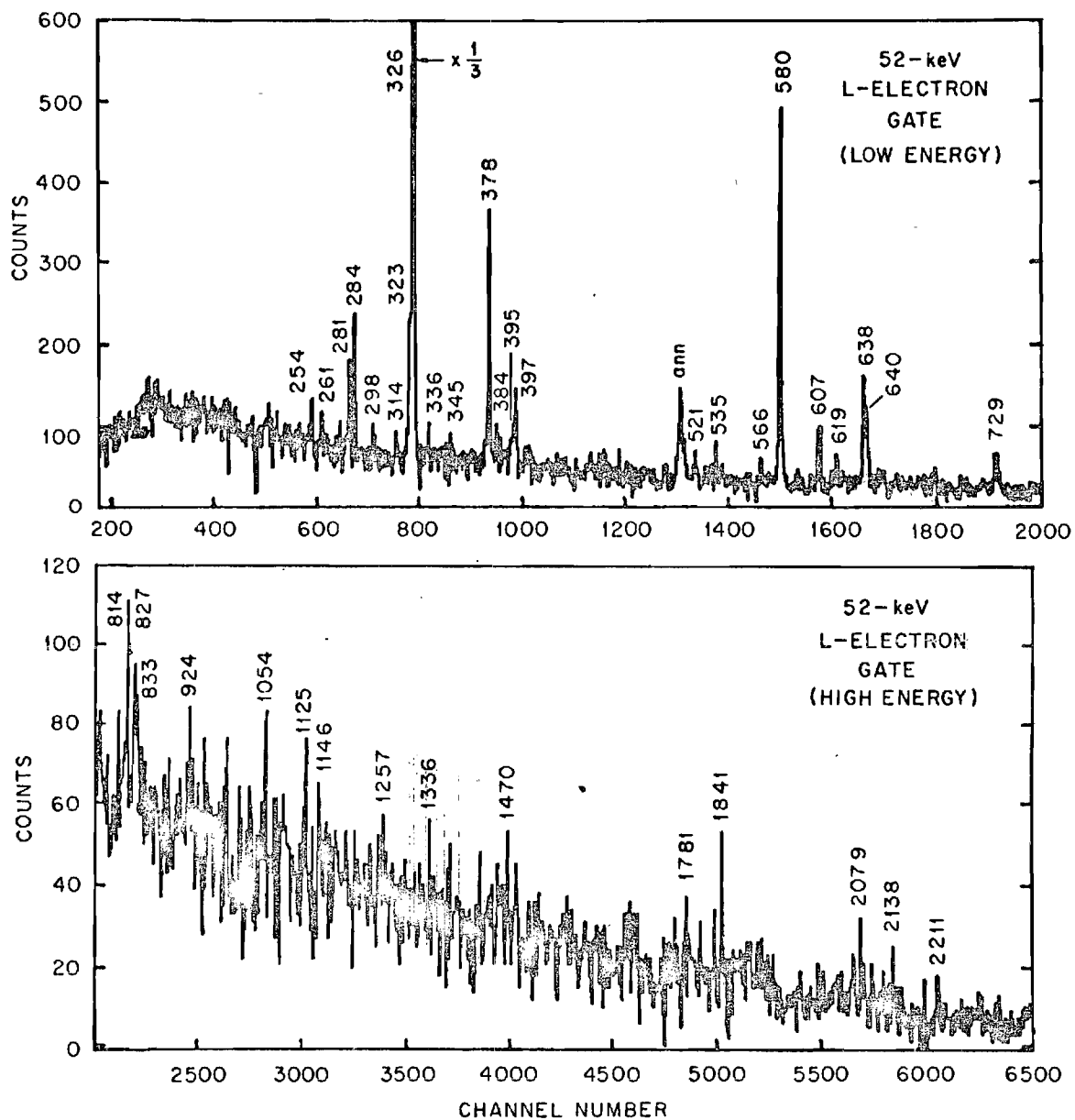


Figure 4-8. The Gamma-Rays in Coincidence with the 52 keV L Electrons Observed in the Decay of ^{191m}Tl and Taken in the $e\text{-}\gamma\text{-t}$ Experiment, Run 191-5.

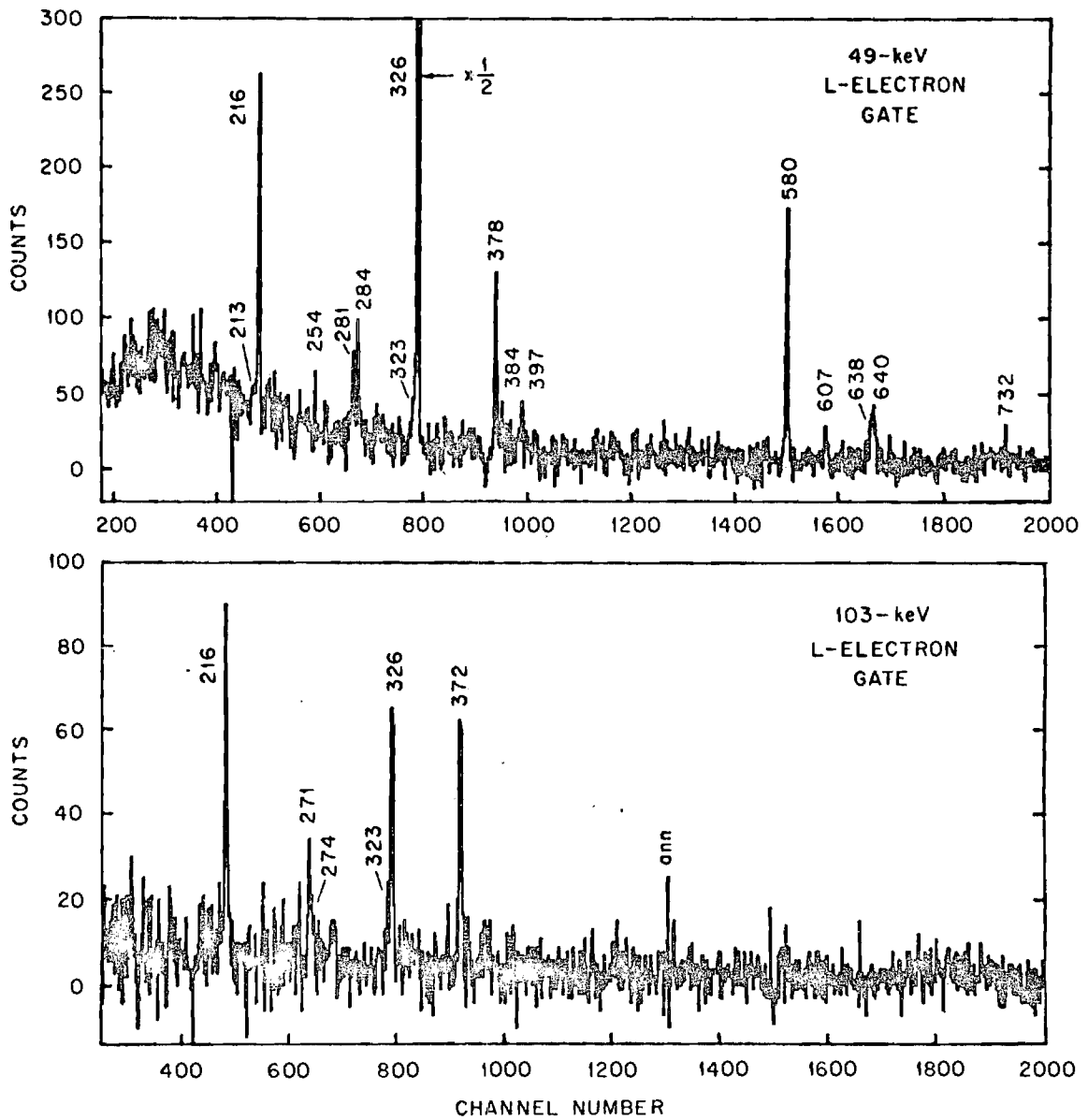


Figure 4-9. The Gamma-Rays in Coincidence with the 49 and 103 keV L Electrons Observed in the Decay of ^{191}mTl and Taken in the e- γ -t Experiment, Run 191-5.

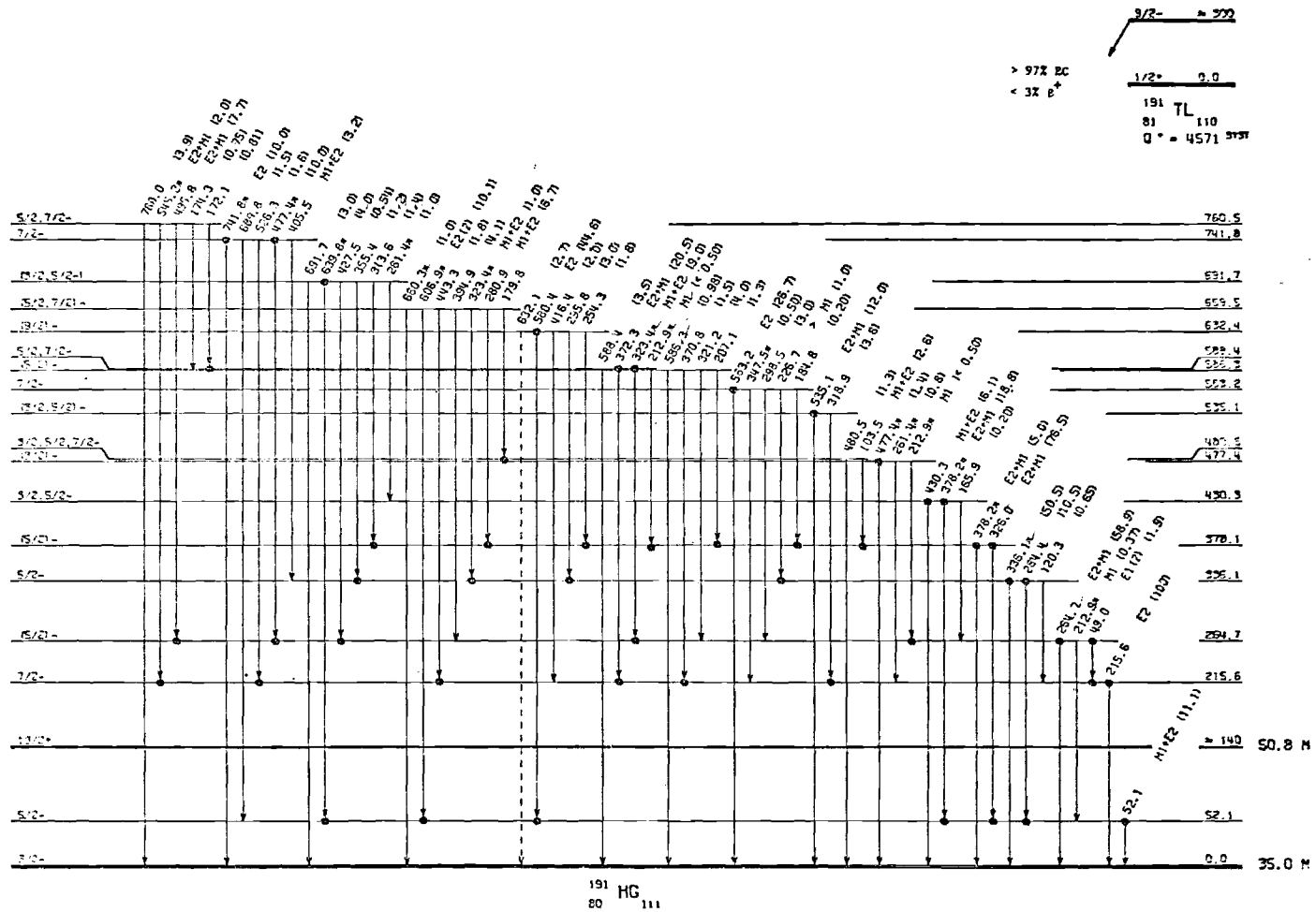


Figure 4-10 (a). The Decay Scheme for ^{191m}Tl : Part I - Transitions from Levels below 800 keV. Transitions seen in coincidence with others below it are indicated with dots on the tip of the arrow; those in coincidence with transitions above have dots on the tail of the arrow. Transition energies and multiplicities, and gamma-ray intensities are given. Dashed lines indicate questionable levels or transitions. Gamma-rays placed more than once are denoted by ■ .

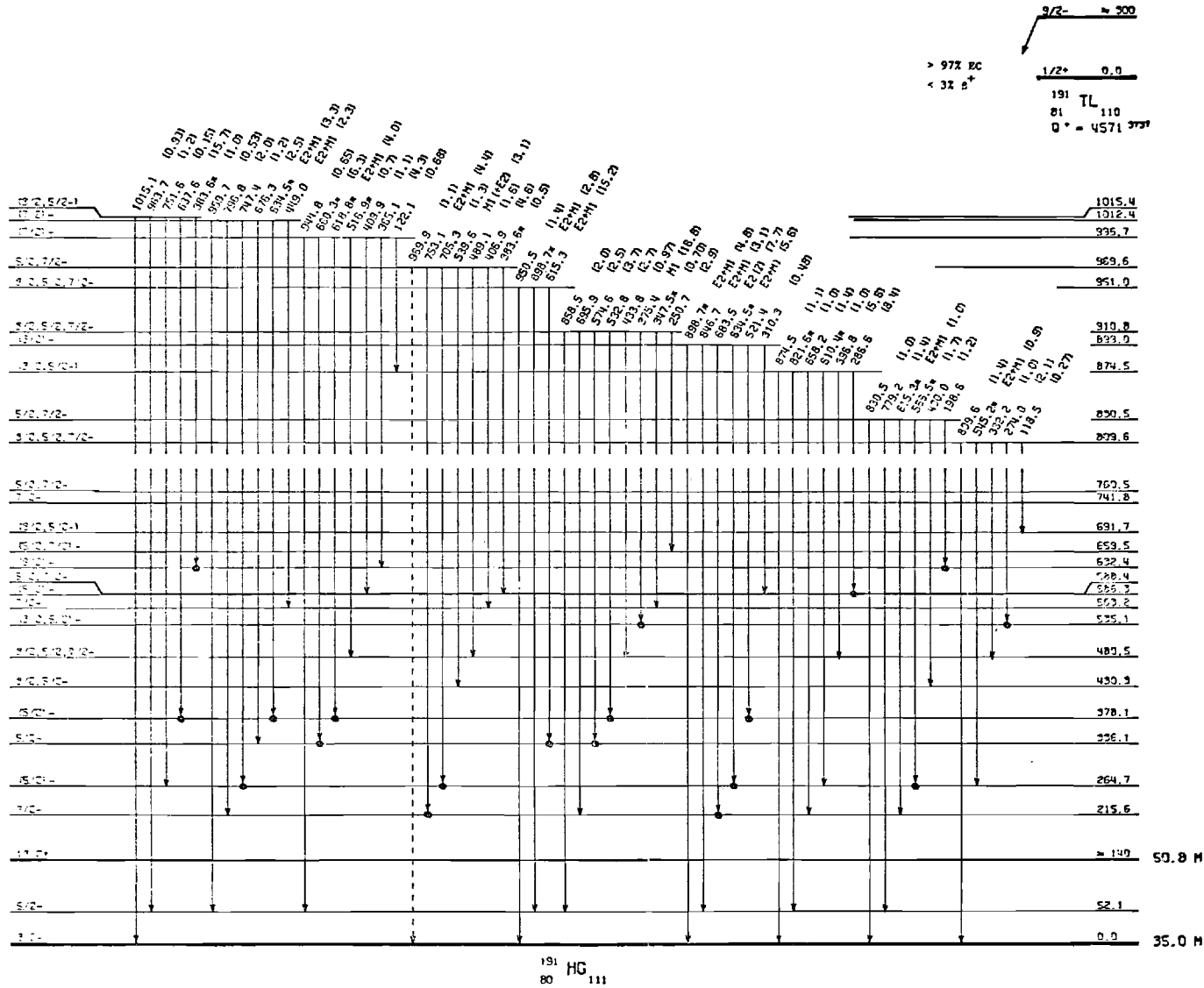


Figure 4-10(b). The Decay Scheme for ^{191m}Tl : Part II - Transitions from Levels between 800 and 1016 keV.

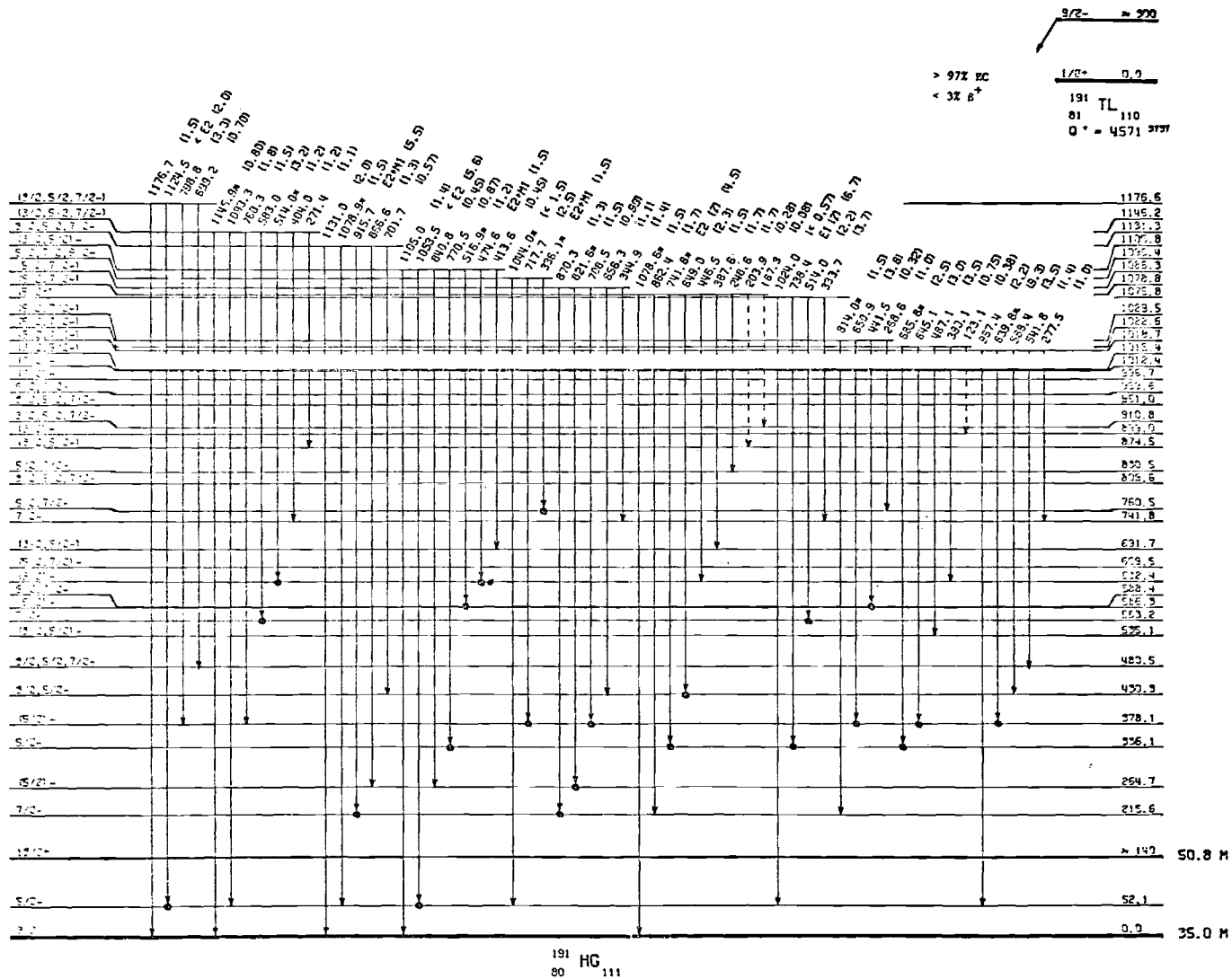


Figure 4-10(c). The Decay Scheme for ^{191m}Tl : Part III - Transitions from Levels between 1016 and 1190 keV.

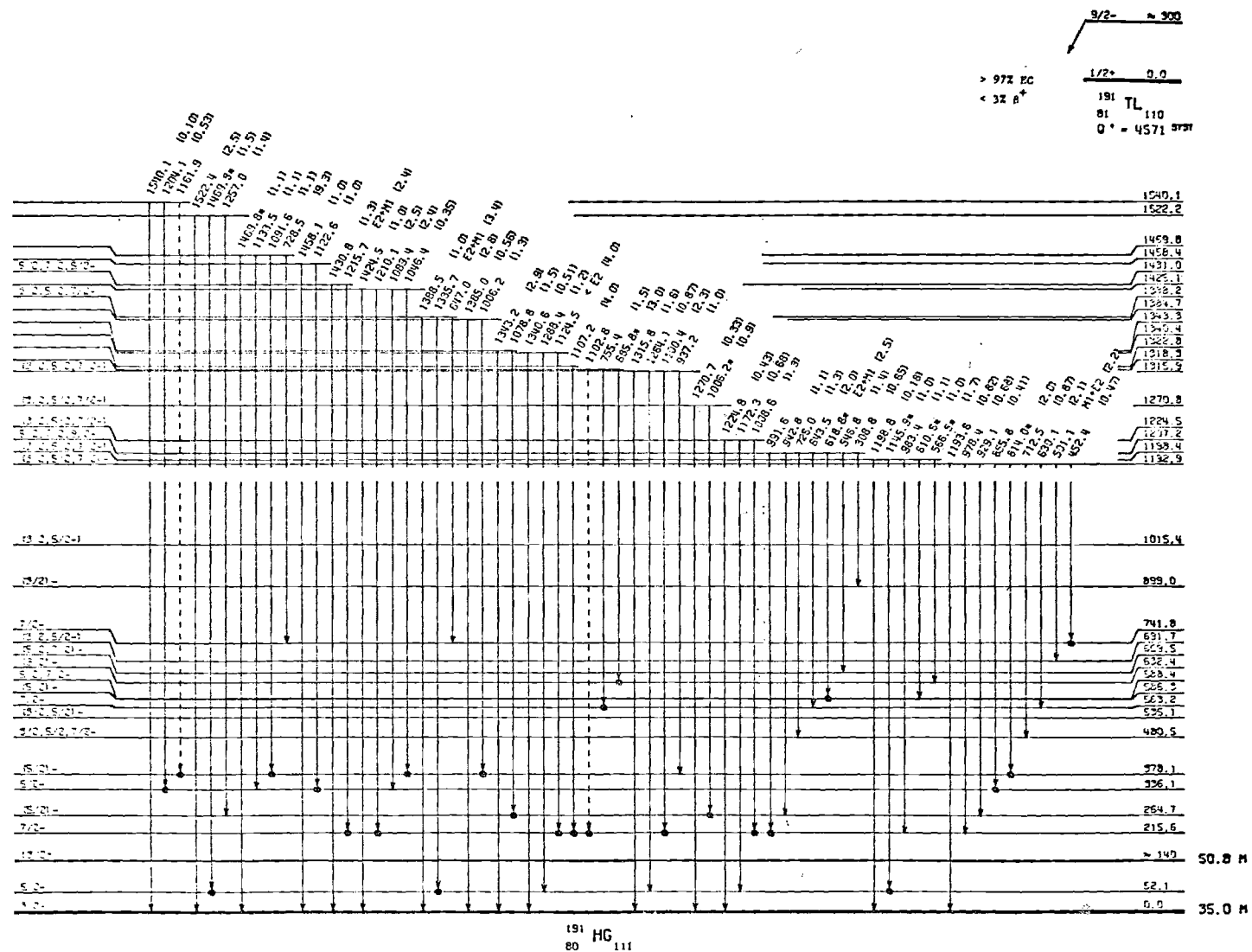


Figure 4-10(d). The Decay Scheme for ^{191m}Tl : Part IV - Transitions from Levels between 1190 and 1550 keV.

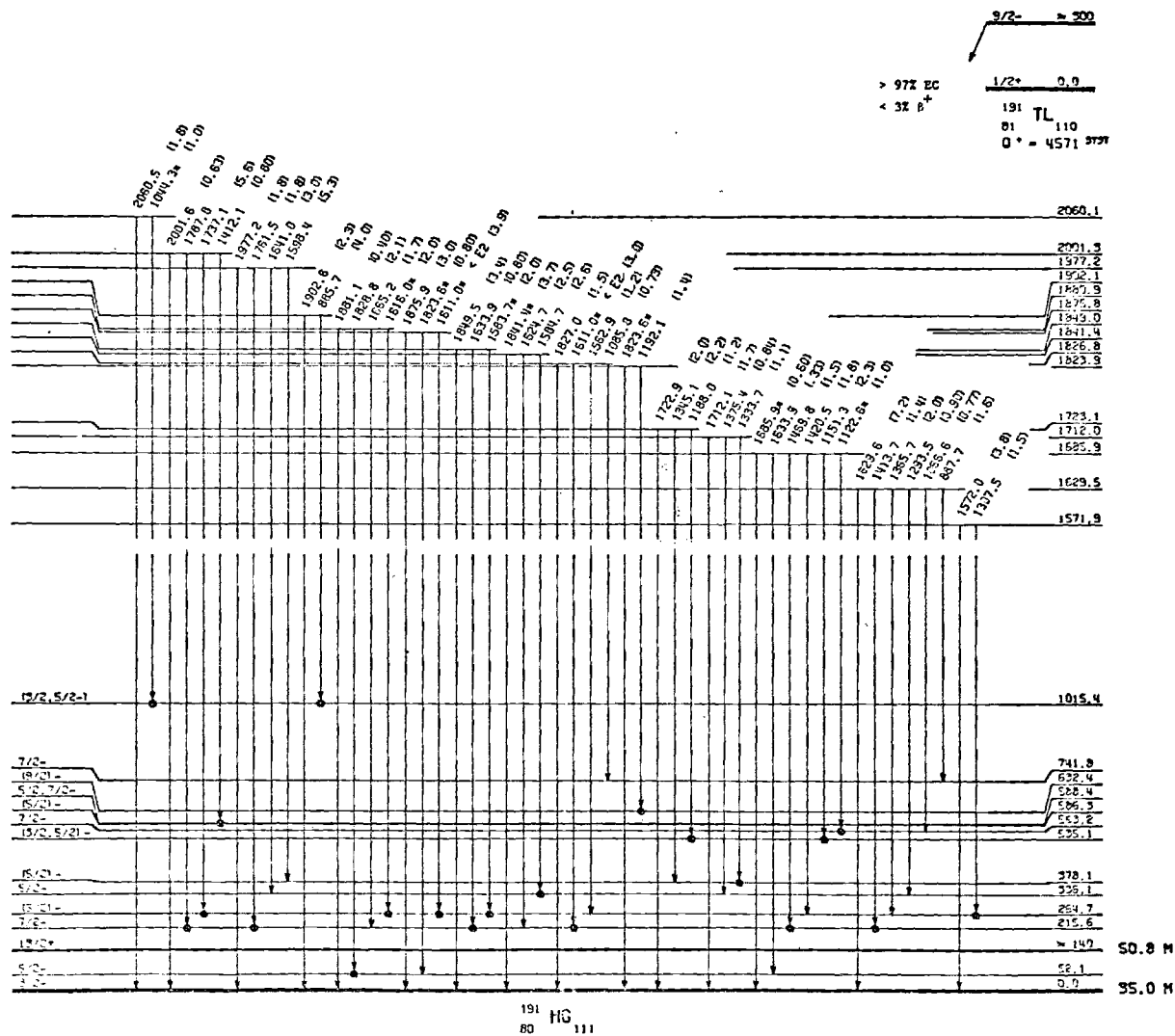


Figure 4-10(e). The Decay Scheme for ^{191m}Tl : Part V - Transitions from Levels between 1550 and 2100 keV.

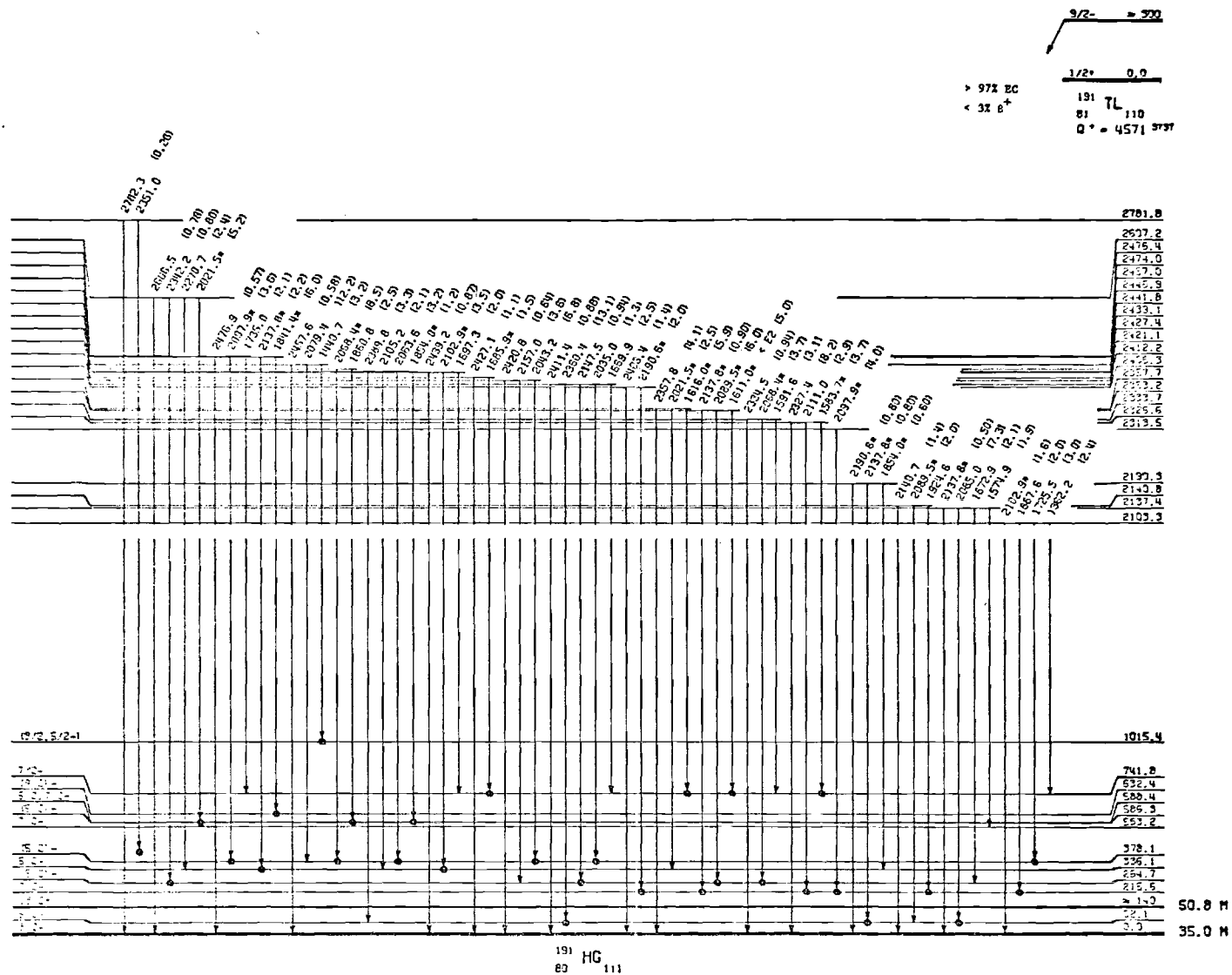


Figure 4-10(f). The Decay Scheme for ^{191m}Tl : Part VI - Transitions from Levels above 2100 keV.

Levels in ^{191}Hg

The only previous knowledge of levels in this nucleus comes from the in-beam work of Lieder et al.,²⁸⁾ who determined the yrast levels of the $i_{13/2}$ band up to $37/2^+$ and a high-spin negative parity band having spins and parities of $21/2^-$ through $37/2^-$ which has been placed relative to the $i_{13/2}$ band. The ground state spin-parity of $3/2^-$ and the approximate placement of the $13/2^+$ level 140 keV above the ground state were assigned through systematic considerations (see Chapter V).

The first excited level placed at 52.1 keV was assigned a spin-parity of $5/2^-$ on the basis of systematic trends (of the $f_{5/2}$ state) in the odd-Hg isotopes (see Chapter V) and its strong transition intensity observed in the conversion electron work. The remaining spins and parities were assigned, using the ground and first excited states as reference points, from the multipolarities of the various transitions feeding these two states. The multipolarities were deduced through a comparison of calculated conversion coefficients with theoretical ones from Hager and Seltzer.¹¹³⁾ The conversion coefficients determined were mainly from Hg K-conversion lines, many of which were contaminated with Au K-, Hg or Au L- or M- conversion lines, which had to be removed in order for these K-conversion coefficients to be determined. Because of the contamination problems, the conversion coefficients of several of the stronger lines could not be determined.

The ^{191}Hg level scheme based mainly on coincidence relationships involving the ground state and first four excited states (52.1, 215.6, 264.7, and 336.1 keV). This framework aided in locating the higher-

lying levels. Energy sums and differences were used to confirm these levels. Note that only a few high-lying levels were determined from a single coincidence, the bulk of the levels required two or more confirmed coincidence relationships in order to define them. The levels were checked and corrected using a total transition intensity balance (where available) among the transitions populating and depopulating each level. Despite the fact that over 350 γ -rays were assigned to depopulate the 93 levels, many of the weaker $A = 191$ lines seen in γ -ray singles spectra and some in the coincidence gates could not be assigned to the decay of either ^{191m}Tl or $^{191g,m}\text{Hg}$. More coincidence data and better singles statistics might have been helpful in the assignments of these lines.

Other Decays

Decay of ^{195g}Tl

The γ -ray spectra from mass-separated $A = 195$ sources were studied in several experiments detailed in Table 4-6. The spectral multiscaling data collected in two of the experiments yielded half-lives of both the Tl and other nuclides and aided in the identification of γ -rays associated with their decay. The sum of all spectra taken in Run 195-2 (which are of considerably superior statistical quality to that of Run 195-1) is shown in Figures 4-11 and 4-12. Gamma-ray transitions following the decay of ^{195}Pb , ^{195}Hg , and other minor contaminants have been indicated, while those following the decay of ^{195}Tl have been labeled only with the decay energy. A spectrum

Table 4-6. Details of ^{195}Tl Experiments

Run Number	Reaction(s) and Projectile Energy	Detectors Used and Their Energy Ranges ^a	Measurement(s) Made and Data Acquisition System Used	Collection Times and Counting Times	Number of Coincidence Events Collected
195-1 ^b	Nat. Re($^{16}\text{O,pxn}$) ^{195}Pb $^{195}\text{Pb} \rightarrow ^{195}\text{Tl}$ 141.3 MeV	11% Ge(Li) 30-3200 keV (8192 channel(s))	γ -ray singles multiscaling using the TN-1700	2 hour collections; counted as 8 sequential 15-min spectra (2 sources counted)	
195-2 ^b	Nat. W($^{16}\text{O,pxn}$) ^{195}Tl 142.9 MeV	16% Ge(Li) ^{c,d} 45-3300 keV and 10% Ge(Li) 25-2100 keV	γ -ray singles multiscaling using the TN-1700 and γ - γ -t coincidences using the SEL 840A system	(1) 2.2 hour collections; counted as 16 sequential 500-sec spectra (9 sources counted) (2) γ - γ -t collected for 20 hours	4.7×10^6
195-3 ^e	Nat. Re($^{16}\text{O,pxn}$) ^{195}Pb $^{195}\text{Pb} \rightarrow ^{195}\text{Tl}$ 141.3 MeV	16% Ge(Li) and off-line Si(Li) electron detector both 30-1750 keV (4096 channels)	Ce^- and γ -ray singles multi-scaling and e- γ -t coincidences using the off-line Tennecomp TP-5000 system	(1) 25 minute collections; counted as 20 sequential 1-min spectra (2) e- γ -t collected for 3 hours	4×10^5

Table 4-6 (Continued)

Run Number	Reaction(s) and Projectile Energy	Detectors Used and Their Energy Ranges ^a	Measurement(s) Made and Data Acquisition System Used	Collection Times and Counting Times	Number of Coincidence Events Collected
195-4 ^e	Nat. W(¹⁶ O,xn) ¹⁹⁵ Pb ¹⁹⁵ Pb → ¹⁹⁵ Tl Nat. W(¹⁶ O,pxn) ¹⁹⁵ Tl 124.6 MeV	18% Ge(Li) 35-2500 keV and 15% Ge(Li) 40-2500 keV	γ-γ-t coincidences using the SEL 840A system	γ-γ-t collected for about 5 hours	2.9 x 10 ⁶

^aAll coincidence measurements made on one of the Tennecomp TP-5000 systems had data collected 8192 channels each for the two events and the TAC; the data were similarly collected on the SEL 840A system 9500 channels each for the three parameters.

^bChemically-separated sources were used.

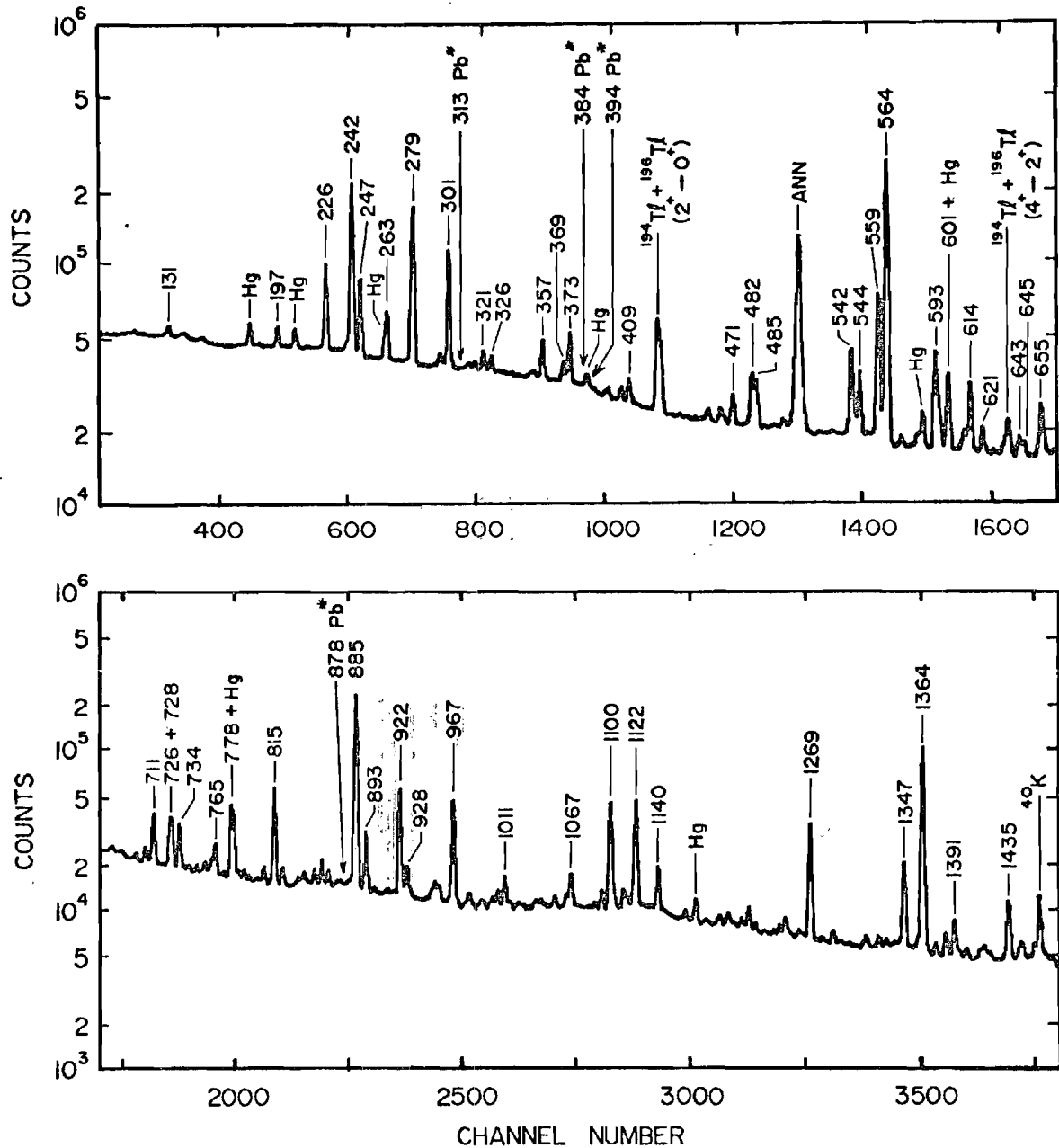


Figure 4-11. Low Energy Portion of the Chemically-Separated A = 195 Singles Gamma-Ray Spectrum: Total Sum of Run 195-2. Those transitions following the decay of ^{195}Hg or other contaminating species have been given special labels, while those associated with the decay of ^{195}Tl have been labeled only with the decay energy. Note that the approximate positions of the strongest ^{195}Pb gamma-rays are shown (indicated with an *) for comparison with Figure 4-13.

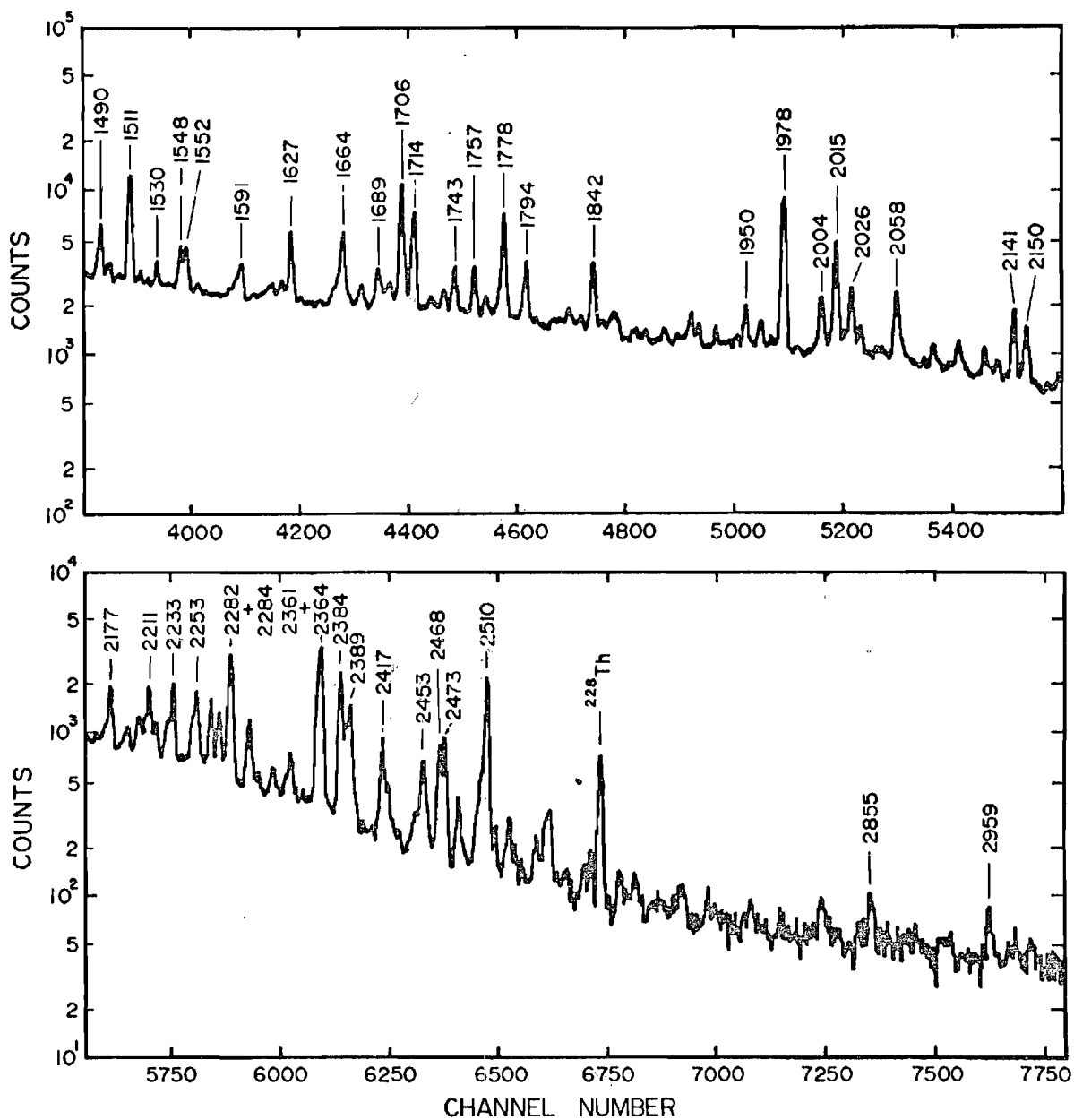


Figure 4-12. High Energy Portion of the Chemically-Separated A = 195 Singles Gamma-Ray Spectrum: Total Sum of Run 195-2. Those transitions following the decay of ^{195}Hg or other contaminating species have been given special labels, while those associated with the decay of ^{195}Tl have been labeled only with the decay energy.

of a non-chemically-separated source of ^{195}Tl plus $^{195}\text{Pb}^{114}$) is shown in Figure 4-13 for comparison. This figure has the gamma-rays from the ^{195}Tl decay labeled as such, while those from the ^{195}Pb decay are labeled only with the decay energy.

The half-life of the ^{195g}Tl was determined by following the decay of several strong lines in the chemically-separated sample of Run 195-2. The half-life deduced (1.13 ± 0.06 hours) is in good agreement with previously reported values.^{24,115)} The relative intensities of γ -rays from the decay of ^{195g}Tl were also measured in the above two experiments. The results of Run 195-2 have been adopted because of their superior statistical quality and are shown in the ^{195g}Tl decay scheme — Figure 4-14.

Conversion electrons were studied in Run 195-3. Using the conversion coefficients for the strong lines reported by Vandlik et al.²⁴⁾ an internal normalization factor was obtained and the K- (plus some L- and M-) conversion coefficients for the other transitions were deduced. The results of a comparison of those conversion coefficients with theoretical values¹¹³⁾ are reported in Figure 4-14 in the form of multipolarity assignments of the transitions involved.

Two separate experiments, Runs 195-2 and 195-4, were done to collect γ - γ -t coincidence data from the ^{195}Tl decay. In addition, e- γ -t data were collected in Run 195-3. The results of analysis of the coincidence relationships from these experiments are summarized in Figure 4-14.

The decay scheme of ^{195g}Tl , shown in Figure 4-14, was constructed through the use of both coincidence results and energy sums and

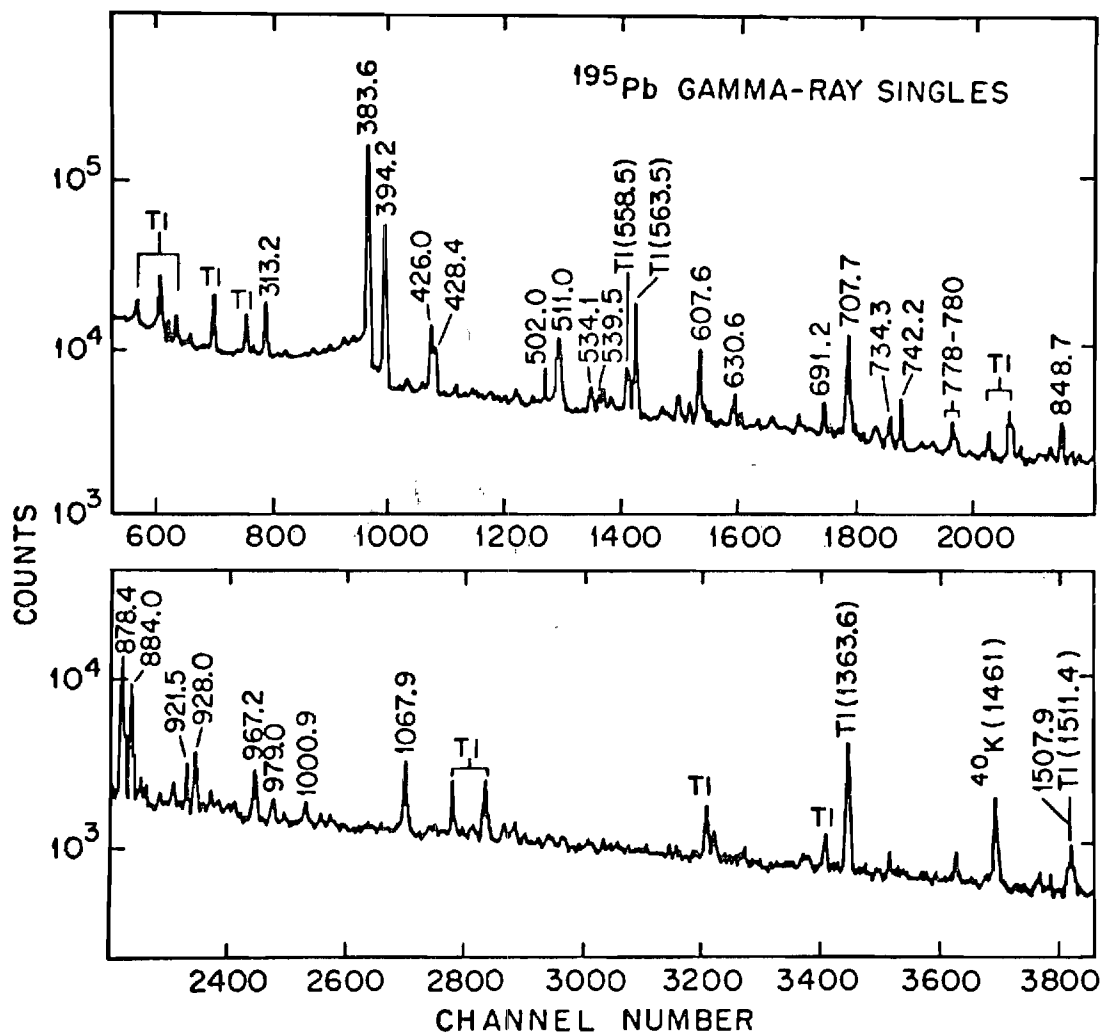


Figure 4-13. Singles Gamma-Ray Spectrum of Non-Chemically Separated $A = 195$ Sources (from ref. 114). Those transitions following the decay of ^{195}Tl have been given special labels, while those associated with the decay of ^{195}Pb have been labeled only with the decay energy.

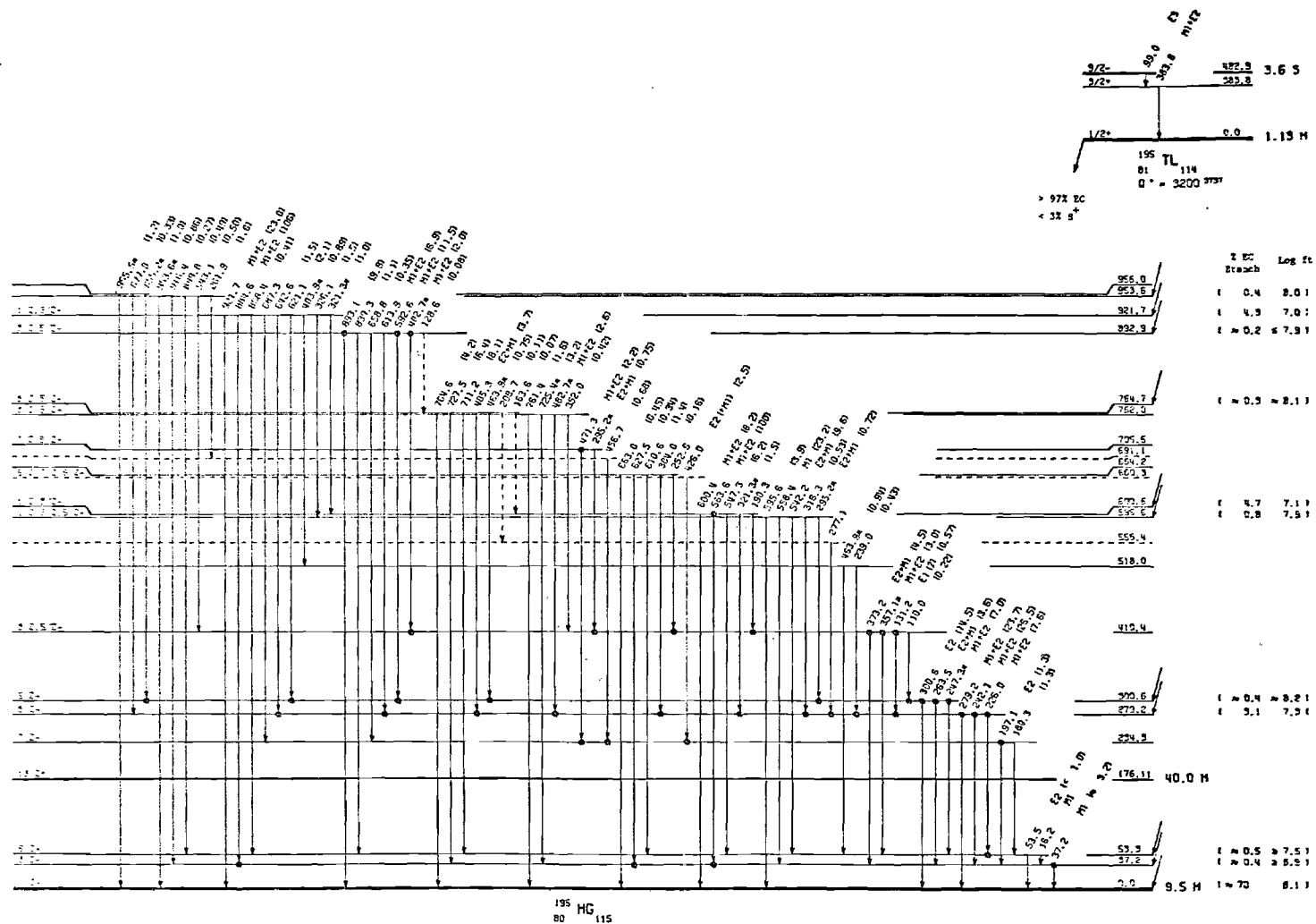


Figure 4-14(a). The Decay Scheme for ^{195m}Tl (with some ^{195m}Tl Admixture): Part I - Transitions from Levels below 1000 keV. Transitions seen in coincidence with others below it are indicated with dots on the tip of the arrow; those in coincidence with transitions above have dots on the tail of the arrow. Transition energies and multipolarities and gamma-ray intensities are given. Branching ratios and log ft values are also shown for some of the levels. Dashed lines indicate questionable levels or transitions. Gamma-rays placed more than once are denoted by \oplus .

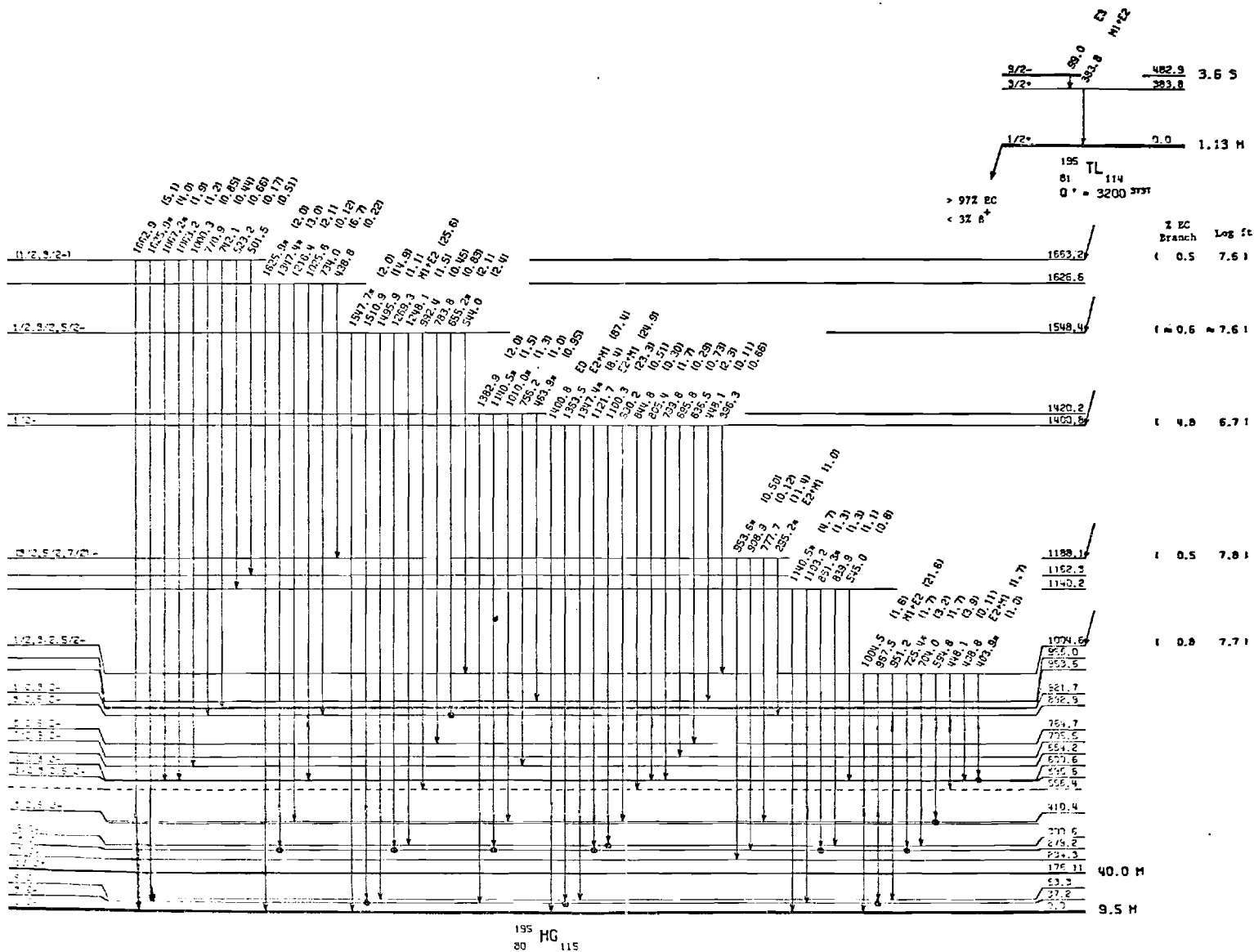


Figure 4-14(b). The Decay Scheme for ^{195g}Tl (with some ^{195m}Tl Admixture): Part II - Transitions from Levels between 1000 and 1700 keV.

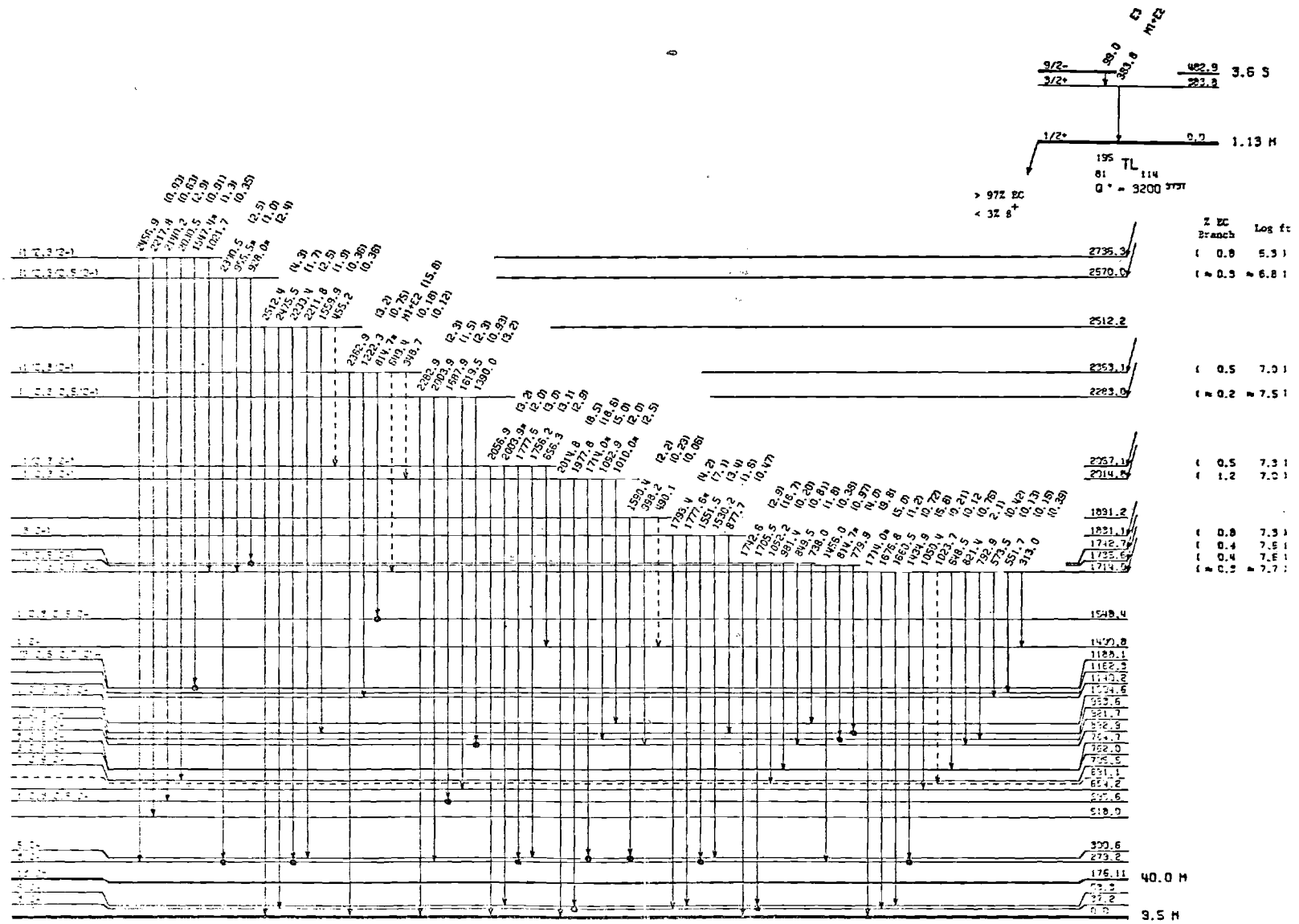


Figure 4-14(c). The Decay Scheme for ^{195g}Tl (with some ^{195m}Tl Admixture): Part III - Transitions from Levels above 1700 keV.

differences. As indicated in this figure, most of the transitions are placed by coincidence relationships. A transition intensity balance (where available) was used to check and correct the levels through their populating and depopulating transitions. The intensity balance was used to estimate the EC branching ratios to some of the ^{195}Hg levels. (The β^+ branching was neglected because it is predicted to be $< 3\%$ of the total decay.) These branching ratios were combined with the electron capture decay energy (Q_{EC}) determined from systematics,^{116,117)} in order to obtain $\log ft$ values for the EC transitions from the ground state of the parent Tl nucleus to some of the individual levels in the daughter Hg nucleus. These values are based on the γ -ray intensity assigned to this decay. It is possible, however, that a significant proportion of the decay goes to a large number of high energy states which decay by weak unobserved high-energy γ -transitions. Our measurements are superior to the best previous work,²⁴⁾ and show several new levels, notably at 234.3, 410.4, 518.1, 664.2, and 705.5 keV, and also confirm, by coincidence observations, many of the previously assigned levels. An interpretation of some of this new level structure is given in Chapter V.

Decay of $^{189\text{m}}\text{Tl}$

Gamma-ray singles data were taken in a number of experiments listed in Table 4-7. Most of the information relating to measurement of energies and relative intensities from total singles results and half-lives and γ -ray identification (by decay) from singles spectral multi-scaling came from the two best experiments, Runs 189-1 and 189-2. From

Table 4-7. Details of ^{189}Tl Experiments^a

Run Number	Reaction(s) and Projectile Energy	Detectors Used and Their Energy Ranges ^b	Measurement(s) Made and Data Acquisition System Used	Collection Times and Counting Times	Number of Coincidence Events Collected
189-1	$^{181}\text{Ta}(^{16}\text{O},8\text{n})^{189}\text{Tl}$ 143 MeV	16% Ge(Li) and on-line Si(Li) electron detector (5.5 keV FWHM) both 30-1500 keV (4096 channels)	Ce^- and γ -ray singles multi-scaling and e- γ -t coincidences using the on-line Tennecomp TP-5000 system	(1) 4 minute collections; counted as 16 sequential 15-sec spectra (2) e- γ -t collected for 3 hours	4×10^5
189-2	$^{181}\text{Ta}(^{16}\text{O},8\text{n})^{189}\text{Tl}$ 143 MeV	(1) 18% Ge(Li) 50-3450 keV (8192 channels) (2) 16% Ge(Li) and 15% Ge(Li) both 30-2300 keV	(1) γ -ray singles multiscaling using the off-line Tennecomp TP-5000 system (2) γ - γ -t coincidences using the SEL 840A system	(1) 6 minute collection; counted as 12 sequential 30-sec spectra (2) γ - γ -t collected for 5 hours	4.2×10^6

Table 4-7 (Continued)

Run Number	Reaction(s) and Projectile Energy	Detectors Used and Their Energy Ranges ^b	Measurement(s) Made and Data Acquisition System Used	Collection Times and Counting Times	Number of Coincidence Events Collected
189-3	$^{181}\text{Ta}(^{16}\text{O}, 8n)^{189}\text{Tl}$ 145.6 MeV	16% Ge(Li) and on-line Si(Li) electron detector (5.5 keV FWHM) both 25-2000 keV (2048 channels)	Ce^- and γ -ray singles multi-scaling and e- γ -t coincidences using the on-line Tennecomp TP-5000 system	(1) 200 sec collections; counted as 10 sequential 20-sec spectra (2) e- γ -t collected for 5 hours	2×10^6

^aOnly the experiments yielding significant results are given.

^bAll coincidence measurements made on one of the Tennecomp TP-5000 systems had data collected with 8192 channels each for the two events and the TAC; the data were similarly collected on the SEL 840A system with 9500 channels each for the three parameters.

data obtained in those two experiments, the half-life of the $9/2^-$ high-spin isomer in ^{189}Tl is determined to be 1.42 ± 0.09 minutes. This value compares favorably with the only previous measurement of the half-life by Vandlik, et al.,²⁰⁾ which was attributed to the ground state decay; however, it has been shown that this half-life belongs to the $9/2^-$ isomer (see Chapter V). The energies and relative intensities for all of the γ -rays assigned to the decay of 1.4 min ($9/2^-$) $^{189\text{m}}\text{Tl}$ are shown in Figure 4-15.

Conversion electrons from the decay of $^{189\text{m}}\text{Tl}$ were studied in Runs 189-1 and 189-3. The latter experiment gave a total conversion electron spectrum of better statistical quality and had a slightly better energy resolution; thus, most of the final results come from this measurement. The pure E2 and M1 transitions previously known from the decays of the contaminating ^{189}Hg isomers¹¹⁸⁾ were used to obtain a normalization factor for the conversion electrons from the decay of $^{189\text{m}}\text{Tl}$. Using this, the K- (and in a few cases L- and M-) conversion coefficients for 1.4 min $^{189\text{m}}\text{Tl}$ ($9/2^-$) transitions were calculated. The multipolarities deduced from a comparison of these conversion coefficients with theoretical calculations,¹¹³⁾ are given in Figure 4-15. Data on e- γ -t coincidences also were obtained during these two experiments.

Coincidence data on γ -rays from $^{189\text{m}}\text{Tl}$ decay were obtained in a number of separate experiments. The most prominent γ - γ -t experiment involved the data recorded during Run 189-2. The results of coincidence analyses from all experiments are summarized in the decay scheme shown in Figure 4-15.

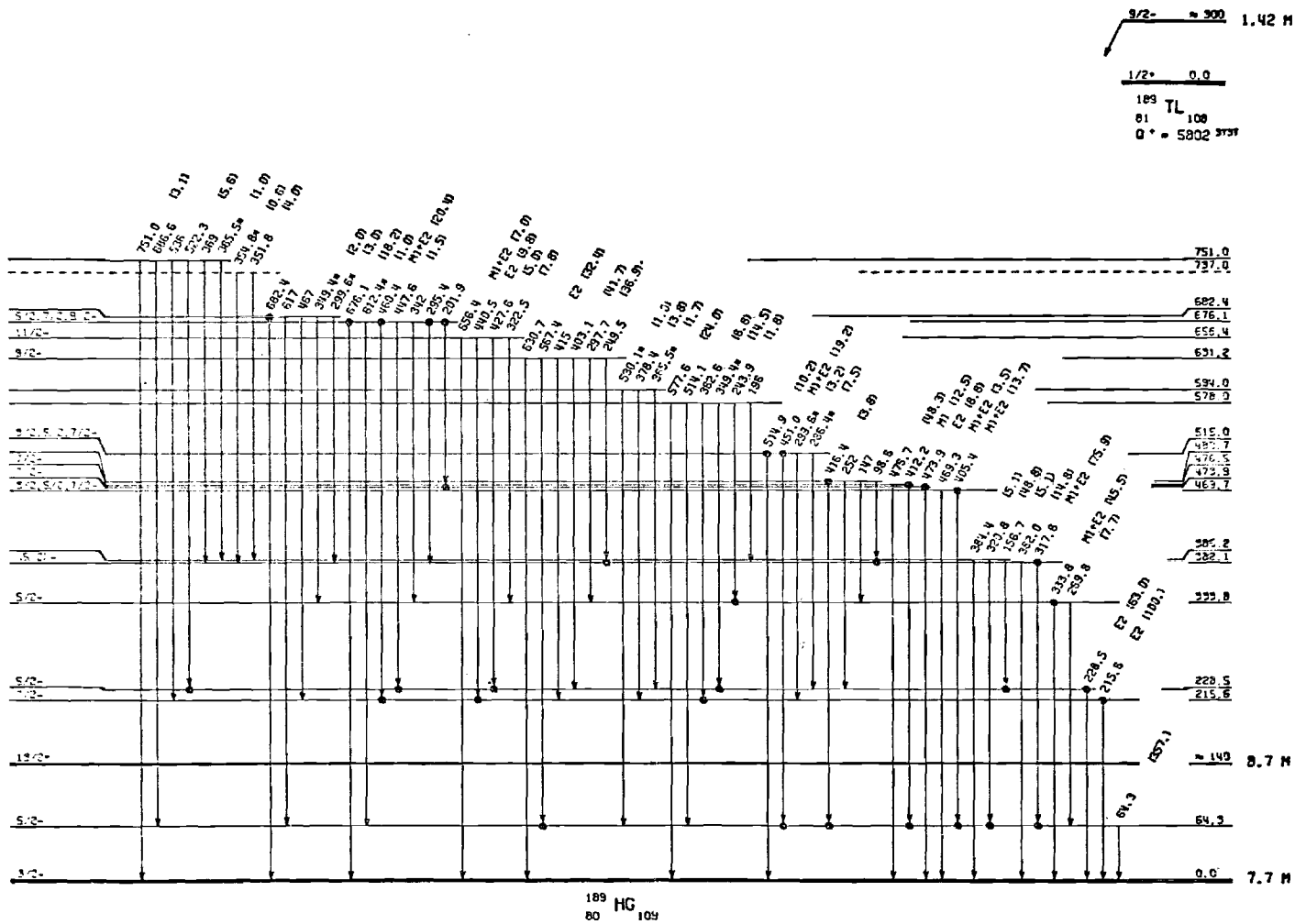


Figure 4-15(a). The Decay Scheme for $^{189\text{m}}\text{Tl}$: Part I - Transitions from Levels below 760 keV. Transitions seen in coincidence with others below it are indicated with dots on the tip of the arrow; those in coincidence with transitions above have dots on the tail of the arrow. Transition energies and multiplicities, and gamma-ray intensities are given. Dashed lines indicate questionable levels or transitions. Gamma-rays placed more than once are denoted by # .

The ^{189m}Tl decay scheme (Figure 4-15) was constructed in the same manner as the $^{191m},^{195g}\text{Tl}$ schemes, based mainly on the extensive use of coincidence relationships as well as energy sums and differences. Previous work²⁰⁾ on the decay of ^{189m}Tl is limited to a determination of the half-life and the energies of three γ -rays. The experiments done at UNISOR have allowed the construction of a decay scheme with 117 γ -rays assigned to 40 levels built on a $3/2^-$ ground state, a $5/2^-$ first excited state at 64.3 keV, and a $13/2^+$ isomer at approximately 140 keV which were placed on the basis of systematic considerations (see Chapter V).

Decay of ^{193g}Tl

Gamma-ray singles and singles-multiscaling data were studied in various ways in several experiments outlined in Table 4-8. The majority of the singles information came from three of these experiments, Runs 193-1 through 193-3, all of which used spectral multiscaling to obtain the half-life of the ^{193}Tl ground state and to identify γ -rays associated with its decay. The best information concerning the ^{193g}Tl half-life came from Run 193-2, due to the high statistical quality of the data. From the decay properties of the strong γ -transitions, the half-life was deduced to be 22.6 ± 0.7 min, in good agreement with the values given by Vandlik, et al.²³⁾ and Nuclear Data Sheets.¹¹⁹⁾ The relative intensities of the ^{193g}Tl γ -rays were also measured in these three experiments. The results of these measurements are given in Figure 4-16 with the final γ -ray energy values also determined from the singles data collected during these experiments.

Table 4-8. Details of ^{193}Tl Experiments

Run Number	Reaction(s) and Projectile Energy	Detectors Used and Their Energy Ranges ^a	Measurement(s) and Data Acquisition System Used	Collection Times and Counting Times	Number of Coincidence Events Collected
193-1 ^b	Nat. W($^{16}\text{O},\text{xn}$) ^{193}Pb $^{193}\text{Pb} \rightarrow ^{193}\text{Tl}$ 125.3 MeV	10% Ge(Li) 40-2100 keV (4096 channels)	γ -ray singles multiscaling using the Canberra 8100	45 minute collections (and decays) from ^{193}Pb experiment; counted as 10 sequential 400-sec spectra	
193-2	Nat. W($^{16}\text{O},\text{xn}$) ^{193}Pb $^{193}\text{Pb} \rightarrow ^{193}\text{Tl}$ and Nat. W($^{16}\text{O},\text{pxn}$) ^{193}Tl 142.9 MeV	17% Ge(Li) \sim 30-2700 keV and off-line Si(Li) electron detector \sim 30-1200 keV (both 4096 channels)	Ce^- and γ -ray singles multi-scaling and e- γ -t coincidences using the off-line Tennecomp TP-5000 system	(1) 45 minute collections; counted as 15 sequential 3-min spectra (2) e- γ -t collected for 20 hours	5×10^6
193-3 ^c	Nat. Re($^{16}\text{O},\text{pxn}$) ^{193}Pb $^{193}\text{Pb} \rightarrow ^{193}\text{Tl}$ 128.9 MeV	17% Ge(Li) \sim 30-2700 keV and 18% Ge(Li) \sim 25-1600 keV (both 4096 channels)	γ -ray singles multiscaling and γ - γ -t coincidences using the off-line Tennecomp TP-5000 system	(1) 40 minute collections; counted as 10 sequential 4-min spectra (2) γ - γ -t collected for 3 hours	4×10^5

Table 4-8. Details of ^{193}Tl Experiments

Run Number	Reaction(s) and Projectile Energy	Detectors Used and Their Energy Ranges ^a	Measurement(s) and Data Acquisition System Used	Collection Times and Counting Times	Number of Coincidence Events Collected
193-4	Nat.W($^{16}\text{O,pxn}$) ^{193}Tl and Nat.Re($^{16}\text{O,pxn}$) ^{193}Pb $^{193}\text{Pb} \rightarrow ^{193}\text{Tl}$ both run at 143.0 MeV	16% Ge(Li) and off-line Si(Li) electron detector both ~ 30 -1700 keV (4096 channels)	Ce^- and γ -ray singles multiscaling using the off-line Tennecomp TP-5000 system	60 minute collections; counted as 15 sequential 4-min spectra	
193-5 ^b	Nat.W($^{16}\text{O,xn}$) ^{193}Pb $^{193}\text{Pb} \rightarrow ^{193}\text{Tl}$ 125.3 MeV	16% Ge(Li) and 10% Ge(Li) both ~ 40 -2500 keV	γ - γ -t coincidences using the SEL-840A system	γ - γ -t collected for about 5 hours	2.7×10^6
193-6 ^b	Nat.W($^{16}\text{O,xn}$) ^{193}Pb $^{193}\text{Pb} \rightarrow ^{193}\text{Tl}$ 113.0 MeV	2 16% Ge(Li) detectors both ~ 35 -2650 keV	γ - γ -t coincidences using the on-line Tennecomp TP-5000 system	γ - γ -t collected for about 15 hours	4×10^6
193-7	Nat.W($^{16}\text{O,xn}$) ^{193}Pb $^{193}\text{Pb} \rightarrow ^{193}\text{Tl}$ and Nat.W($^{16}\text{O,pxn}$) ^{193}Tl 142.9 MeV	17% Ge(Li) ~ 30 -2700 keV and 18% Ge(Li) ~ 25 -1600 keV (both 4096 channels)	γ -ray singles multiscaling and γ - γ -t coincidences using the off-line Tennecomp TP-5000 system	(1) 45 minute collections; counted as 15 sequential 3-min spectra (2) γ - γ -t collected for 6 hours	2×10^6

Table 4-8. Details of ^{193}Tl Experiments

Run Number	Reaction(s) and Projectile Energy	Detectors Used and Their Energy Ranges ^a	Measurement(s) and Data Acquisition System Used	Collection Times and Counting Times	Number of Coincidence Events Collected
193m-1	$^{186}\text{W}(^{14}\text{N},7\text{n})^{193}\text{Tl}$ 130.8 MeV	17% Ge(Li) ^d ~30-2650 keV (8192 channels) and 16% Ge(Li) ~25-1750 keV	γ -ray singles multiscaling and γ - γ -t coincidences using the on-line Tennecomp TP-5000 system	(1) 2 minute collections; counted as 12 sequential 10-sec spectra (2) γ - γ -t collected for 6.4 hours	6.5×10^6
193m-2 ^b	Nat.W($^{16}\text{O},\text{xn})^{193}\text{Pb}$ $^{193}\text{Pb} \rightarrow ^{193}\text{Tl}$ 113.0 MeV	16% Ge(Li) and on-line Si(Li) electron detector (5.5 keV FWHM) both 30-1500 keV (4096 channels)	Ce^- and γ -ray singles multi-scaling and e- γ -t coincidences using the on-line Tennecomp TP-5000 system	(1) 5 minute collections; counted as 10 sequential 30-sec spectra (2) e- γ -t collected for about 12 hours	8×10^5
193m-3 ^b	Nat.Re($^{16}\text{O},\text{pxn})^{193}\text{Pb}$ $^{193}\text{Pb} \rightarrow ^{193}\text{Tl}$ 141.3 MeV	16% Ge(Li) and on-line Si(Li) electron detector (2.5 keV FWHM) both ~30-1500 keV (4096 channels)	Ce^- and γ -ray singles multi-scaling and e- γ -t coincidences using the on-line Tennecomp TP-5000 system	(1) 5 minute collections; counted as 10 sequential 30-sec spectra (2) e- γ -t collected for 4.6 hours	2.4×10^6

Table 4-8 (Continued)

^aAll coincidence measurements made on one of the Tennecomp TP-5000 systems had data collected with 8192 channels each for the two events the TAC; the data were similarly collected on the SEL 840A system with 9500 channels each for the three parameters.

^bThe primary nucleus under study was ¹⁹³Pb.

^cChemically-separated sources were used.

^dThe Cu + Cd absorber was used on this detector for about one-half of the experimental data collection.

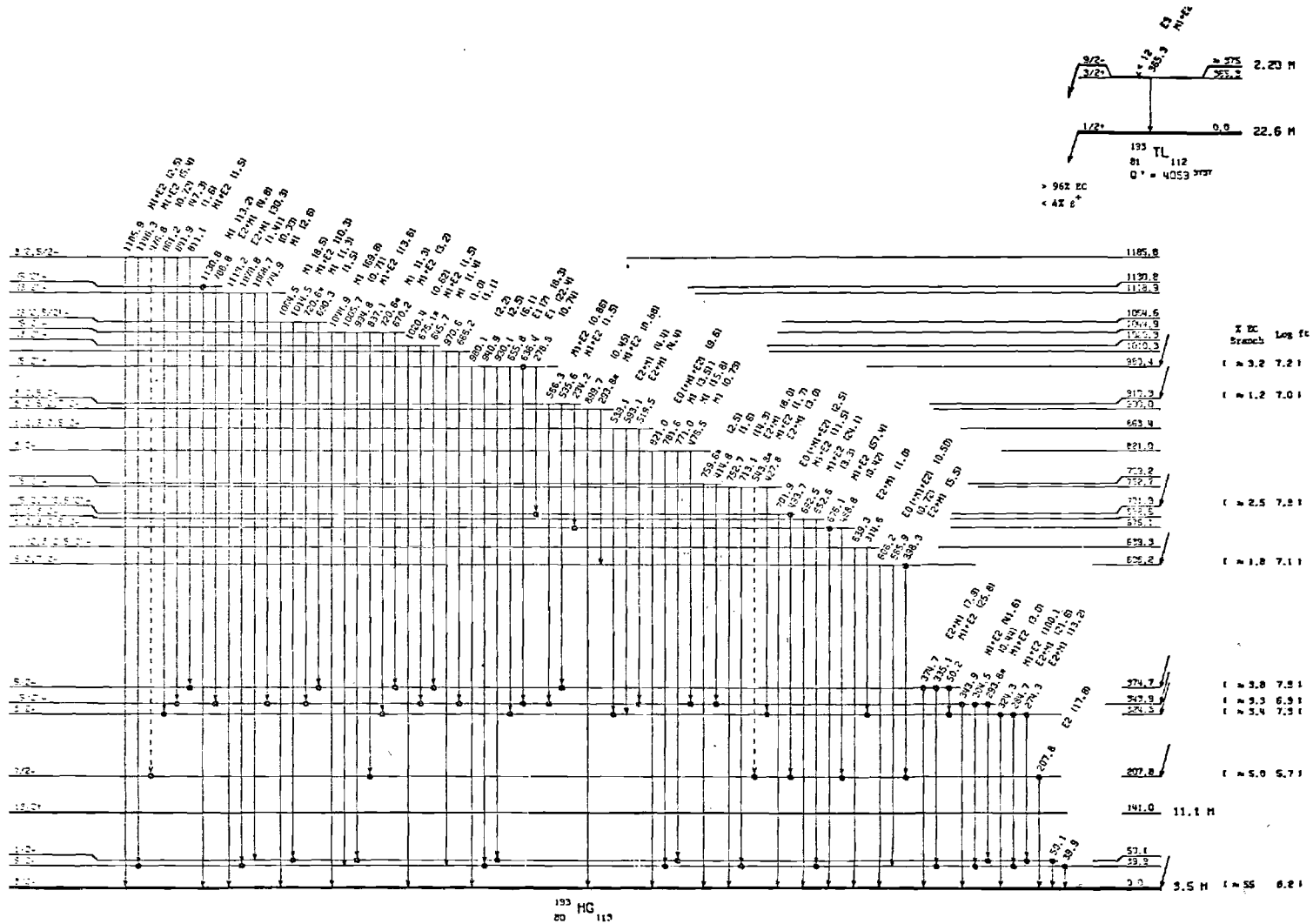


Figure 4-16(a). The Decay Scheme of ^{193m}Tl (with some ^{193m}Tl Admixture): Part I - Transitions from Levels below 1200 keV. Transitions seen in coincidence with others below it are indicated with dots on the tip of the arrow; those in coincidence with transitions above have dots on the tail of the arrow. Transition energies and multipolarities and gamma-ray intensities are given. Branching ratios and log ft values are also shown for some of the levels. Dashed lines indicate questionable levels or transitions. Gamma-rays placed more than once are denoted by γ .

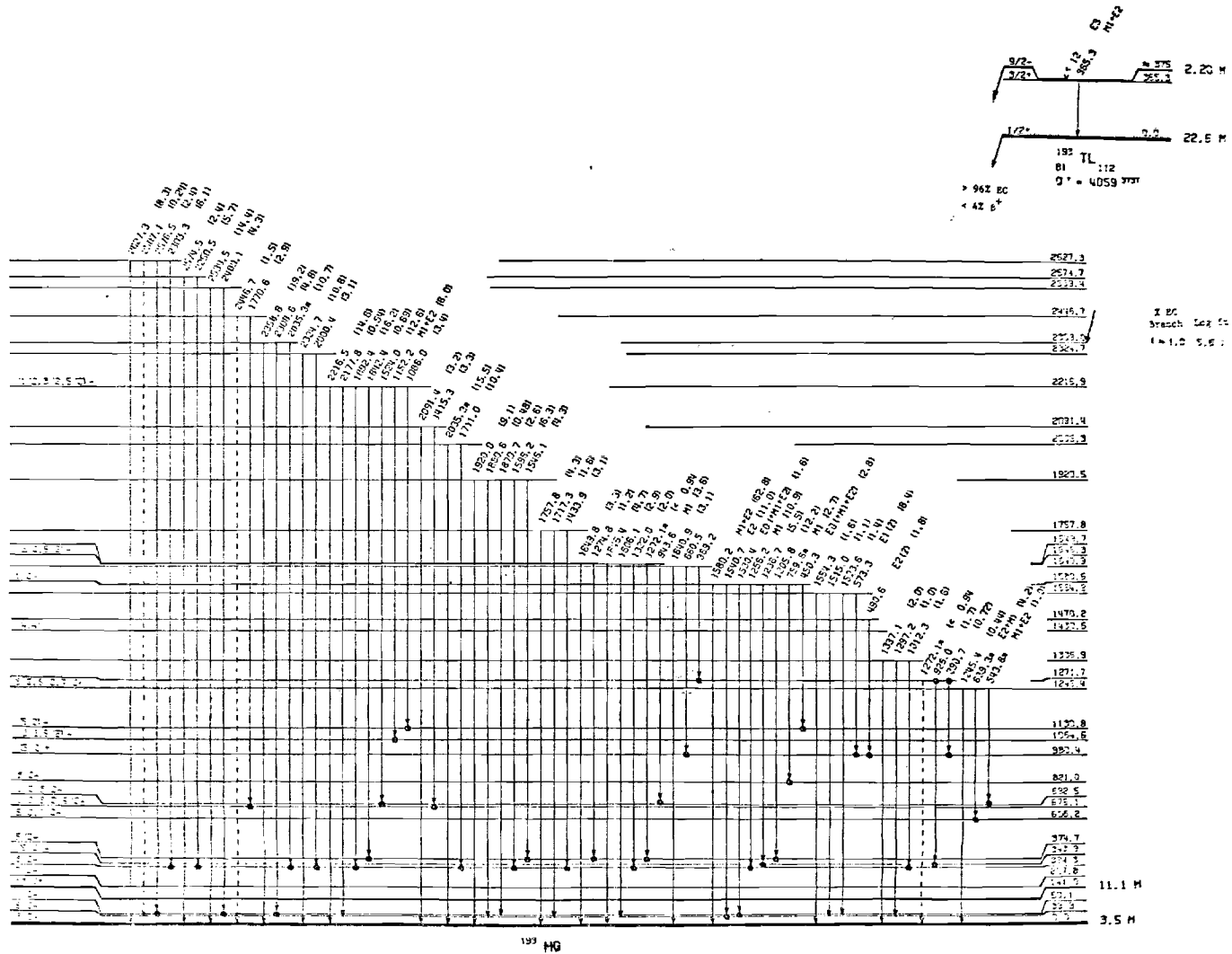


Figure 4-16(b). The Decay Scheme for ^{193g}Tl (with some ^{193m}Tl Admixture): Part II - Transitions from Levels above 1200 keV.

Runs 193-2 and 193-4 studied conversion electrons from transitions in ^{193}Hg due to the decay of ^{193g}Tl . By summing the individual multiscaled spectra to achieve the best possible statistics and using the conversion coefficients for pure E2 and M1 transitions (from Plajner et al.^{120,121}) in the ^{193}Hg decays, a normalization factor was obtained for the γ -rays and conversion electrons. The K- (and several L- and M-) conversion coefficients were deduced for previously unknown transitions in the decay of ^{193g}Tl . Figure 4-16 shows the results of a comparison of the conversion coefficients with theoretical ones from Hager and Seltzer¹¹³) in the form of multipolarity assignments of the transitions.

Four experiments were used to obtain the γ - γ -t coincidence data from the ^{193g}Tl decay, Runs 193-3 and 193-5 through 193-7. The most useful coincidence data were those from e- γ -t measurements taken in Run 193-2. The coincidence relationships derived from these five experiments are shown in Figure 4-16 for all assigned transitions.

The ^{193g}Tl decay scheme (mixed with decays from ^{193m}Tl), shown in Figure 4-16, was constructed, as for the other odd-Hg isotopes, using the coincidence relationships derived above and energy sums and differences. A much less detailed scheme proposed by Vandlik et al.²³) and systematic considerations were used as starting points. We have high confidence in this result because of our ability to determine essentially all levels by coincidence measurements. Branching percentages and log ft values for some of the levels in ^{193}Hg are also shown in Figure 4-16. (See Chapter V for a detailed discussion of some of the more interesting

transitions from this nucleus as they compare with the transitions from the neighboring odd-Hg isotopes.)

Decay of ^{193m}Tl

In addition to the large amount of work done on the 22.6 min ground state decay of ^{193}Tl , an additional experiment, Run 193m-1, was done emphasizing the 2.2 min $9/2^-$ isomer, which is predicted from systematics to be $\leq 18\%$ β^+ /EC and $\geq 82\%$ isomeric transition (IT) in this nucleus (see Chapter V). (Detailed ^{193m}Tl experimental measurements are given in Table 4-8.) In this experiment, γ -ray emissions were studied by singles spectral multiscaling and γ - γ -t list data taken simultaneously. The half-life for the ^{193m}Tl obtained from the singles multiscaling data is 2.20 ± 0.15 min, and is in good agreement with previous reports.¹¹⁸⁾ Approximately one-half of the γ - γ -t list data were collected with the Cd + Cu absorber, and thus a good indication of the peaks due to summing effects was obtained by comparing the two halves of the total projected coincidences derived from these data. The results of the coincidence analysis of the γ - γ -t data is presented in Figure 4-17 as part of the total decay scheme for the ^{193m}Tl .

Conversion electron data were taken as singles multiscaling and e- γ -t data in conjunction with two ^{193}Pb decay experiments, Runs 193m-2 and 193m-3. The total sums of the multiscaled data for the conversion electron and γ -ray singles from Run 193m-3 were used (because of their superior quality and better electron resolution) along with the normalization between the two spectra obtained from known lines in the ^{193}Hg

decay (which is present as a contaminating species), to deduce conversion coefficients for the unknown lines attributed to the decay of ^{193m}Tl . These results were compared to the theoretical values¹¹³⁾ to yield the multipolarities of the transitions cited in Figure 4-17. The e- γ -t coincidence data collected in Run 193m-3 were employed solely to provide coincidence relationships between highly converted low energy transitions in the conversion electron spectrum and medium- to high-energy transitions in the γ -ray spectrum. The results of both coincidence analyses along with energies, relative intensities, and multipolarities are shown in Figure 4-17.

The decay scheme of ^{193m}Tl shown in Figure 4-17 was constructed using the above data and most of the levels have been established from coincidences. Systematic trends allowed the assignments for the ground state ($3/2^-$) and the state at 208 keV ($7/2^-$) to be made. This, coupled with the information from the ^{193}Tl ground state decay, became and basis for the ^{193m}Tl decay scheme. More will be said about the transitions from this decay in Chapter V, concerning specifically the transitions feeding the ground state through the 208 keV level.

Decay of ^{197g}Tl

The γ -ray emissions from mass-separated $A = 197$ sources were studied in several experiments as detailed in Table 4-9. The information relating to measurement of singles rates came from Runs 197-1 and 197-2. In both of these experiments, spectral multiscaling was used to determine half-lives for the $A = 197$ γ -rays, in order to identify those with the

Table 4-9. Details of ^{197}Tl Experiments

Run Number	Reaction(s) and Projectile Energy	Detectors Used and Their Energy Ranges ^a	Measurement(s) and Data Acquisition Systems Used	Collection Times and Counting Times	Number of Coincidence Events Collected
197-1 ^b	Nat. Re($^{16}\text{O}, \text{pxn}$) ^{197}Pb $^{197}\text{Pb} \rightarrow ^{197}\text{Tl}$ 141.3 MeV	11% Ge(Li) $\sim 30\text{-}3200$ keV (8192 channels)	γ -ray singles multiscaling using the TN-1700	1 hour collections; counted as one source as 8 sequential 15- min spectra ^c	
197-2 ^b	Nat. W($^{16}\text{O}, \text{xn}$) ^{197}Pb $^{197}\text{Pb} \rightarrow ^{197}\text{Tl}$ 142.9 MeV and Nat. Re($^{16}\text{O}, \text{pxn}$) ^{197}Pb $^{197}\text{Pb} \rightarrow ^{197}\text{Tl}$ 128.9 MeV	16% Ge(Li) ^d $\sim 40\text{-}2700$ keV and 10% Ge(Li) $\sim 25\text{-}2000$ keV	γ -ray singles multiscaling using the TN- 1700 and γ - γ -t coincidences using the SEL 840A system	(1) 1 hour collections ^c ; counted as one source as 8 sequential 1-hr spectra (2) γ - γ -t collected for 8 hours	9×10^5
197-3 ^e	Nat. Re($^{16}\text{O}, \text{pxn}$) ^{197}Pb $^{197}\text{Pb} \rightarrow ^{197}\text{Tl}$ 128.9 MeV	17% Ge(Li) $\sim 30\text{-}2700$ keV and off-line Si(Li) electron detector $\sim 30\text{-}1200$ keV (both 4096 channels)	Ce^- and γ -ray singles multi- scaling and e- γ -t coincidences using the off- line Tennecomp TP-5000 system	(1) 1 hour collections; counted as 20 sequential 3- min spectra (2) e- γ -t collected for about 4 hours	5×10^5

Table 4-9 (Continued)

^aAll coincidence measurements made on one of the Tennecomp TP-5000 systems had data collected with 8192 channels each for the two events and the TAC; the data were similarly collected on the SEL 840A system with 9500 channels each for the three parameters.

^bChemically-separated sources were used.

^cCollection times were optimized for the study of ¹⁹⁷Pb decay. These ¹⁹⁷Pb sources were all put together and chemically-separated to give a source of ¹⁹⁷Tl.

^dSingles measurements were done as 8192 channels. The Cu + Cd absorber was used on this detector throughout the experiment.

^eThe primary nucleus under study was ¹⁹⁷Pb.

decay of ^{197g}Tl . The best information concerning the ^{197g}Tl half-life came from Run 197-2, due to the fact that there were no contaminations from ^{197}Pb and ^{197}Hg and that the long collection times allowed the ^{197g}Tl decay to be studied for about three half-life periods. The half-life so determined, 2.83 ± 0.15 hours, is in good agreement with the values previously reported.^{25,122)}

Conversion electrons were detected during a separate experiment, Run 197-3 (see Table 4-9), done in conjunction with the study of the decay of the ^{197}Pb . Using the conversion coefficients for strong previously known electron lines in the ^{197}Tl decay,²⁵⁾ an internal normalization factor was obtained, and the K- (plus some L- and M-) conversion coefficients for the ^{197g}Tl transitions were deduced. The results of a comparison of the conversion coefficients with the theoretical values of Hager and Seltzer¹¹³⁾ are reported in Figure 4-18 as multipolarities deduced for the transitions.

Coincidence data on the γ -rays from ^{197g}Tl decay were also obtained in Runs 197-1 and 197-2. In addition, e- γ -t data were collected in the off-line conversion electron arrangement simultaneously with conversion electron singles data in Run 197-3. The results of the analysis of the coincidence relationships, together with energies, relative intensities, and multipolarities for the transitions in the decay of ^{197g}Tl and log ft values for the levels in ^{197}Hg are given in Figure 4-18.

The decay scheme of ^{197g}Tl , shown in Figure 4-18, was constructed in the usual manner, described above, using coincidence relationships and energy sums and differences. Most of the levels have been placed by

coincidence data and checked by an intensity balance of the γ -rays proposed to populate and depopulate each level. This work is mostly confirmatory, with the results of previous studies^{25,42)} being quite similar to these results. More will be said about the detailed level structure in the discussions from Chapter V.

CHAPTER V

INTERPRETATION OF EXPERIMENTAL RESULTS AND SYSTEMATICS
OF LEVELS IN ODD-A HG ISOTOPESPopulation of Levels in Odd-A Hg Isotopes from Tl
Isomeric and Ground-State Decays

The Nilsson diagram of single-particle proton states in the range of $Z = 50$ to 82 is illustrated in Figure 5-1, in which the approximate deformation ($\epsilon \sim \beta = -0.15$, oblate) is shown for odd-A isotopes of Tl. As seen in this diagram, the single-particle states $s_{1/2}$, $d_{3/2}$, $h_{11/2}$, $d_{5/2}$, and $g_{7/2}$ are expected to be present in the (near spherical) odd proton ($Z = 81$) Tl isotopes. (At higher deformations the $h_{9/2}$ state is also expected to intrude into the Tl level configuration from above the $Z = 82$ closed shell.¹²²) Figure 5-2 shows the energy relationships among the low-lying states ($s_{1/2}$, $d_{3/2}$, $d_{5/2}$, and $h_{9/2}$) in the odd-mass Tl isotopes.^{110,111,119,122,124,128} These isotopes all have $s_{1/2}$ ground states and $h_{9/2}$ isomeric states. The $h_{9/2}$ level drops noticeably relative to the $1/2^+$, $3/2^+$, and $5/2^+$ states in going from ^{201}Tl to ^{189}Tl . This is the $h_{9/2}$ shell model state from above the $Z = 82$ shell closure. In the heavier Tl nuclei, ($A \geq 197$), the $h_{9/2}$ isomer deexcites only by an E3 isomeric transition; thus, only the $1/2^+$ ground state in these nuclei populates levels in Hg through β^+/EC decay. In ^{195}Tl , however, β^+/EC decay from the isomer is expected to begin competing with the E3 isomeric transition. This β^+/EC branching is predicted by our decay data to be no greater than 1%, however. In

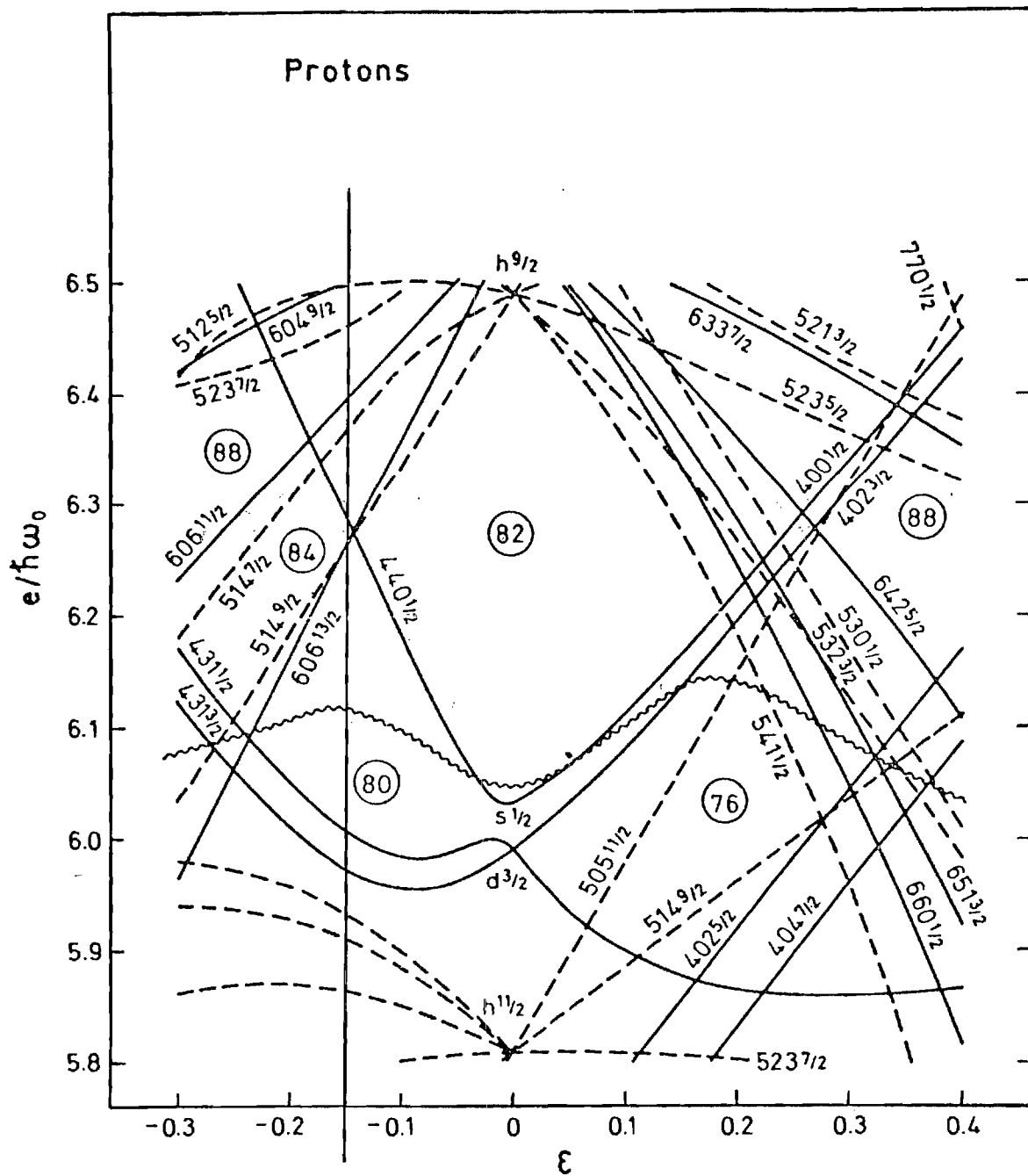


Figure 5-1. Nilsson Diagram for Odd-Proton States, $50 < Z < 82$. The line at $\epsilon \approx -0.15$ shows the approximate deformation for the $189\text{-}197\text{Tl}$ isotopes.

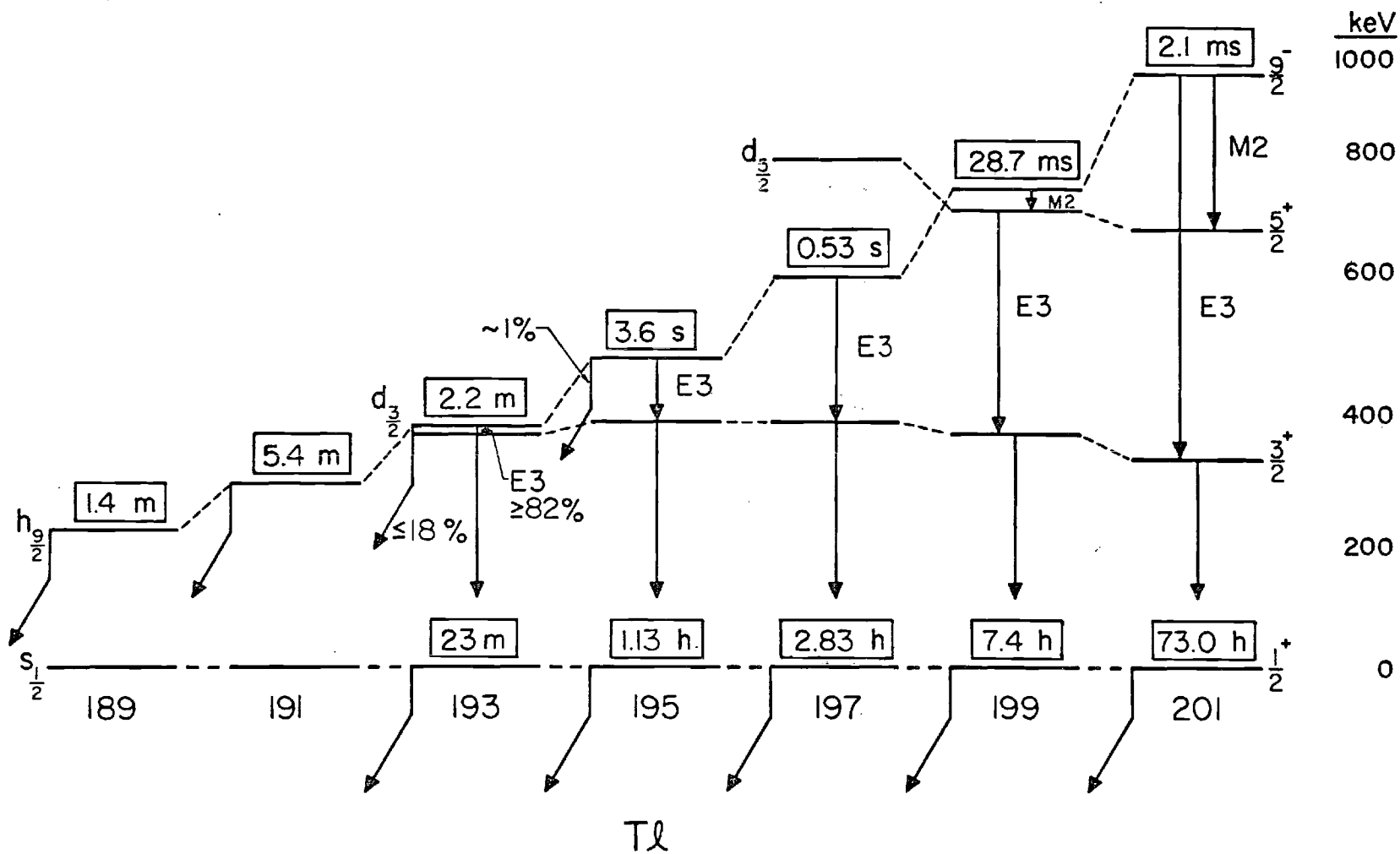
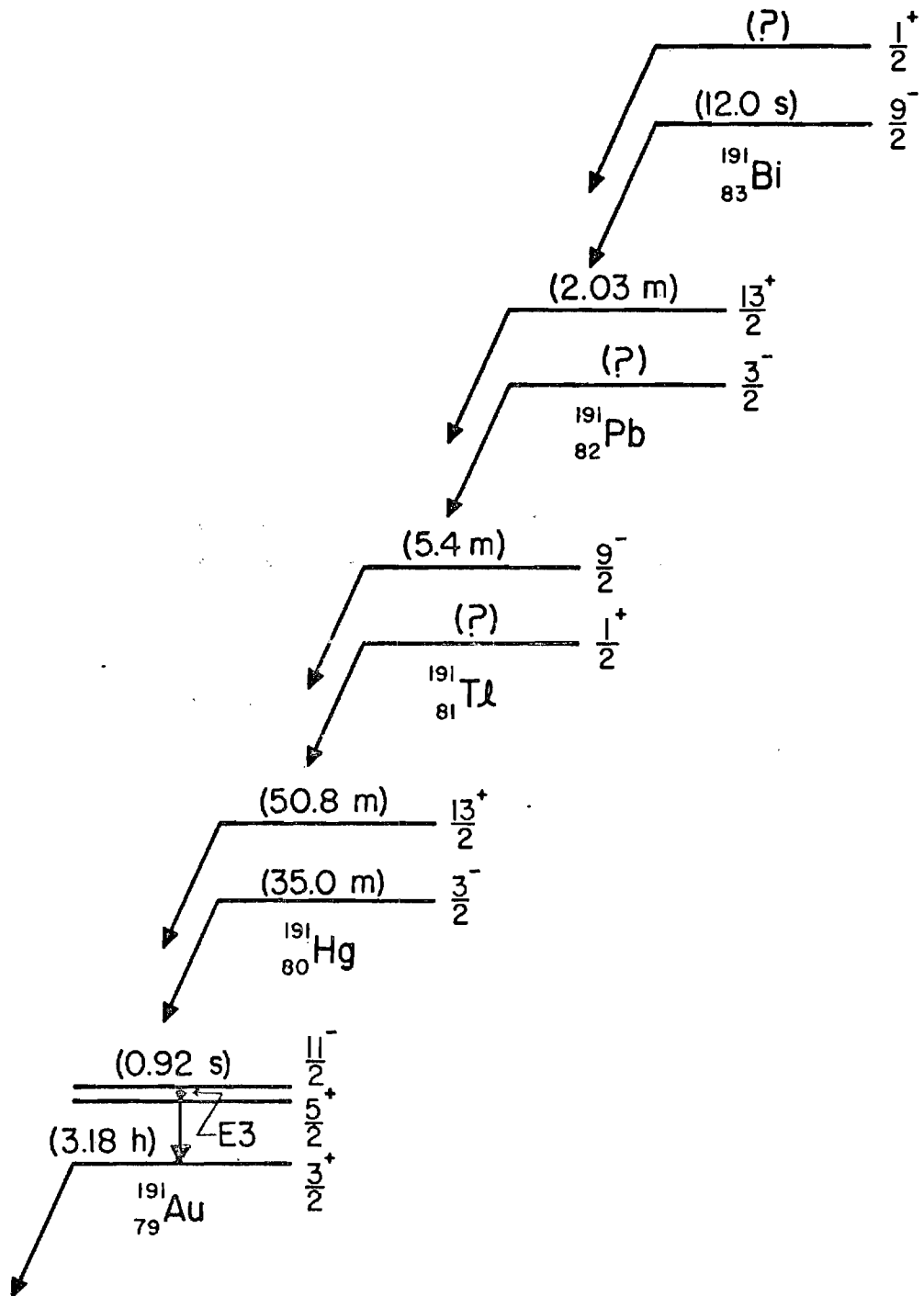


Figure 5-2. The Single-Particle Shell Model States Observed in the Odd-Mass $^{189-201}\text{Tl}$ Isotopes Showing the Isomer and Ground State Relationships.

^{193}Tl , significant β^+ /EC decay from the isomer is seen and is estimated to be $\leq 18\%$ β^+ /EC decay from systematics. Finally, in the $^{189,191}\text{Tl}$ decays, no indication of more than one half-life for each nucleus has been observed. This result, coupled with the fact that the ground state is not observed via in-beam γ -ray spectroscopy with heavy ions,¹²⁴⁾ leads us to the conclusion that the 1.42-min and 5.35-min half-lives for ^{189}Tl and ^{191}Tl , respectively, must be due to decay from the $9/2^-$ isomers. The systematic trends illustrated in Figure 5-2 show how this conclusion can be explained. The $3/2^+$ state is energetically stable relative to the ground state throughout these Tl nuclei. At ^{191}Tl , the $9/2^-$ state drops below the $3/2^+$ state, removing the pathway for the E3 isomer. The $9/2^- \rightarrow 1/2^+$ M4 transition might lead to γ deexcitation to the ground state, but this is not observed to compete with direct β^+ /EC from the $h_{9/2}$ level. Therefore, since heavy-ion reactions tend to populate high-spin states preferentially, the levels in $^{189,191}\text{Hg}$ are expected to be fed mostly through the decay from the $9/2^-$ isomer in $^{189,191}\text{Tl}$. (See Figure 5-3 for a skeletal view of the decay patterns observed and expected in the $A = 191$ decay chain.)

Isomeric and Ground-State Relationships Among Odd-A Mercury Isotopes

The odd-neutron Nilsson diagram in the region of $N = 82$ is shown in Figure 5-4, where the approximate deformation ($\epsilon \sim \beta = -0.15$, oblate) is illustrated for odd-N Hg isotopes. From this diagram, the single-particle states $p_{1/2}$, $f_{5/2}$, $p_{3/2}$, and $i_{13/2}$ are expected in the odd-N Hg isotopes ($N = 109 - 117$). The relationships among the low-spin ground states and high-spin isomers in the odd-mass Hg isotopes are depicted in Figure 5-5. The figure shows the predominant states

Figure 5-3. Skeletal Decay Chain for $A = 191$.

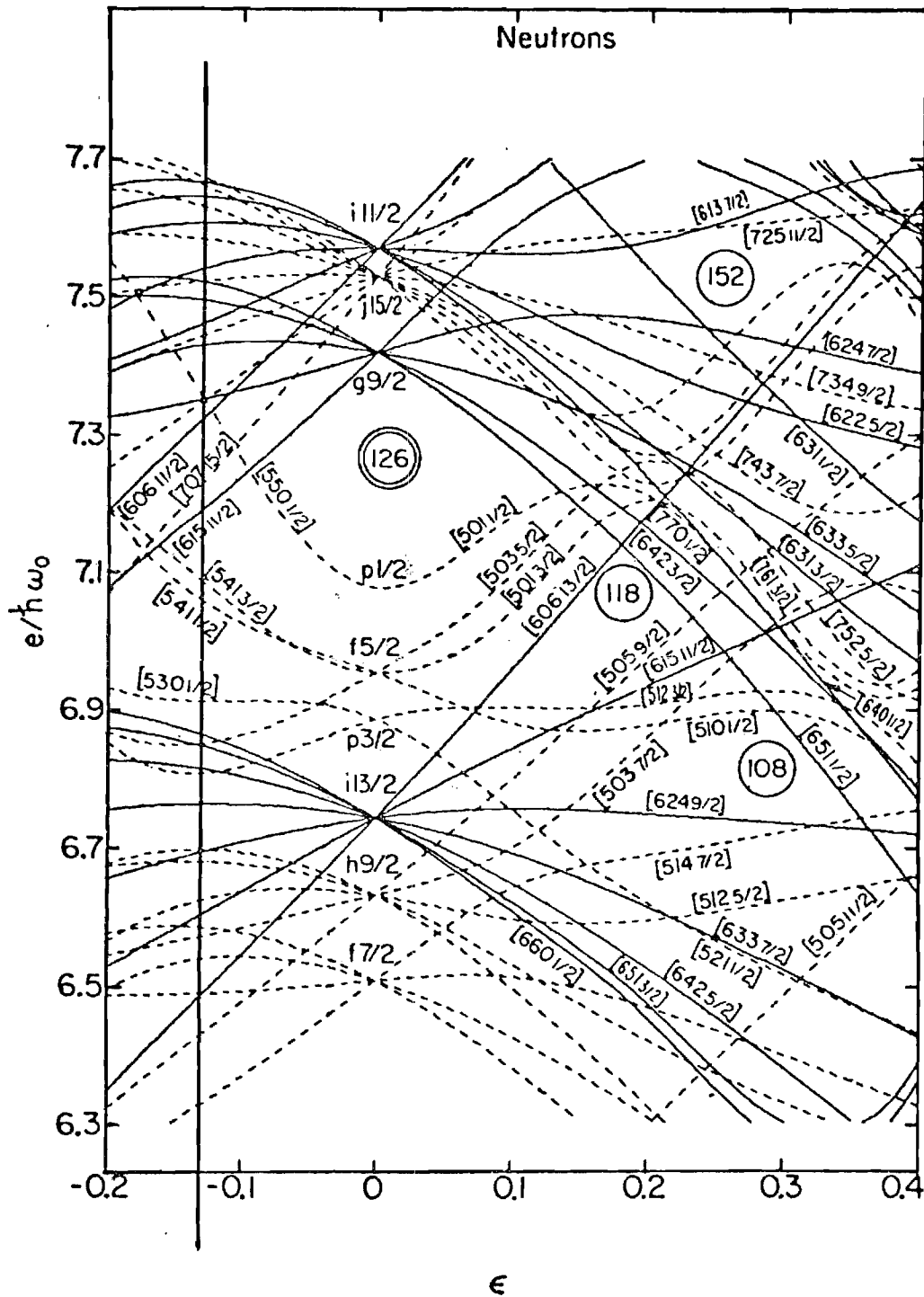


Figure 5-4. Nilsson Diagram for Odd-Neutron States, $82 \leq N \leq 126$. The line at $\epsilon \approx -0.14$ shows the approximate deformation for the $189-197\text{Hg}$ isotopes.

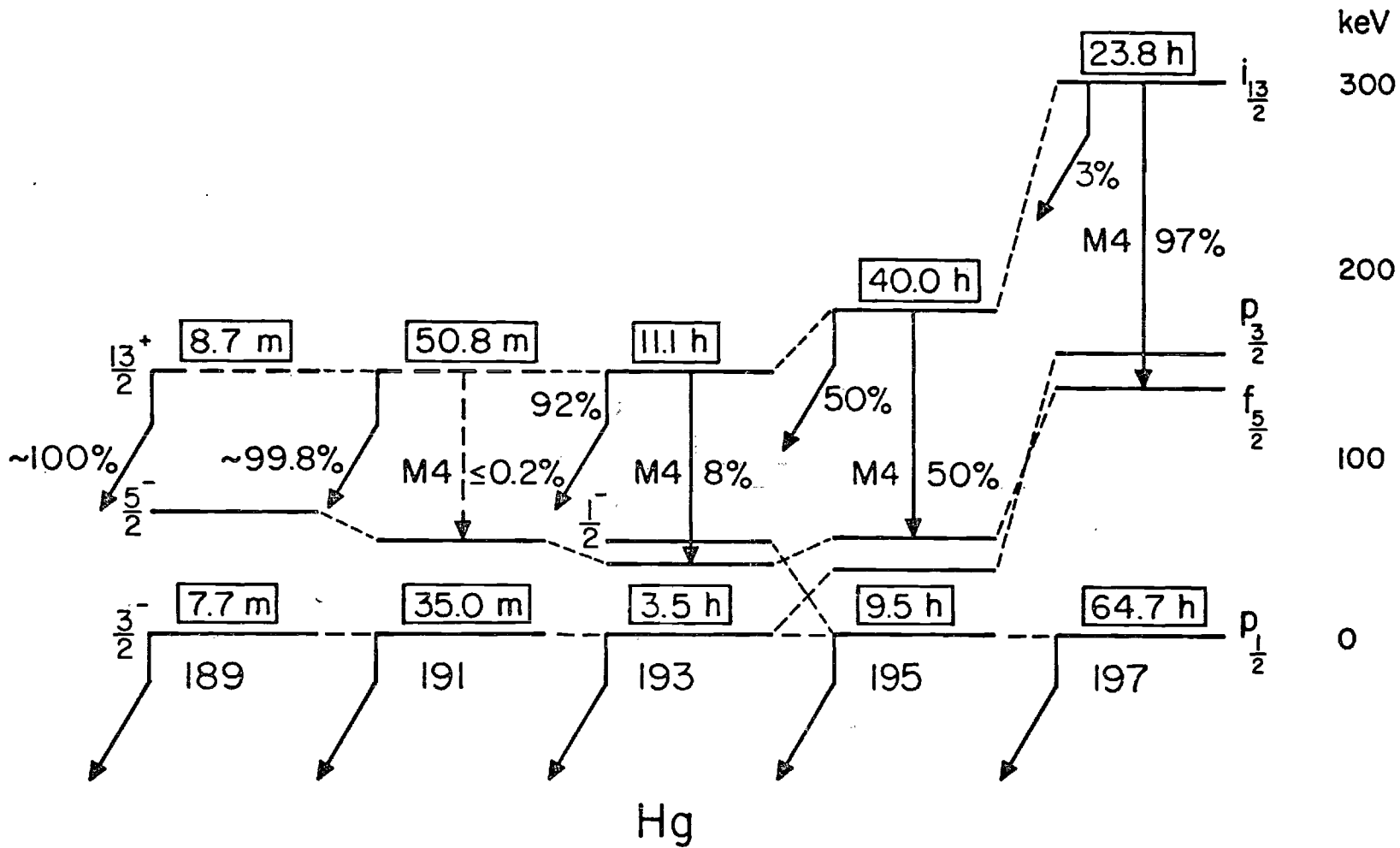


Figure 5-5. The Single-Particle Shell Model States Observed in the Odd-Mass $^{189-197}\text{Hg}$ Isotopes Showing the Isomer and Ground State Relationships.

present ($p_{1/2}$, $p_{3/2}$, and $i_{13/2}$) and their relative energies in these Hg nuclei. The heavier Hg isotopes ($A \geq 195$) have $p_{1/2}$ ground states, while those of ^{193}Hg and lower have $p_{3/2}$ ground states. The $3/2^-$ state drops relative to the $1/2^-$ state with decreasing N and crosses at ^{193}Hg . The $5/2^-$ and $13/2^+$ states also drop relative to the $1/2^-$ state with decreasing N as indicated in Figure 5-5. The half-lives for the two isomers $^{189\text{m}}\text{Hg}$ and $^{191\text{m}}\text{Hg}$ have been measured at UNISOR in the study of the decay $^{189,191}\text{Hg} \rightarrow ^{189,191}\text{Au}$, (111,118) but the positions of the $13/2^+$ isomers relative to their respective ground states are not known. This is due to the very small branching ratio seen in the M4 isomeric transition in those nuclei, the isomer only having been observed to deexcite by β^+/EC decay. The positions of the $13/2^+$ isomers in $^{189,191}\text{Hg}$ in Figure 5-5 have been estimated using the systematic trends illustrated in Figure 5-6. This figure shows the remarkable stability of the $i_{13/2}$ state relative to the $p_{3/2}$ state and the rising of the $f_{5/2}$ state relative to both states as the neutron number decreases. These systematic trends also permit an estimation of upper limits for the M4(IT)/ β -branching ratios in $^{189,191}\text{Hg}$. The estimated $\leq 0.2\%$ M4 in ^{191}Hg and estimated $\leq 8 \times 10^{-3}\%$ M4 in ^{189}Hg indicate essentially 100% β^+/EC from the isomeric states.

Systematic Trends and Band Structures in the Odd-Mass Hg Isotopes

The Negative Parity States

Systematic trends for the low-lying levels in the odd-Hg isotopes, $^{189,191}\text{Hg}$, are shown in Figure 5-7. The $p_{1/2}$, $p_{3/2}$, $f_{5/2}$, and $i_{13/2}$ states examined earlier (Figures 5-5 and 5-6) are shown for references. Note that isotopes $^{201-205}\text{Hg}$ are not included in these systematics,

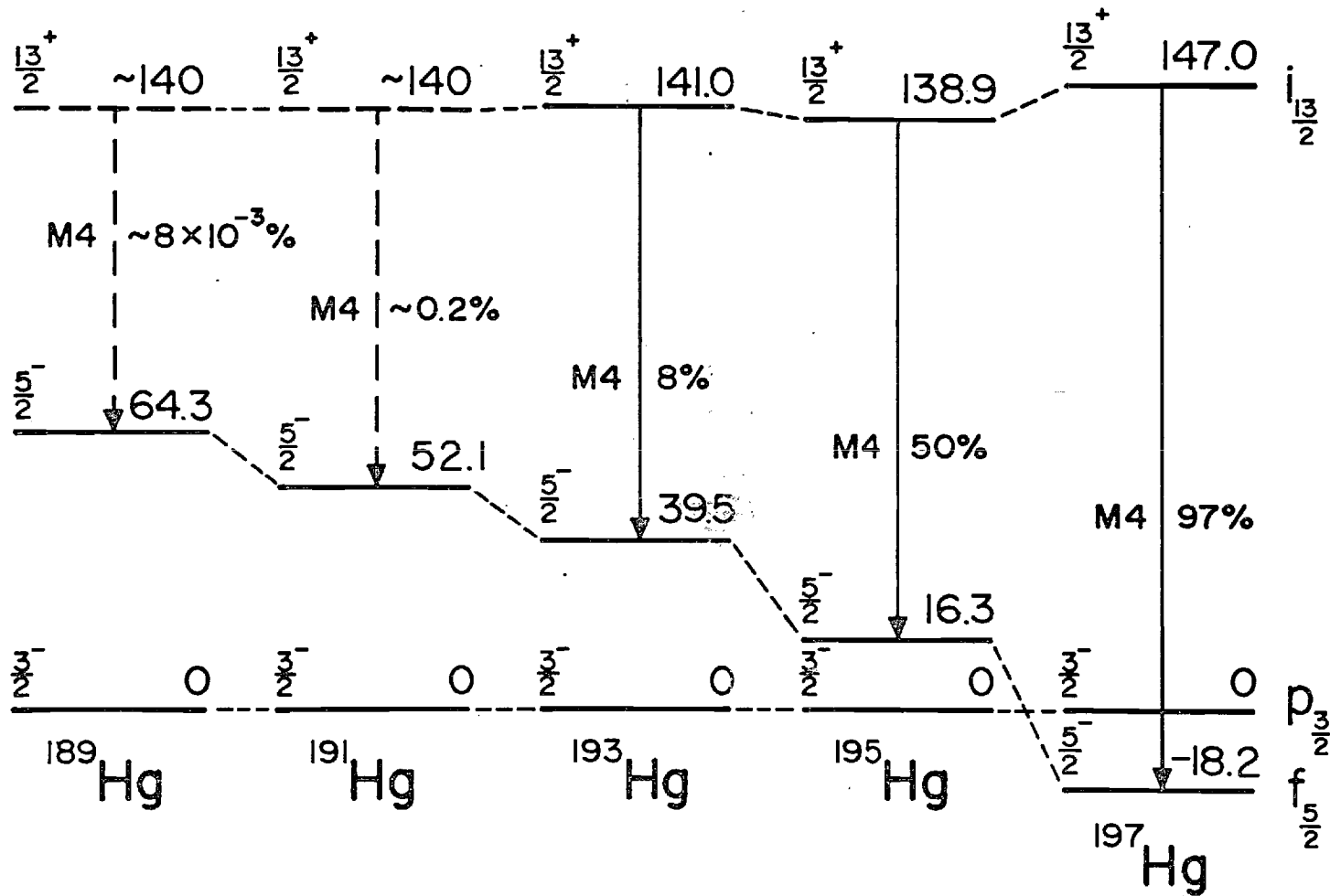


Figure 5-6. The $i_{13/2}$ and $f_{5/2}$ Single-Particle States Shown Relative to the $p_{3/2}$ Single-Particle State in the Odd-Mass $^{189-197}\text{Hg}$ Isotopes.

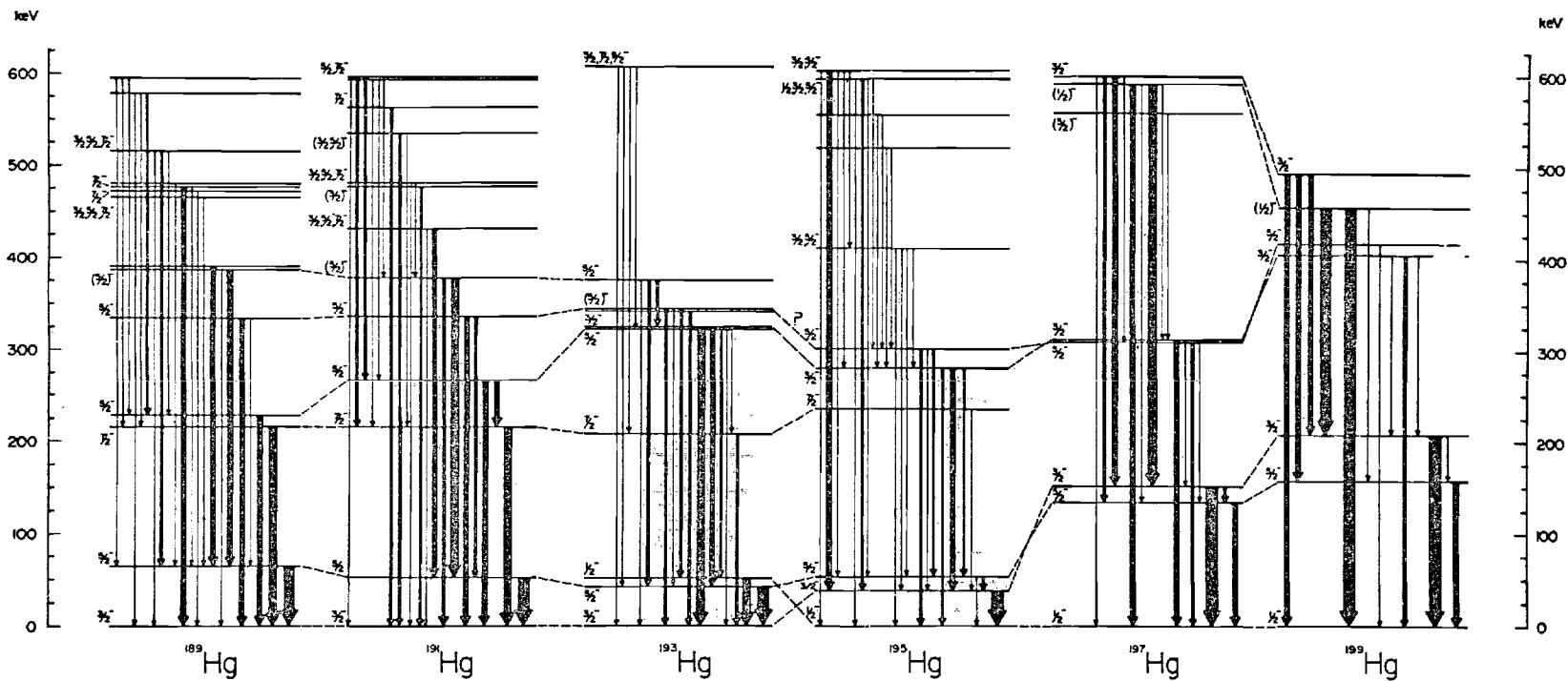


Figure 5-7. Level Systematics for Low-Lying (Energy < 600 keV) States in the Odd-Mass $^{189-197}\text{Hg}$ Isotopes. The widths of the arrows are indicative of approximate relative intensities of the transitions. Dashed connecting lines are to guide the eye and suggest possible level trends.

because existing experimental information¹²⁶⁻¹³⁰ does not provide complete and consistent level structures. The most interesting feature that we have found in these level systematics is evidence for a possible deformed rotational band in ^{189}Hg . The anomalously large number of levels between 400 and 500 keV in ^{189}Hg (see Figure 5-7) compared to $^{191-197}\text{Hg}$ is an indication of additional nuclear degrees of freedom coming into play, such as a series of deformed states. The predicted deformed band (compared to the $p_{3/2}$ and $f_{5/2}$ bands) in ^{189}Hg is shown in Figure 5-8. A reasonably strong 284.6 keV transition feeding the 476.5 keV level is the most promising candidate as the first excited member of such a deformed band. If the rotational constant $h^2/2\mathcal{I}$ is taken to be ~ 14.0 keV (from the values found in the even-even Hg bands and ^{187}Au), the spin of the 476.5 keV level is calculated to be $7/2^-$ and the 284.6 keV transition is predicted to be the $11/2^- \rightarrow 7/2^-$ transition in this band. Looking at a Nilsson level diagram for $N = 109$ and the expected deformation, $\beta \sim 0.27$ (prolate) (again from the even-Hg nuclei and ^{187}Au), the predicted band is $7/2^- [503\uparrow]$. In addition, the transition from this 476.5 keV level to the 64.3 keV level ($5/2^-$) is a pure M1 transition. Our speculation for the existence of this deformed band is also confirmed by earlier experimental work at UNISOR and elsewhere on the lighter-mass Tl isotopes (the deformed bandhead energies have been found to be at 375, 522, 825 keV in ^{184}Hg ¹³¹) and $^{186,188}\text{Hg}$ ¹³²) respectively, and are predicted to be at ~ 1284 keV for ^{190}Hg and the ground state¹³³) and ~ 215 keV* in $^{185,187}\text{Hg}$, respectively).

* Preliminary UNISOR results indicate the deformed rotational band in ^{187}Hg has a bandhead energy between 160 and 180 keV.

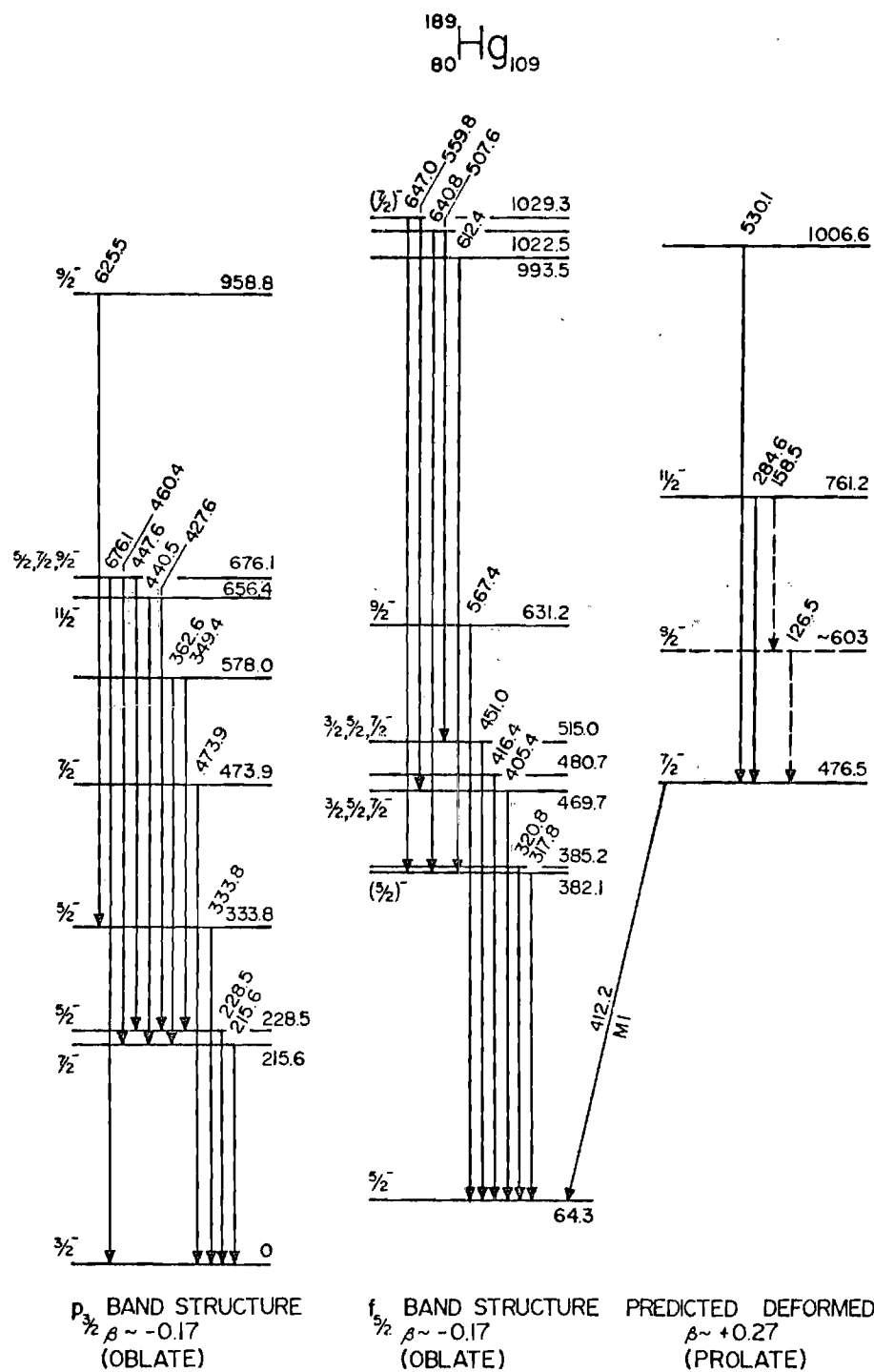


Figure 5-8. The Observed Band Structures in ^{189}Hg Showing the Relationships among the $p_{3/2}$, $f_{5/2}$, and Deformed Bands.

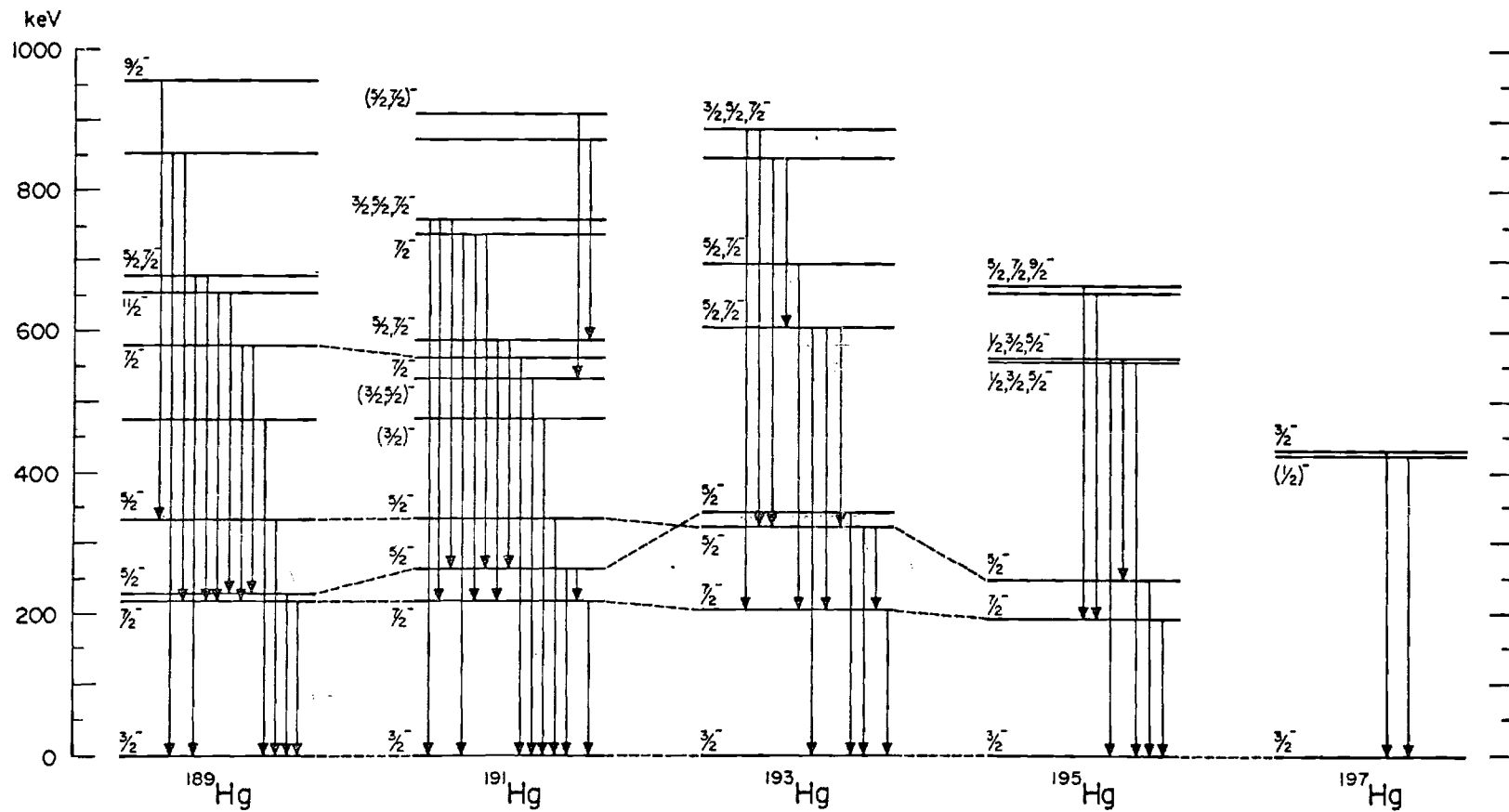


Figure 5-9. Band Structure Built on the $p_{3/2}$ Single-Particle State in $^{189-197}\text{Hg}$. Note the possible decoupled band structure ($3/2^-$, $7/2^-$, $5/2^-$) present. Dashed connecting lines are to guide the eye and suggest possible level trends.

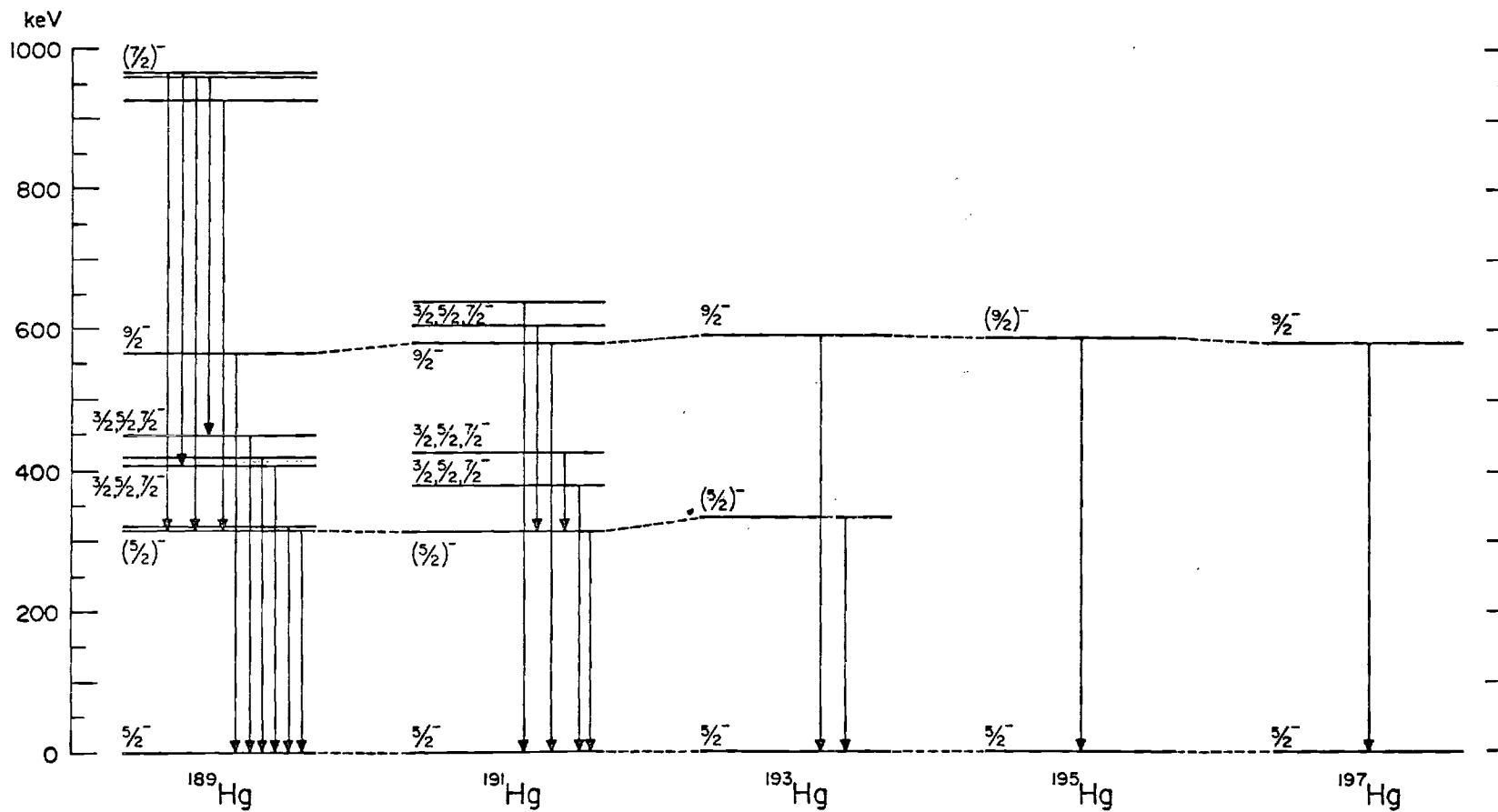


Figure 5-10. Band Structure Built on the $f_{5/2}$ Single-Particle State in $^{189-197}\text{Hg}$. Dashed connecting lines are to guide the eye and suggest possible level trends.

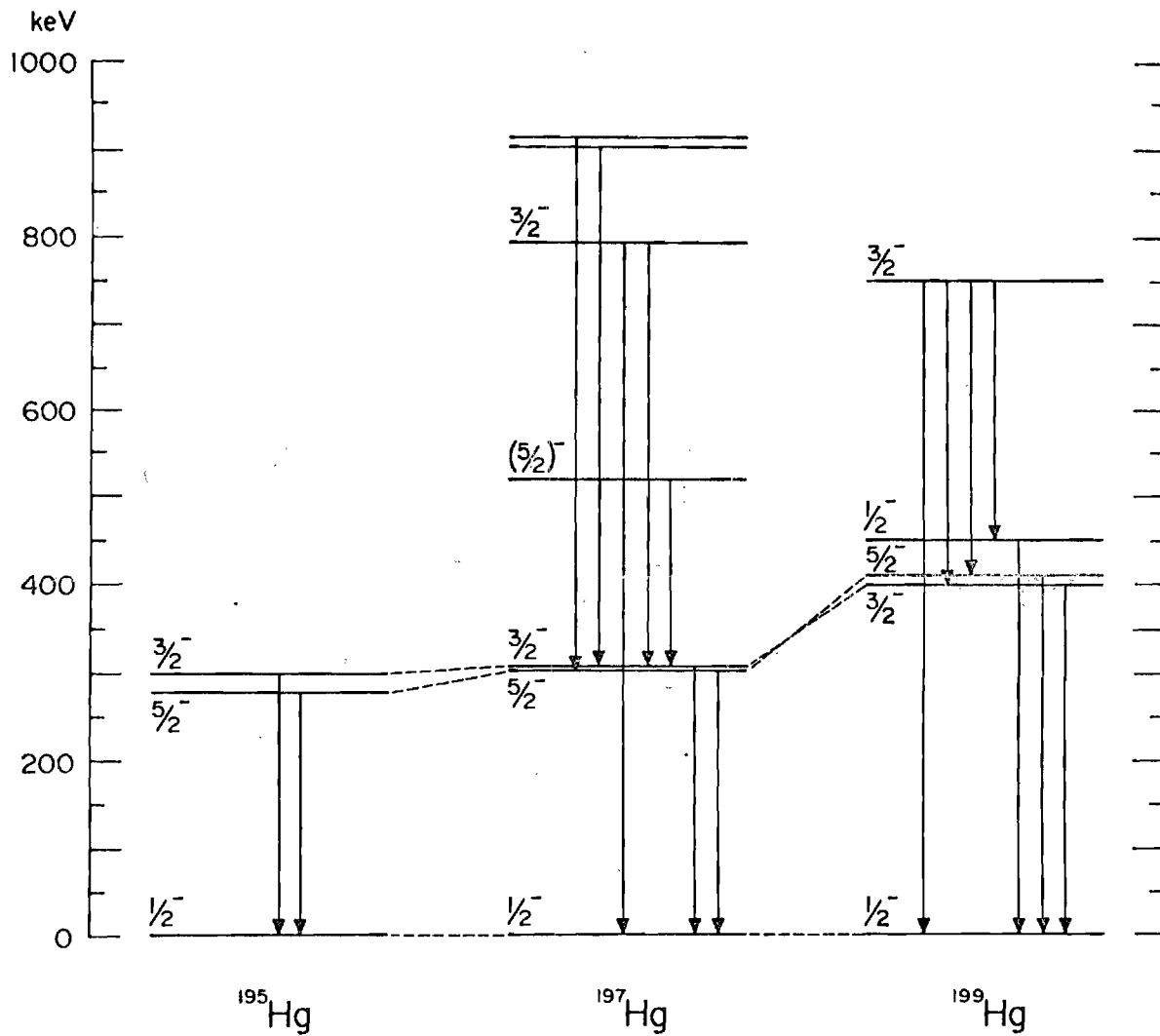


Figure 5-11. Band Structure Built on the $p_{1/2}$ Single-Particle State in $^{195-199}\text{Hg}$. Dashed connecting lines are to guide the eye and suggest possible level trends.

These systematics indicate the deformed band in ^{189}Hg is expected at ~ 595 keV, in reasonably good agreement with our 476.5 keV candidate. The observation of strong retardation of the 476.5 keV M1 via a lifetime measurement will confirm this interpretation.

Several other matters also need emphasizing in our discussion of levels in $^{189-199}\text{Hg}$ nuclei. First, (d,t) single-nucleon transfer reaction experiments⁴¹⁾ have been made on ^{197}Hg , and (d,p) and (d,t) on ^{199}Hg . These experiments indicate that the strengths of the $p_{1/2}$, $p_{3/2}$, and $f_{5/2}$ single-particle orbitals are concentrated in the first five excited states of these nuclei, and that some fragmentation of their single-particle character among these low-lying levels is present (presumably due to mixing with collective degrees of freedom).

Second our work provides evidence for band structures based on the $p_{3/2}$, $f_{5/2}$, and $p_{1/2}$ states in $^{189-199}\text{Hg}$ (as illustrated in Figures 5-9 through 5-11). The $3/2$, $7/2$, and $5/2$ structure seen in the $p_{3/2}$ band have been located in the present work for the $^{189-195}\text{Hg}$ nuclei, with the $7/2^- \rightarrow 3/2^-$ transition intensity reflecting the approximate amount of high-spin β^+/EC feeding present from the high-spin isomers in the parent nuclei. The ^{195}Hg band members are hard to place, because they are populated only weakly through the small β^+/EC branch from $^{195\text{m}}\text{Tl}$ decay. The odd-mass Hg nuclei of $A = 197$ and above do not show this structure, because these states have spins too high to be populated through decay of the $1/2^+$ ground states of the Tl parents. This $p_{3/2}$ band structure is indicative of a decoupled band pattern which points to the presence of rotational character in these nuclei. Bands built on the $p_{1/2}$ and $f_{5/2}$ states do not, however, seem to show any recognizable

structure which supports a rotational character.

A final item concerns the systematics of one particular level above those shown in Figure 5-7. This level is shown in Figure 5-12 for $^{193-197}\text{Hg}$, where the decay pattern from a proposed $1/2^-$ high-energy level is depicted. Many transitions with significant strength depopulate this level, but a high intensity $M1 + E2$ transition from this level to the first $3/2^-$ level dominates the picture. Furthermore, the most interesting feature by far is the fact that this level deexcites by a strong EO transition to the $1/2^-$ ($p_{1/2}$) state in the $^{193-197}\text{Hg}$ nuclei. No explanation has yet been found for these strongly populated $1/2^-$ levels connected by large EO matrix elements to the low-lying $p_{1/2}$ states, and no such EO transitions are known in the corresponding even- Hg isotopes. This unique structure was not found in the $^{189,191}\text{Tl}$ decays, because no low-spin decay is present to populate a $1/2^-$ state.

As mentioned in Chapter II, several particle (or quasiparticle)-phonon coupling models have been invoked in attempts to describe low-lying states in odd- Hg nuclei. Comparisons of the present data with predictions from these models for ^{193}Hg , (16,17) ^{195}Hg , (12,13,15-17) and ^{197}Hg (12,13,15-17) are shown in Figures 5-13 through 5-15, respectively. As can be seen from these figures, the level density is approximately reproduced, but the energy fit and ordering of the levels is relatively poor. Thus, despite the complex many-parameter models in use, none seem to be useful in predicting the level structure for the odd-mass Hg transitional nuclei. No theoretical calculations are available so far for $^{189,191}\text{Hg}$.

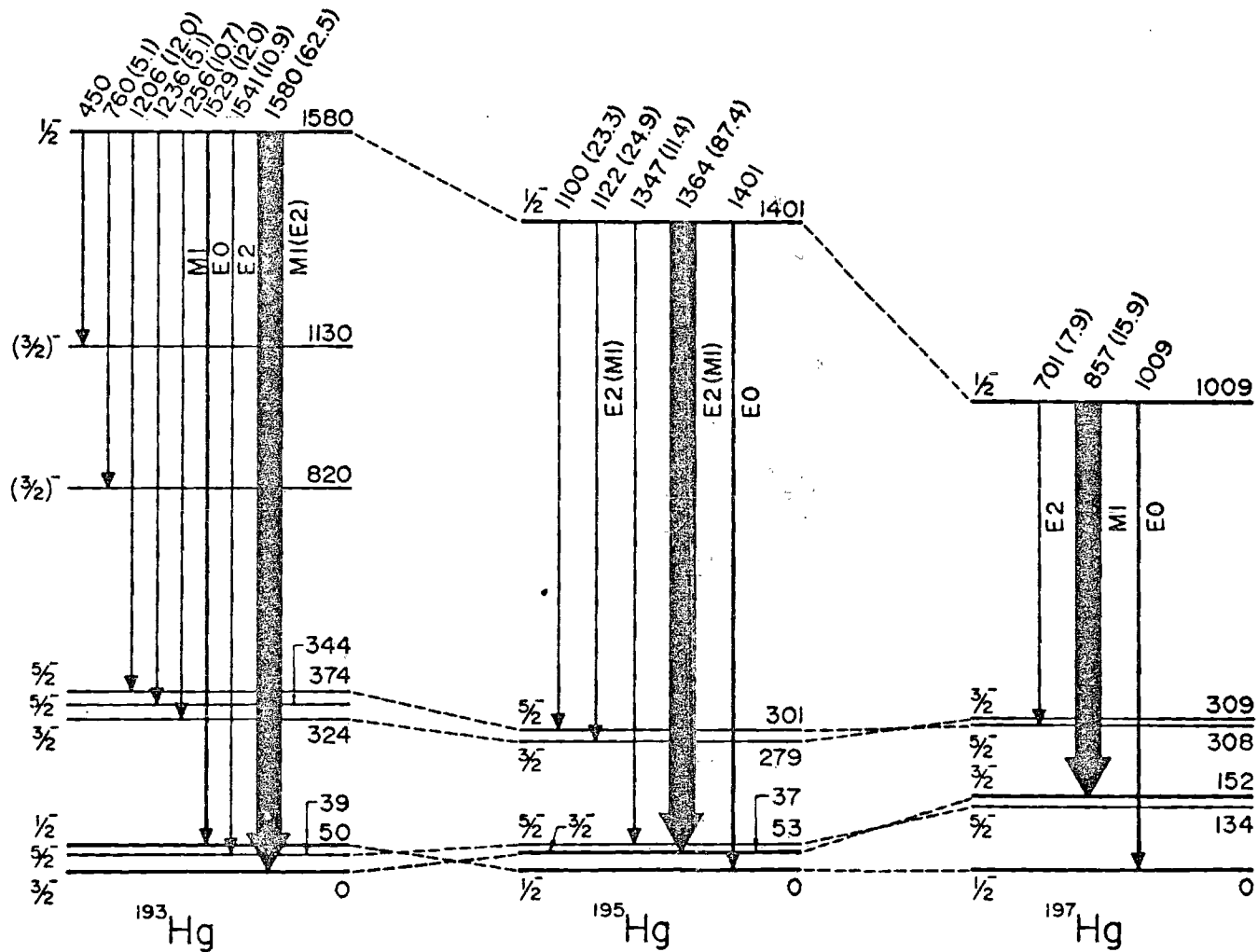


Figure 5-12. The Depopulation of the Strongly Fed High-Energy $1/2^-$ States in $^{193-197}\text{Hg}$ are Shown Feeding the $p_{1/2}$ Single-Particle States by E0 Transitions. Note that the width of the $1/2^- \rightarrow$ (first) $3/2^-$ arrows are indicative of the large intensities of these transitions.

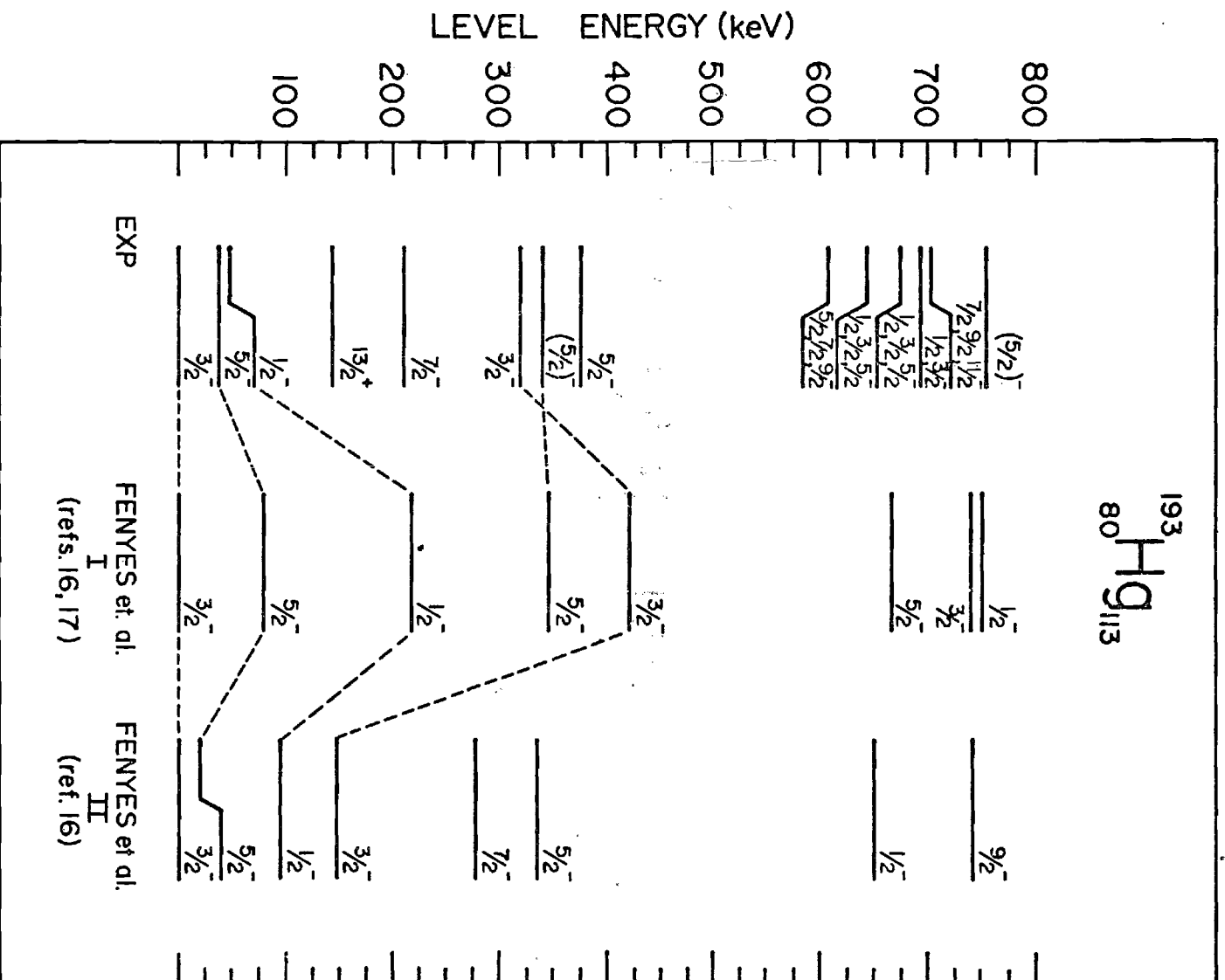


Figure 5-13. A Comparison of Experimental and Theoretical Negative Parity States in ^{193}Hg . The $13/2^+$ level is shown for reference. Connecting lines are to guide the eye to the location of the first few states of spin $1/2$, $3/2$, and $5/2$ and are not meant to imply a structural correspondence between experiment and the various theories. Note that Fenyes et al. (I) only gives states of spin $1/2$, $3/2$, and $5/2$.

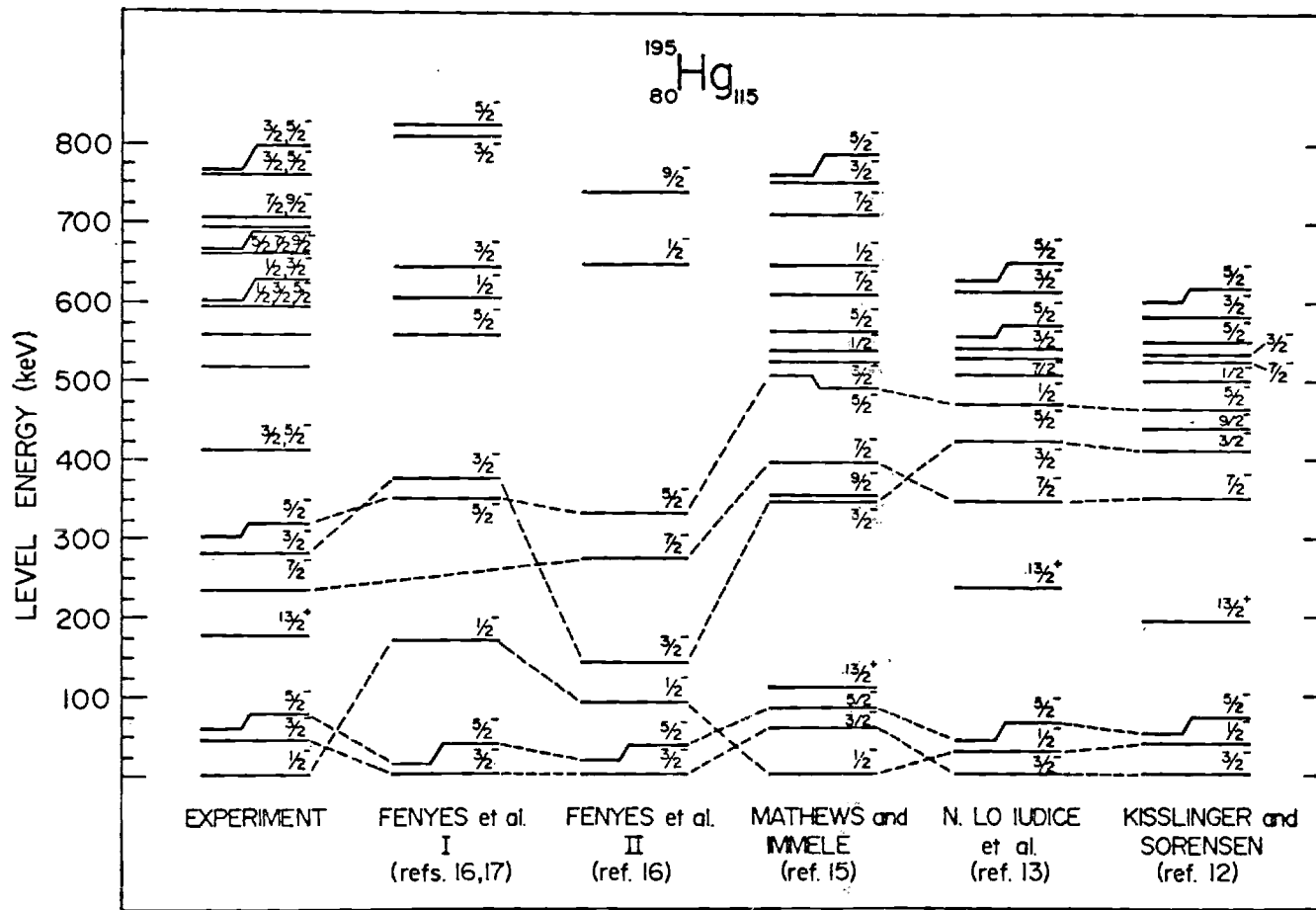


Figure 5-14. A Comparison of Experimental and Theoretical Negative Parity States in ^{195}Hg . The $13/2^+$ level is shown for reference. Connecting lines are to guide the eye to the location of the first few states of spin $1/2$, $3/2$ and $5/2$ and are not meant to imply a structural correspondence between experiment and the various theories. Note that Fenyés et al. (I) only give states of spin $1/2$, $3/2$, and $5/2$.

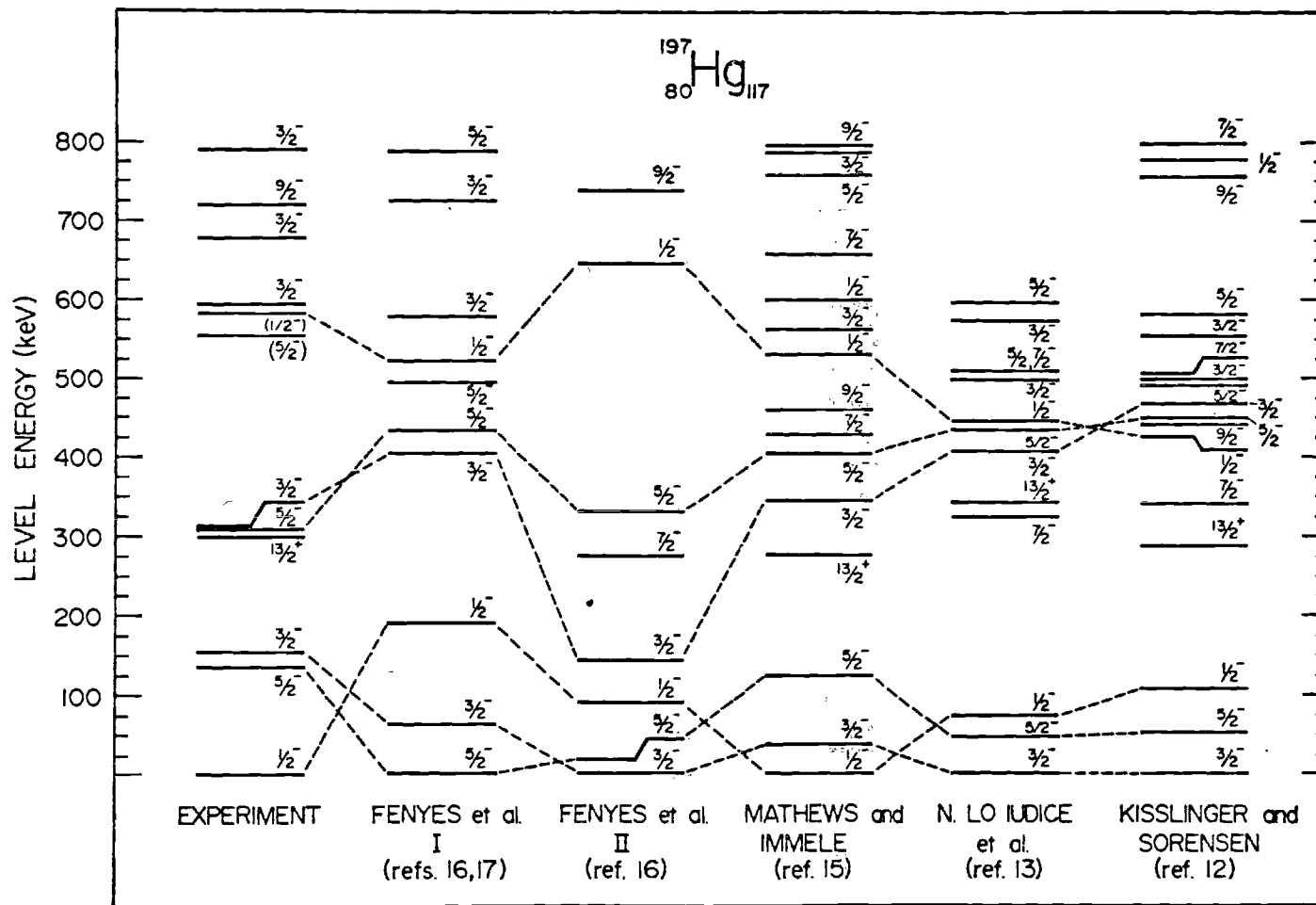


Figure 5-15. A Comparison of Experimental and Theoretical Negative Parity States in ^{197}Hg . The $13/2^+$ level is shown for comparison. Connecting lines are to guide the eye to the location of the first few states of spin $1/2$, $3/2$, and $5/2$ and are not meant to imply a structural correspondence between experiment and the various theories. Note that Fenyes et al. (I) only give states of spin $1/2$, $3/2$, and $5/2$.

The Positive Parity States and the $i_{13/2}$ Band

Current experimental information on the positive parity states in the odd-Hg isotopes ($A = 189-197$) is depicted in Figure 5-16. Most of the results presented come from the in-beam work done at Jülich²⁸⁾ on $^{191,193}\text{Hg}$, at Berkeley³⁷⁾ on $^{195,197}\text{Hg}$, and at Rossendorf⁴²⁾ on ^{197}Hg . The yrast states that are populated in these in-beam experiments show decoupled band behavior (see Figure 2-3 for an explanation) consistent with predictions of the rotation-aligned coupling model^{18,74)} for hole states built on oblate cores. Figure 5-17 shows a comparison of this yrast positive parity structure for the Hg isotopes ($A = 190-195$), illustrating the decoupled nature of the odd-Hg isotopes.²⁸⁾ In addition, the recent work of Khoo et al.¹³⁴⁾ on the $i_{13/2}$ band in ^{191}Pt (isotonic to ^{193}Hg) has shown that the odd-mass Pt isotopes most likely have triaxial shapes. Their detailed β -decay and in-beam work investigated the non-yrast, as well as yrast states in ^{191}Pt . The non-yrast levels provided the crucial test of triaxiality, and are shown to give excellent agreement with the results of the triaxial rotor model.^{8,9)} The odd-Hg isotopes have also been thought by Khoo et al.¹³⁴⁾ and by us⁴⁸⁾ to be triaxial, due to the triaxial nature of the even-Hg cores (see Chapter II) and the decoupled pattern of the yrast members of the $i_{13/2}$ band. This success for ^{191}Pt has heightened our search for the odd-Hg non-yrast states. As can be seen in Figure 5-16, our results so far are extremely limited, and no definite conclusion can be given as to the exact structure followed by the odd-Hg nuclei. However,

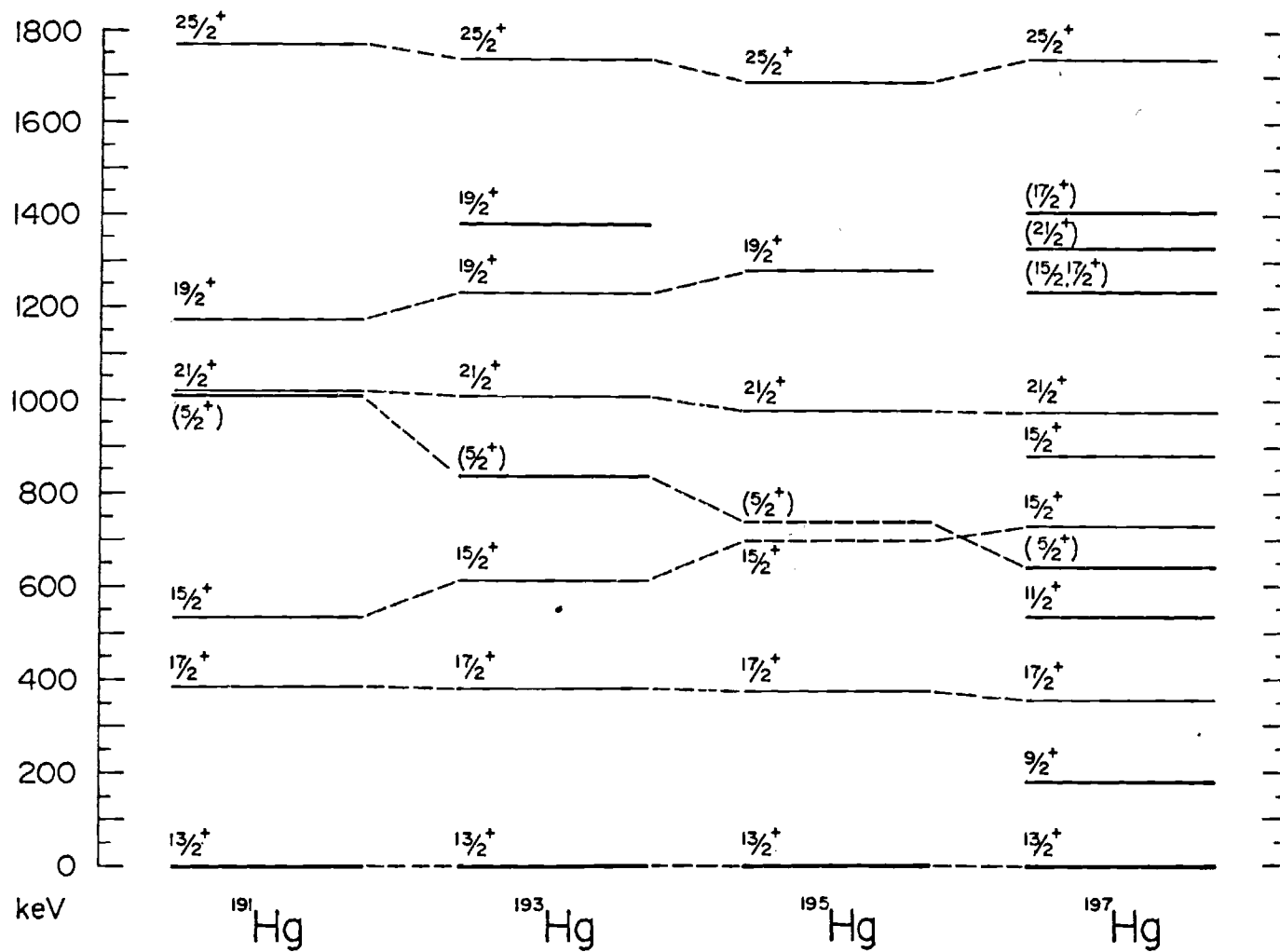


Figure 5-16. The Positive Parity States Observed in $^{191-197}\text{Hg}$ through In-Beam and Decay Studies. The in-beam results were taken from refs. 28, 29, and 42. Dashed connecting lines are to guide the eye and suggest possible level trends.

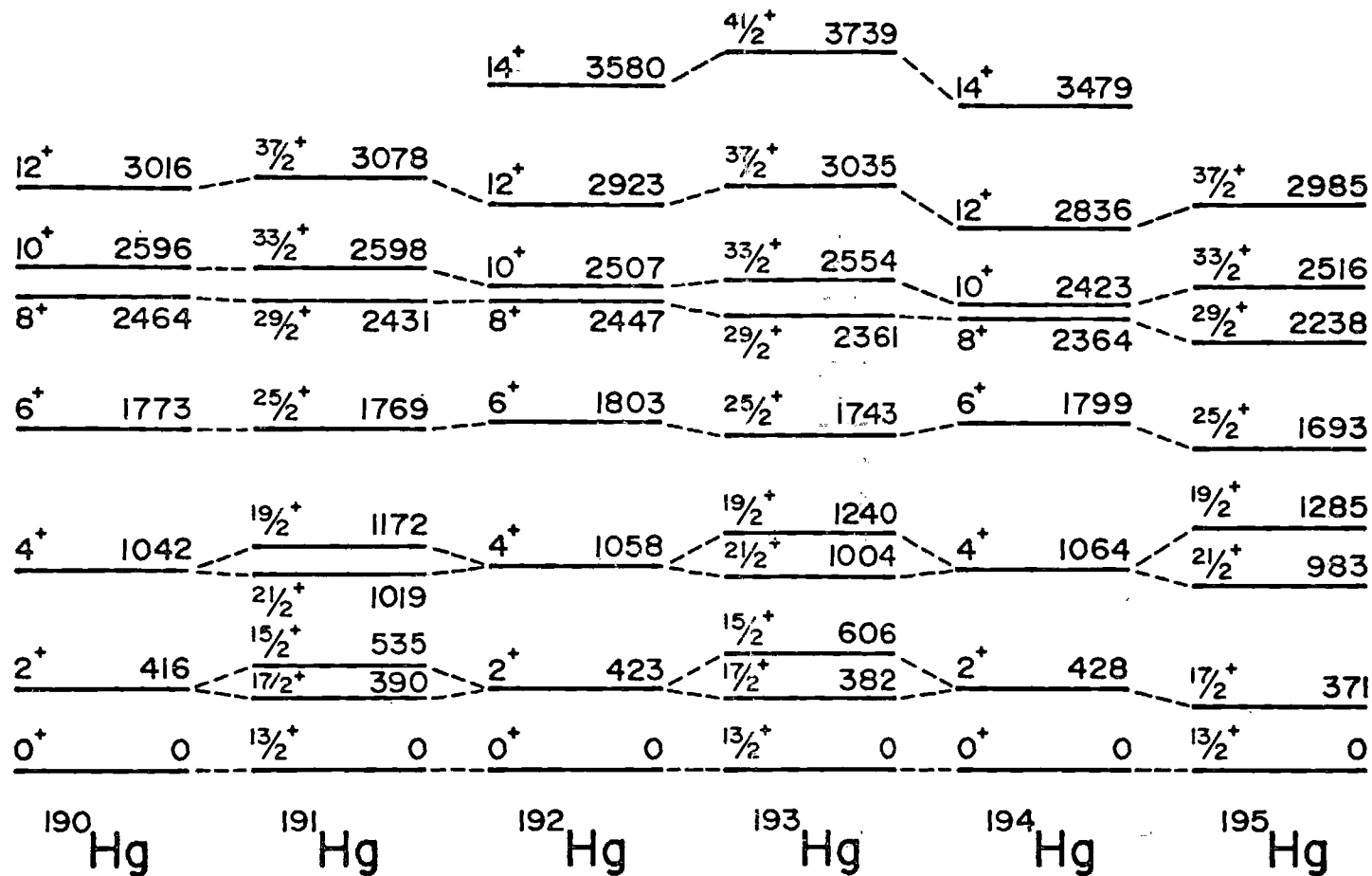


Figure 5-17. A Systematic Comparison of the Level Structure of Positive Parity States in ^{190}Hg - ^{195}Hg (taken from Lieder et al.) Showing the Decoupled Band Structure Following the Rotation-Aligned Picture of Stephens. Dashed connecting lines are to guide the eye and suggest possible level trends.

comparison of the known experimental levels in Figure 5-18 with the triaxial rotor model,⁹⁾ the triaxial rotor model including VMI,¹⁹⁾ and the rotation-alignment model⁹⁾ exhibits very impressive agreement with the two triaxial rotor models including their predictions of the two known non-yrast levels. This seems to lend additional credence to the prediction of triaxial shapes for the odd-mass Hg isotopes, although no final conclusion can yet be drawn. Another possible explanation of these bands is provided by the calculations of Baker and Goss¹³⁵⁾ (made specifically for ¹⁸⁷Ir), which indicate the importance of β_4 (hexadecapole) (in addition to the well-known β_2 -quadrupole) deformations in this region. At present there are no calculations available for other nuclei in this region that incorporate β_4 deformations. It should be noted that ¹⁸⁷Ir lies near to the axially symmetric prolate limit of the triaxially deformed region centered near ¹⁹⁵Hg.¹³⁶⁾ A third alternative is the Alaga-Paar model¹³⁷⁾ which couples the $i_{13/2}$ hole with phonon vibrational modes. It remains to be seen whether either of the latter two proposals can provide comparably good agreement with experimental results.

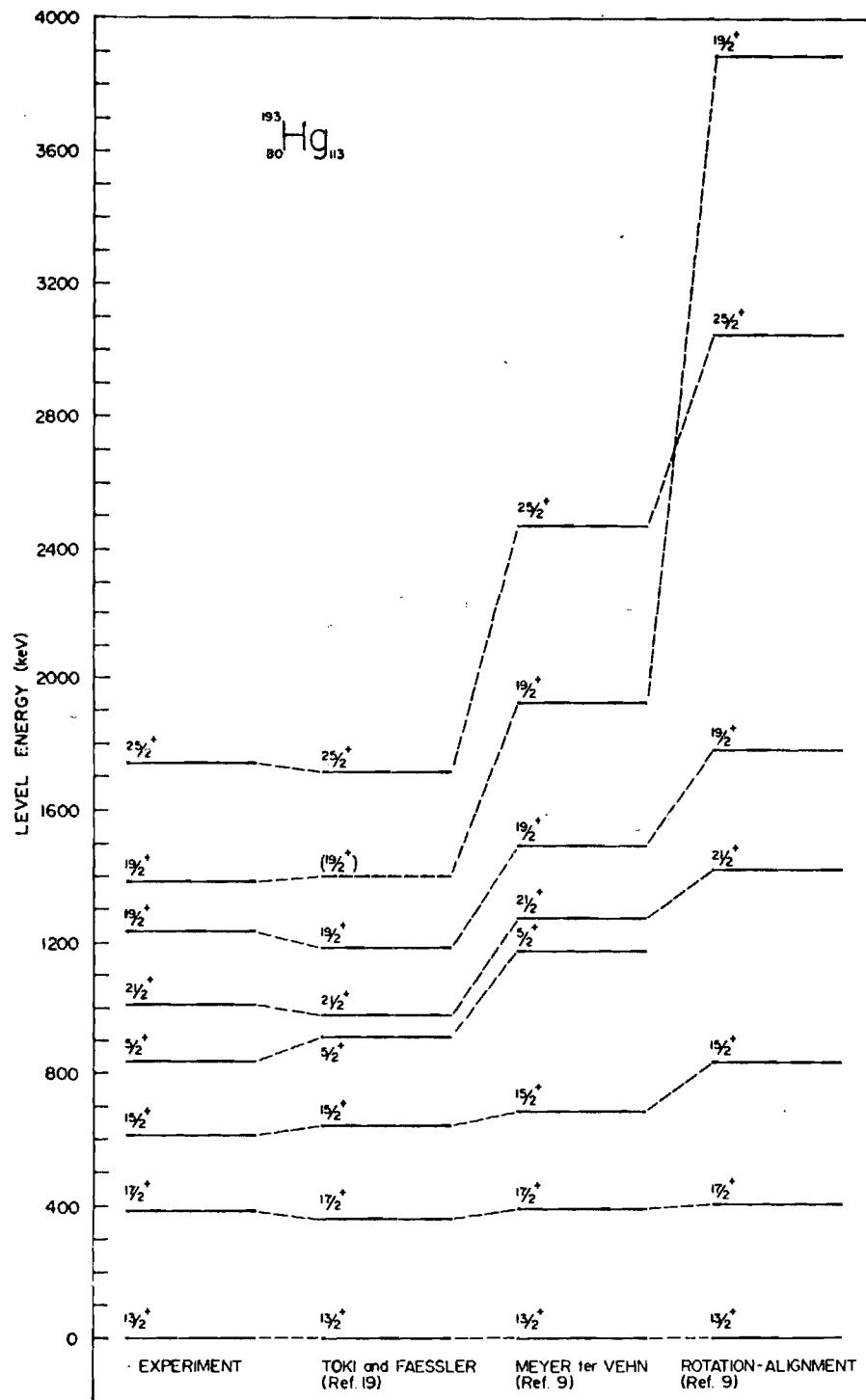


Figure 5-18. Comparison of Experimental Results for the $113/2$ Band with the Triaxial Rotor Model Plus VMI (Toki and Faessler), Triaxial Rotor Model (Meyer ter Vehn), and Rotation-Alignment Model Theoretical Predictions.

CHAPTER VI

CONCLUSIONS AND PROPOSED FUTURE EXPERIMENTAL WORK

Several observations concerning the results and interpretation of the work done for this dissertation can be drawn from the results discussed above. The relative population of levels in the odd-Hg nuclei changes as the nuclei become more neutron deficient, with the ratio of β^+ /EC decay branches from the isomeric and ground states of the respective $^{189-197}\text{Tl}$ parents being essentially 100/0, 100/0, 18/82, 1/99, and 0/100. Low-lying negative parity states in the odd-Hg isotopes are too complex to systematize well, but decoupled band structure is indicated in $^{189-195}\text{Hg}$, built on the $p_{3/2}$ state, that points to the existence of possible rotational character in these nuclei.

A study of ^{191}Pt , a nucleus isotonic to ^{193}Hg , gives a strong indication of the presence of triaxiality in this region. An alternative work by Baker and Goss¹³⁵⁾ suggests that the nuclei in this region can be explained as axially symmetric with hexadecapole (β_4 -deformation), in addition to the normal quadrupole (β_2 -deformation) degrees of freedom. However, this argument has, so far, only been applied to ^{187}Ir , a nearly axially symmetric nucleus, and therefore this question remains open.

In addition to the ^{191}Pt results, the even-Hg cores have low-lying 2_2^+ and 3_1^+ states separated by approximately the $2^+ \rightarrow 0^+$ energy

spacing (see Figure 2-2) which is also indicative of the pattern exhibited by triaxial nuclei.^{58,59)} Finally, we have indicated the excellent comparison of the present work and the in-beam results of Lieder et al.²⁸⁾ with the triaxial rotor model calculations of Meyerter Vehn⁹⁾ and Toki.¹⁹⁾ However, a conclusive piece of evidence necessary to show that triaxiality is present in odd-Hg isotopes would be placement of the non-yrast $i_{13/2}$ band members. However, these have not yet been identified. Rotational character is certainly indicated in some form by the unique parity high-spin $i_{13/2}$ states in this region. It remains an open question, however, whether an alternative model,¹³⁷⁾ based on coupling the $i_{13/2}$ hole with vibrational modes, can provide comparably good agreement with the experimental data presented here and reported in the literature for ^{191}Pt .

In spite of a relatively complex formalism, present vibrational models (for low-spin states) do not perform well when compared to our experimental results. Part of this may be due to the rotational character possibly exhibited by both the positive and negative parity states of the odd-Hg nuclei. A more physically realistic interpretation of this region might include both rotational and vibrational degrees of freedom and the mixing between these modes of excitation. Such a picture has been proposed by Arima and Iachello^{79,80)} in their interacting boson model, as a solution to the failing of vibrational models in general. Recently, extensive work on even-even nuclei⁷⁹⁾

has been reported by these authors, but it remains to be seen whether this model will provide an explanation of odd-mass nuclei in this region.

An extremely interesting feature suggested by the systematic trends observed in these odd-mass Hg levels is the possible presence of shape coexistence in ^{189}Hg . This phenomena has been found in $^{184,186,188}\text{Hg}$ (131,132) and predicted in $^{185,187}\text{Hg}$. (133) A possible deformed band having three observed members exists in ^{189}Hg with a bandhead energy of 476.5 keV above the ground state and a predicted spin-parity assignment of $7/2^-$. This assignment is consistent with a $7/2^- [503\uparrow]$ Nilsson state at the predicted deformation of $\beta \sim +0.27$ (prolate) for 109 neutrons. In order to prove or disprove the existence of this deformed band, a lifetime measurement will have to be made to see if transitions depopulating levels in the "deformed" band have lifetimes expected to be in the psec to μsec range implying that the transition probabilities are strongly retarded due to the change in nuclear deformation.

Another interesting feature found in the present work is the observation of a relatively intense E0 transition depopulating a very strongly fed, relatively high-lying level which feeds the $p_{1/2}$ single-particle level in $^{193,195,197}\text{Hg}$. The E0 transitions increase in energy as one goes more neutron deficient. No E0 transitions have been observed in the neighboring even-Hg nuclei. The interpretation of these levels, thus, is intriguing and uncertain.

As a final result of the present work, an extremely good set of experimental data now exists for the odd-mass Hg isotopes, $A = 189-197$. The remaining task clearly lies in the realm of theoretical calculations with models such as those outlined above.

In addition to the suggested theoretical exploration as a result of the present work, future experimental investigations are also indicated. The most urgent tasks should be lifetime measurements in ^{189}Tl decay (and possibly ^{191}Tl decay), to confirm the presence of shape coexistence in the Hg daughters, and a more thorough search for the $i_{13/2}$ non-yrast states. Also, band structure built on the $p_{3/2}$, $p_{1/2}$, and $f_{5/2}$ single-particle states should be further investigated. In this respect, studies of the decays from the ground states of $^{189,191}\text{Tl}$ might prove helpful, as well as a more detailed study of the decay of the $^{195\text{m}}\text{Tl}$ isomer. In order to populate the ground states of $^{189,191}\text{Tl}$, it will be necessary to enter the mass chains at $^{189,191}\text{Bi}$ (see Figure 5-3). The ground state-isomer situation in $^{189,191}\text{Pb}$ seems to be analogous to that in $^{189,191}\text{Hg}$ in that the isomeric and ground states both decay by essentially 100% β^+/EC . Therefore, as is found in these Tl nuclei, heavy-ion reactions will populate preferentially the $\text{Pb } 13/2^+$ isomer, which will predominately feed high-spin levels in Tl. However, entering these chains at Bi will give β^+/EC decay from the $9/2^-$ ground state populating both low- and high-spin states in Pb (similar to the situation found in odd-Tl to odd-Hg decay). Thus the $3/2^-$ ground state of Pb will be significantly populated, and this in turn will

decay to the $1/2^+$ ground state in $^{189,191}\text{Tl}$. The $\sim 1\%$ β^+ /EC branch in the decay of the 3.6 sec ^{195}Tl $9/2^-$ isomer can be studied through short (4-10 sec) on-line collections of directly produced (Heavy Ion, xn) ^{195}Tl sources, in order to optimize the $^{195\text{m}}\text{Tl}$ production over that of the 1.1 hour ground state. In addition, much more extensive in-beam studies of low- and high-spin states in the Hg nuclei, similar to those on ^{197}Hg (42) are needed before a more complete picture of these nuclei might emerge. Finally an extension of the systematic trends both above ^{199}Hg and below ^{189}Hg is required. Better radioactive decay, in-beam, and single-particle transfer reaction data will be necessary to add $^{201-205}\text{Hg}$ to the systematics. Extension of our decay work to the decay of more neutron-deficient nuclei $^{187-183}\text{Tl} \rightarrow ^{187-183}\text{Hg}$ has already been started at UNISOR.

BIBLIOGRAPHY

1. M. G. Mayer, Phys. Rev. 75, 1969 (1949).
2. O. Haxel, J. H. D. Jensen, and H. E. Suess, Phys. Rev. 75, 1766 (1949).
3. M. G. Mayer and J. H. D. Jensen, Elementary Theory of Nuclear Shell Structure, John Wiley and Sons, Inc., New York (1957).
4. A. Bohr, Kgl. Dan. Vidensk. Selsk. Mat.-Fys. Medd. 26, No. 14 (1952).
5. A. Bohr and B. R. Mottelson, Kgl. Dan. Vidensk. Selsk. Mat.-Fys. Medd. 27, No. 16 (1953).
6. E. K. Hyde, I. Perlman, and G. T. Seaborg, The Nuclear Properties of Heavy Elements, Vol. I, Prentice-Hall, Inc., Englewood Cliffs, N.J. (1964).
7. R. A. Sorensen, Rev. Mod. Phys. 45, 353 (1973).
8. J. Meyer ter Vehn, Nucl. Phys. A249, 111 (1975).
9. J. Meyer ter Vehn, Nucl. Phys. A249, 141 (1975).
10. A. de-Shalit, Phys. Rev. 122, 1530 (1961).
11. R. Kalish and A. Gal, Nucl. Phys. A175, 652 (1971).
12. L. S. Kisslinger and R. A. Sorensen, Rev. Mod. Phys. 35, 853 (1963).
13. N. Lo Iudice, D. Prosperi, and E. Salusti, Nucl. Phys. A127, 221 (1969).
14. G. J. Mathews, F. M. Bernthal, and J. D. Immele, Phys. Rev. C 11, 587 (1975).
15. G. J. Mathews and J. D. Immele, Report MNC-4028-0021, University of Maryland (1974), p. 32.
16. T. Fényes, I. Mahunka, Z. Máté, R. V. Jolos, and V. Paar, Nucl. Phys. A247, 103 (1975).
17. R. V. Jolos, Report P4-9357, Dubna (1975).

18. F. S. Stephens, *Revs. Mod. Phys.* 47, 43 (1975).
19. H. Toki and A. Faessler, *Nucl. Phys.* A253, 231 (1975).
20. T. B. Vandlik, J. Vandlik, N. G. Zaitseva, Z. Máté, I. Mahunka, M. Mahunka, T. Fényes, H. Tyrroff, and M. Jahim, *JETP Lett. (USSR)* 15, 271 (1972).
21. T. Fényes, I. Mahunka, M. Mahunka, Z. Máté, A. Piotrowski, L. Trón, H. Tyrroff, J. Vandlik, and N. G. Zaitseva, Proceedings of the International Conference on Properties of Nuclei Far from the Region of Beta-Stability, CERN 70-30, Vol. 2, 1081 (1970).
22. J. Vandlik, N. G. Zaitseva, Z. Máté, I. Mahunka, H. Tyrroff, and T. Fényes, *Bull. Acad. Sci. USSR, Phys. Ser.* 38, 26 (1974).
23. T. B. Vandlik, J. Vandlik, N. G. Zaitseva, Z. Máté, I. Mahunka, M. Mahunka, H. Tyrroff, T. Fényes, and V. I. Fominykh, *Bull. Acad. Sci. USSR, Phys. Ser.* 38, 21 (1974).
24. T. B. Vandlik, J. Vandlik, N. G. Zaitseva, I. Mahunka, M. Mahunka, Z. Máté, H. Tyrroff, and T. Fényes, *Bull. Acad. Sci. USSR, Phys. Ser.* 37, 15 (1973).
25. T. B. Vandlik, J. Vandlik, N. G. Zaitseva, I. Mahunka, Z. Máté, H. Tyrroff, T. Fényes, and V. I. Fominykh, *Bull. Acad. Sci. USSR, Phys. Ser.* 37, 9 (1973).
26. K. F. Chackett and G. A. Chackett, *J. Inorg. Nucl. Chem.* 13, 1 (1960).
27. G. Andersson, I. B. Haller, and R. Ringh, *J. Inorg. Nucl. Chem.* 17, 15 (1961).
28. R. M. Lieder, H. Beuscher, W. F. Davidson, A. Neskakis, and C. Mayer-Böricke, *Nucl. Phys.* A248, 317 (1975).
29. R. M. Diamond and F. S. Stephens, *Nucl. Phys.* 45, 632 (1963).
30. M. Karras, G. Andersson, and M. Nurmia, *Ark. Fys.* 23, 57 (1963).
31. J. D. Knight and E. W. Baker, *Phys. Rev.* 100, 1334 (1955).
32. G. Andersson, E. Arberman, and B. Jung, *Ark. Fys.* 11, 297 (1957).
33. R. K. Gupta and S. Jha, Proceedings of the International Conference on Nuclear Structure, Kingston, Canada, D. A. Bromley and E. W. Vogt (eds.), University of Toronto Press, (1960), p. 617.

34. B. Jung and J. Svedberg, Ark. Fys. 19, 447 (1961).
35. B. Jung and G. Andersson, unpublished work quoted in 34, (1961).
36. A. Backlin, B. Fogelberg, V. Berg, and S. G. Malmskog, Nucl. Phys. A138, 429 (1969).
37. D. Proetel, D. Benson, Jr., A. Gizon, J. Gizon, M. R. Maier, R. M. Diamond, and F. S. Stephens, Nucl. Phys. A226, 237 (1974).
38. G. Andersson, E. Arberman, I. Bergstrom, and A. Wapstra, Phil. Mag. 46, 70 (1955).
39. G. Andersson, J. O. Burgman, and B. Jung, Phil. Mag. 3, 105 (1958).
40. J. Knight and E. Baker, Phys. Rev. 99, 1646 (1955).
41. R. A. Moyer, Phys. Rev. C 5, 1678 (1972).
42. P. Kemnitz, L. Funke, H. Strusny, D. Venos, E. Will, and G. Winter, Proceedings of the 3rd International Conference on Nuclei Far from Stability, 19-26 May, 1976, Cargèse, Corsica (France), CERN 76-13, p. 464.
43. E. E. Zganjar, B. D. Kern, J. L. Weil, K. J. Hofstetter, H. K. Carter, W. D. Schmidt-Ott, R. L. Mlekodaj, E. H. Spejewski, C. R. Bingham, L. L. Riedinger, J. L. Wood, G. Gowdy, R. W. Fink, J. H. Hamilton, and A. V. Ramayya, Bull. Am. Phys. Soc. 19, 699 (1974).
44. J. L. Weil, K. J. Hofstetter, B. D. Kern, E. F. Zganjar, J. L. Wood, A. Xenoulis, G. Gowdy, E. H. Spejewski, R. L. Mlekodaj, H. K. Carter, W.-D. Schmidt-Ott, A. V. Ramayya, J. H. Hamilton, E. Bosworth, C. R. Bingham, L. L. Riedinger, F. Turner, and J. Lin, Bull. Am. Phys. Soc. 19, 1019 (1974).
45. E. F. Zganjar, J. L. Wood, R. W. Fink, G. Gowdy, L. L. Riedinger, C. R. Bingham, B. D. Kern, J. L. Weil, J. H. Hamilton, A. V. Ramayya, R. L. Mlekodaj, E. H. Spejewski, W. D. Schmidt-Ott, H. K. Carter, and J. Lin, Bull. Am. Phys. Soc. 19, 1125 (1974).
46. G. M. Gowdy, J. L. Wood, R. W. Fink, E. F. Zganjar, L. L. Riedinger, C. R. Bingham, F. Turner, B. D. Kern, J. L. Weil, R. L. Mlekodaj, H. K. Carter, E. H. Spejewski, W. D. Schmidt-Ott, J. H. Hamilton, and A. V. Ramayya, Bull. Am. Phys. Soc. 19, 1125 (1974).

47. A. G. Schmidt, G. M. Gowdy, R. W. Fink, and C. R. Bingham, *Bull. Am. Phys. Soc.* 21, 559 (1976).
48. G. M. Gowdy, J. L. Wood, R. W. Fink, E. F. Zganjar, and A. G. Schmidt, *Bull. Am. Phys. Soc.* 21, 559 (1976).
49. J. L. Wood, G. M. Gowdy, R. W. Fink, D. A. McClure, M. S. Rapaport, R. A. Braga, E. H. Spejewski, R. L. Mlekodaj, H. K. Carter, A. G. Schmidt, J. D. Cole, A. V. Ramayya, J. H. Hamilton, H. Kawakami, E. F. Zganjar, C. R. Bingham, L. L. Riedinger, A. C. Kahler, L. L. Collins, E. L. Robinson, J. Lin, B. D. Kern, J. L. Weil, K. S. R. Sastry, F. T. Avignone, M. A. Ijaz, and K. S. Toth, Proceedings of the 3rd International Conference on Nuclei Far from Stability, 19-26 May, 1976, Cargèse, Corsica (France), CERN 76-13, p. 364.
50. J. H. Hamilton, E. H. Spejewski, R. L. Mlekodaj, W.-D. Schmidt-Ott, R. W. Fink, A. Xenoulis, K. R. Baker, J. L. Wood, G. Gowdy, H. K. Carter, B. D. Kern, K. J. Hofstetter, J. L. Weil, E. F. Zganjar, K. S. R. Sastry, F. T. Avignone, C. R. Bingham, L. L. Riedinger, L. Harwood, F. Turner, I. A. Sellin, D. J. Pegg, J. Lin, A. V. Ramayya, S. Lee, G. Garcia-Bermudez, E. Bosworth, K. S. Toth, and N. R. Johnson, *Bull. Acad. Sci. USSR, Ser. Phys.* 38, 22 (1974).
51. J. H. Hamilton, K. R. Baker, C. R. Bingham, E. L. Bosworth, H. K. Carter, J. D. Cole, R. W. Fink, G. Garcia Bermudez, G. M. Gowdy, K. J. Hofstetter, M. A. Ijaz, A. C. Kahler, B. D. Kern, W. Lourens, B. Martin, R. L. Mlekodaj, A. V. Ramayya, L. L. Riedinger, W. D. Schmidt-Ott, E. H. Spejewski, B. N. Subba Rao, E. L. Robinson, K. S. Toth, F. Turner, J. L. Weil, J. L. Wood, A. Xenoulis, and E. F. Zganjar, *Bull. Acad. Sci. USSR, Phys. Ser.* 40, 1 (1976).
52. B. D. Kern, J. L. Weil, J. H. Hamilton, A. V. Ramayya, C. R. Bingham, L. L. Riedinger, E. F. Zganjar, J. L. Wood, G. M. Gowdy, R. W. Fink, E. H. Spejewski, H. K. Carter, R. L. Mlekodaj, and J. Lin, Atomic Masses and Fundamental Constants, Vol. 5, J. H. Sanders and A. H. Wapstra (eds.), Plenum Publishing Corp., New York, 1976, p. 81.
53. S. G. Nilsson, J. R. Nix, P. Möller, and I. Ragnarsson, *Nucl. Phys.* A222, 221 (1974).
54. C. R. Bingham, L. L. Riedinger, F. E. Turner, B. D. Kern, J. L. Weil, K. J. Hofstetter, J. Lin, E. F. Zganjar, A. V. Ramayya, J. H. Hamilton, J. L. Wood, G. M. Gowdy, R. W. Fink, E. H. Spejewski, W. D. Schmidt-Ott, R. L. Mlekodaj, H. K. Carter, and K. S. R. Sastry, *Phys. Rev. C* 14, 1586 (1976).

55. F. E. Turner and L. L. Riedinger (private communication).
56. B. Amov, T. Vandlik, J. Vandlik, Ts. Vylov, Zh. Zhelev, N. G. Zaitseva, I. Penev, and H. Tyrroff, *Sov. J. Nucl. Phys.* 16, 487 (1973).
57. R. Beraud, Ph.D. dissertation, University of Claude Bernard de Lyon, LYCEN-7305 (1973).
58. A. S. Davydov and G. F. Filippov, *Nucl. Phys.* 8, 237 (1958).
59. A. S. Davydov and V. S. Rostovsky, *Nucl. Phys.* 12, 58 (1959).
60. H. Toki and A. Faessler, *Z. Phys.* A276, 35 (1976).
61. M. A. J. Mariscotti, G. Scharff-Goldhaber, and B. Buck, *Phys. Rev.* 178, 1864 (1969).
62. K. Heyde and P. J. Brussard, *Nucl. Phys.* A104, 81 (1967).
63. V. Paar, *Nucl. Phys.* A164, 576 (1971).
64. A. Covello and G. Sartoris, *Nucl. Phys.* A93, 481 (1967).
65. R. V. Jolos, Soobshcheniya OIYAI, Report P4-7967, Dubna (1974).
66. V. Paar, *Nucl. Phys.* A211, 29 (1973).
67. V. Paar, *Phys. Rev. C* 11, 1432 (1975).
68. V. Paar, Proceedings of the Topical Conference on Problems of Vibrational Nuclei, Zagreb, Yugoslavia, September, 1974, p. 15.
69. S. G. Nilsson, *Kgl. Dan. Vidensk. Selsk. Mat.-Fys. Medd.* 29, No. 16 (1955).
70. W. Ogle, S. Wahlborn, R. Piepenbring, and S. Fredriksson, *Revs. Mod. Phys.* 43, 424 (1971).
71. K. Hecht and G. R. Satchler, *Nucl. Phys.* 32, 286 (1962).
72. V. V. Pashkevich and R. A. Sardaryan, *Nucl. Phys.* 65, 401 (1965).
73. A. K. Kerman, *Kgl. Dan. Vidensk. Selsk. Mat.-Fys. Medd.* 30, No. 15 (1956).
74. F. S. Stephens, R. M. Diamond, J. R. Leigh, T. Kammuri, and K. Nakai, *Phys. Rev. Lett.* 29, 438 (1972).

75. J. L. Wood, R. W. Fink, E. F. Zganjar, and J. Meyer ter Vehn, *Phys. Rev. C* 14, 682 (1976).
76. A. Faessler and H. Toki, *Phys. Lett.* 59B, 211 (1975).
77. Y. Yamazaki and R. K. Sheline, *Phys. Rev. C* 14, 531 (1976).
78. J. M. Eisenberg and W. Greiner, *Nuclear Theory*, Vol. I, North-Holland, Amsterdam (1970).
79. A. Arima and F. Iachello, *Ann. Phys. (New York)* 99, 253 (1976).
80. A. Arima and F. Iachello, *Phys. Rev. C* 14, 761 (1976).
81. E. H. Spejewski, R. L. Mlekodaj, H. K. Carter, W. D. Schmidt-Ott, E. L. Robinson, R. W. Fink, J. M. Palms, W. H. Brantley, B. D. Kern, K. J. Hofstetter, E. F. Zganjar, A. R. Quinton, F. T. Avignone, W. M. Bugg, C. R. Bingham, F. Culp, J. Lin, J. H. Hamilton, A. V. Ramayya, M. A. Ijaz, J. A. Jacobs, J. L. Duggan, W. G. Pollard, R. S. Livingston, C. E. Bemis, E. Eichler, N. R. Johnson, R. L. Robinson, and K. S. Toth, *Proceedings Eight International Electromagnetic Isotope Separator Conference*, eds. G. Andersson and G. Holmen, Chalmers University, Gothenberg, Sweden, (1973), p. 318.
82. M. L. Mallory, E. D. Hudson, and G. Fuchs, *IEEE Transactions on Nucl. Sci.* NS-19, 2, 118 (1971).
83. M. Blann and F. Plasil, "ALICE: A Nuclear Evaporation Code," COO-3494-10, 8p. (1973).
84. M. Blann, "OVERLAID ALICE: A Statistical Model Computer Code including Fission and Preequilibrium Models," COO-3494-29, 52p. (1975).
85. R. L. Mlekodaj, E. H. Spejewski, H. K. Carter, and A. G. Schmidt, *Nucl. Instr. and Meth.* 139, 299 (1976).
86. O. Almen and K. O. Nielsen, *Nucl. Instr. and Meth.* 1, 302 (1957).
87. H. K. Carter, E. H. Spejewski, R. L. Mlekodaj, A. G. Schmidt, F. T. Avignone, C. R. Bingham, R. A. Braga, J. D. Cole, A. V. Ramayya, E. L. Robinson, K. S. R. Sastry, and E. F. Zganjar, *Nucl. Instr. and Meth.* 139, 349 (1976).
88. H. K. Carter and R. L. Mlekodaj, *Nucl. Instr. and Meth.* 128, 611 (1975).
89. M. W. Guidry, Ph.D. dissertation, University of Tennessee, 1974 (unpublished).

90. R. C. Greenwood, R. G. Helmer, and R. J. Gehrke, Nucl. Instr. and Meth. 77, 141 (1970).
91. R. G. Helmer, R. C. Greenwood, and R. J. Gehrke, Nucl. Instr. and Meth. 96, 173 (1971).
92. D. H. White, R. E. Birkett, and T. Thomson, Nucl. Instr. and Meth. 77, 261 (1970).
93. G. Aubin, J. Barrette, G. Lamoureux, and S. Monaro, Nucl. Instr. and Meth. 76, 93 (1969).
94. R. C. Hawkings, Chemistry and Materials Division Progress Report: Atomic Energy of Canada Limited, Report No. PR-CMa, p. 39 (1968).
95. L. J. Jardine, "Gamma-Ray Calibration Standards," UCRL-20476 (1971).
96. M. R. Schmorak, Nucl. Data Sheets 14, 559 (1975).
97. R. L. Bunting, Nucl. Data Sheets 15, 335 (1975).
98. R. L. Heath, W. W. Black, and J. E. Cline, IEEE Trans. Nucl. Sci. NS-13, 3, 455 (1966).
99. W. W. Black and R. L. Heath, Nucl. Phys. A90, 650 (1967).
100. W. W. Black, Nucl. Instr. and Meth. 53, 249 (1967).
101. J. T. Routti and S. G. Prussin, Nucl. Instr. and Meth. 72, 125 (1969).
102. J. T. Routti, "SAMPO, a Fortran IV Program for Computer Analysis of Gamma Spectra from Ge(Li) Detectors, and for Other Spectra with Peaks," UCRL-19452 (1969), 34 p.
103. G. Wallace and G. E. Coote, Nucl. Instr. and Meth. 74, 353 (1969).
104. T. Hirose, S. Morinobu, and H. Ikegami, Nucl. Phys. A146, 220 (1970).
105. R. S. Mowatt, Can. J. Phys. 48, 2606 (1970).
106. L. L. Riedinger, N. R. Johnson, and J. H. Hamilton, Phys. Rev. C 2, 2358 (1970).
107. M. R. Schmorak, Nucl. Data Sheets 9, 195 (1973).

108. N. A. Voinova, D. M. Kaminker, and Yu. V. Sergeenkov, *Nucl. Phys.* A235, 123 (1974).
109. Program developed by D. C. Hensley, ORNL (1975).
110. M. B. Lewis, *Nucl. Data Sheets* 9, 479 (1973).
111. J. L. Wood, G. M. Gowdy, R. W. Fink, E. F. Zganjar, L. L. Riedinger, C. R. Bingham, E. H. Spejewski, R. L. Mlekodaj, H. K. Carter, B. L. Kern, J. L. Weil, and J. H. Hamilton, "The Decay of ^{191m}Hg to ^{191}Au ," *Phys. Rev. C* (to be published, 1977).
112. H. Beuscher, P. Jahn, R. M. Lieder, and C. Mayer-Böricke, *Z. Phys.* 247, 383 (1971).
113. R. S. Hager and E. C. Seltzer, *Nucl. Data Tables* A4, 1 (1968).
114. L. L. Collins, Ph.D. dissertation, University of Tennessee, 1977 (unpublished).
115. M. J. Martin, *Nucl. Data Sheets* B8, 431 (1972).
116. V. E. Viola, Jr., J. A. Swant, and J. Graber, *Atomic Data and Nuclear Data Tables* 13, 35 (1974).
117. I. Mahunka, Z. Máté, and F. Tárkányi, *Atomki Kozlem.* 16, 133 (1974).
118. E. F. Zganjar, J. L. Wood, R. W. Fink, L. L. Riedinger, C. R. Bingham, E. H. Spejewski, R. L. Mlekodaj, H. K. Carter, B. L. Kern, J. L. Weil, and J. H. Hamilton, "The Decay of ^{189m}Hg to ^{189}Au ," *Phys. Rev. C* (to be published, 1977).
119. M. B. Lewis, *Nucl. Data Sheets* B8, 389 (1972).
120. Z. Plajner, J. Frána, I. Rezanka, A. Spalek, and M. Fiser, *Z. Phys.* 233, 122 (1970).
121. C. Vieu, Ph.D. dissertation, University of Paris, Orsay, CSNSM-T-74-01 (1974).
122. M. B. Lewis, *Nucl. Data Sheets* B7, 129 (1972).
123. J. L. Wood and R. W. Fink, "Intruder States and the Quadrupole Pairing Force," (to be published, 1977).
124. J. O. Newton, F. S. Stephens, and R. M. Diamond, *Nucl. Phys.* A236, 225 (1974).

125. M. B. Lewis, Nucl. Data Sheets B6, 355 (1971).
126. R. L. Auble, Nucl. Data Sheets B5, 56 (1971).
127. A. Pakkanen, H. Helppi, T. Komppa, and P. Puumalainen, Z. Phys. 254, 98 (1972).
128. S. Hofmann and D. Walcher, Z. Phys. A272, 351 (1975).
129. R. L. Auble, Nucl. Data Sheets B5, 531 (1971).
130. M. R. Schmorak, Nucl. Data Sheets B6, 425 (1971).
131. J. D. Cole, J. H. Hamilton, A. V. Ramayya, W. G. Nettles, H. Kawakami, E. H. Spejewski, M. A. Ijaz, K. S. Toth, E. L. Robinson, K. S. R. Sastry, J. Lin, F. T. Avignone, W. H. Brantley, and P. V. G. Rao, Phys. Rev. Lett. 37, 1185 (1976).
132. J. H. Hamilton, A. V. Ramayya, E. L. Bosworth, W. Lourens, J. D. Cole, B. Van Nooijen, G. Garcia-Bermudez, B. Martin, B. N. Subba Rao, H. Kawakami, L. L. Riedinger, C. R. Bingham, F. Turner, E. F. Zganjar, E. H. Spejewski, H. K. Carter, R. L. Mlekodaj, W. D. Schmidt-Ott, K. R. Baker, R. W. Fink, G. M. Gowdy, J. L. Wood, A. Xenoulis, B. D. Kern, K. J. Hofstetter, J. L. Weil, K. S. Toth, M. A. Ijaz, and K. S. R. Sastry, Phys. Rev. Lett. 35, 562 (1975).
133. J. Bonn, G. Huber, H. Kluge, and E. W. Otten, Phys. Lett. 38B, 308 (1972).
134. T. L. Khoo, F. M. Bernthal, C. L. Dors, M. Piiparinen, S. Saha, P. J. Daly, and J. Meyer ter Vehn, Phys. Lett. 60B, 341 (1976).
135. F. T. Baker and D. Goss, Phys. Rev. Lett. 36, 852 (1976).
136. U. Götz, H. C. Pauli, K. Alder, and K. Junker, Nucl. Phys. A192, 1 (1972).
137. G. Alaga, Proceedings of the Topical Conference on Problems of Vibrational Nuclei, Zagreb, 1974, eds. G. Alaga, V. Paar, and L. Sips, North-Holland, Amsterdam, p. 344.

VITA

Gregory Michael Gowdy was born in Indianapolis, Indiana on February 2, 1947. He attended Shortridge High School there and upon graduation entered the Massachusetts Institute of Technology. Mr. Gowdy married the former Donna Duffy in Cambridge, Massachusetts on June 21, 1969. He received B.S. degrees, in Chemistry and Physics, from M.I.T. in June 1970. In September, 1970, he entered graduate school in Nuclear Chemistry at the University of Kentucky, transferring to the Nuclear Chemistry program at the Georgia Institute of Technology in January, 1973. He and his wife have one child, Kristyn Mercedes, born September 17, 1974 in Atlanta, Georgia. Mr. Gowdy completed the requirements for a Ph.D. in Nuclear Chemistry on December 4, 1976.